SANDIA REPORT

SAND Number 2005-0182
Unlimited Release
Printed February 2005

Photo-Control of Nanointeractions

Nelson S. Bell, Marcin Piech, Tim Long, Justin Marbury, Greg Jamison, Chad Staiger, Joe Thomes, Barrett G. Potter, Kelly Simmons Potter, Liu Jiang, and John Lean

Prepared by
Sandia National Laboratories
Albuquerque, New Mexico 87185 and Livermore, California 94550

Sandia is a multiprogram laboratory operated by Sandia Corporation,
a Lockheed Martin Company, for the United States Department of Energy's
National Nuclear Security Administration under Contract DE-AC04-94AL85000.

Issued by Sandia National Laboratories, operated for the United States Department of Energy by Sandia Corporation.

Available to DOE and DOE contractors from
U.S. Department of Energy
Office of Scientific and Technical Information
P.O. Box 62
Oak Ridge, TN 37831

Telephone: (865)576-8401
Facsimile: (865)576-5728
E-Mail: reports@adonis.osti.gov
Online ordering: http://www.doe.gov/bridge

Available to the public from
U.S. Department of Commerce
National Technical Information Service
5285 Port Royal Rd
Springfield, VA 22161

Telephone: (800)553-6847
Facsimile: (703)605-6900
E-Mail: orders@ntis.fedworld.gov
Online order: http://www.ntis.gov/help/ordermethods.asp?loc=7-4-0#online

SAND2005-0182
Unlimited Release
Printed February 2005

Photo-Control of Nanointeractions

Nelson S. Bell, Marcin Piech, Tim Long, Justin Marbury, and Greg Jamison
Chemical Synthesis and Nanomaterials

Chad Staiger
Chemical & Biological Systems

Joe Thomes
Firing Set, Fuze, & Switch Tube

Sandia National Laboratories
P.O. Box 5800
Albuquerque, NM 87185-1411

Barrett G. Potter
Kelly Simmons Potter
The University of Arizona
Tucson, AZ 85721

Liu Jiang, John Lean
Former Sandians

Abstract

The manipulation of physical interactions between structural moieties on the molecular scale is a fundamental hurdle in the realization and operation of nanostructured materials and high surface area microsystem architectures. These include such nano-interaction-based phenomena as self-assembly, fluid flow, and interfacial tribology. The proposed research utilizes photosensitive molecular structures to tune such interactions reversibly. This new material strategy provides optical actuation of nano-interactions impacting behavior on both the nano- and macroscales and with potential to impact directed nanostructure formation, microfluidic rheology, and tribological control.

Acknowledgements

Appreciation is extended to all the team members in this study for their perserverence and effort in this program. Special thanks are offered to Liu Jiang, who provided exceptional optimism and interest in the synthesis of the materials, and without which the program would not have had the successes it generated. Thanks are also due to Martin Piech who undertook additional responsibility of leadership and dedication in the project. We also extend our appreciation to the characterization department at Sandia, especially Tom Headley's transmission microscopy and Bonnie McKenzie for scanning electron microscopy efforts on our behalf.

Contents

Figures

Tables

This page intentionally left blank

Executive Summary

Section 1 focuses on the identification and examination of organic structures possessing known photophysical effects that have a high probability for influencing target interaction processes, e.g. physical entanglement, hydrophobicity/philicity, local electrostatic charge or pH changes. Their incorporation into polymeric chemistries will allow their application to inorganic colloids as photo-active surfactants. Studies were performed by the synthesis of photo-switchable molecules with chemically binding deposition to silicon wafer substrates. The response of the materials was tested using contact angle measurements and characterization of the surface energy parameters of the photo-switchable films. These parameters were used to predict changes in wetting behavior for the surfaces against known solvent parameters, and allowed for screening of the effect of these films for additional study.

Section 2 describes the synthesis of colloidal particles functionalized with photoreversible organic moeities which provide photo-control of the state of particle agglomeration. Both azobenzene and spiropyran derivatives were investigated, in the form of monolayers and grafted polymers. Photo-switching in the organic moiety demonstrated changes in the colloidal stability of the particles in certain nonaqueous solvents. A system was chosen for focused study. The functionalized particles developed for this purpose are coated with polymer layers containing benzospiropyran molecules. These molecules can be switched from a non-polar closed form (benzospiropyran) to the open, zwitterionic form (merocyanine) through exposure to ultraviolet (UV) light at 330 nm wavelength. They can be reversibly switched to the closed form by exposure to heat and/or visible light at 540 nm wavelength. The cycles of exposure and recovery lead to reversible states of aggregation in the system.

Section 3 presents photo-physical effects between derivatized particles including formation of particle agglomerates, comparison of sedimentation rates in various solvents, and reversible changes in suspension viscosity. Polymerically coated layers exhibit greater stability in cycling through aggregation and dispersion events than monolayer coated particles.

Section 4 describes studies of the aggregation and deposition of the photo-controlled particles on derivatized substrates. Confocal microscopy was used with one micron particles to determine the affinity of particles in the switched form to undergo agglomeration, and to test the dynamics of switching to restructure the aggregate.

Their incorporation into polymeric chemistries will allow their application to inorganic colloids as photo-active, surfactants to enable the photo-actuated control of interparticle nano-interactions to reduce the defect content of colloidal crystal arrays (artificial opals). Primary demonstration of successful nano-interaction control will be provided by zone refining of assembled colloidal crystals. A successful demonstration will provide proof that colloidal crystal arrays can be used to form complete photonic band gaps by the elimination of defects which currently prevent band gap development. Extension of these fundamental findings can also provide optically tuned microfluidic rheology and tribological control useful in a range of microsystems with an impact in DOE/DP technologies for stockpile safety and security.

Section 1

Evaluation of Photoswitchable Organic Structures and Applicability to Changes in Surface Properties

Introduction

The manipulation of physical interactions between structural moieties on the molecular scale is a fundamental hurdle in the realization and operation of nanostructured materials and high surface area microsystem architectures relying on such nano-interaction-based phenomena as self-assembly, fluid flow, and interfacial tribology. Self-assembly systems using molecular interactions have received attention recently to construct complex structures or composites[1]. Colloids and polymers are assembled using electrostatic methods from surfactants of opposite charge, because these materials form strong ionic bonds and are stable. Derivatization of colloidal gold and silver using 4-aminothiophenol and 4-carboxythiophenol created alternating layers of materials, and the use of polymers mitigates the presence of defects, but cannot eliminate them.[2] Approaches for control of nanoparticle and colloidal assembly have used polymer phase separation as well as microcontact printing for templating the deposition of colloidal materials. Additionally, biomaterials have been examined for use in colloidal systems, specifically DNA as a stabilizer and specific recognition agent for colloidal assembly. Ferritin has been used as a templating agent for particle precipitation, and lysine and streptavidin have been used for templating particle assembly. Nonlinear rheological fluids have been applied to the control of microfluidic networks[3]. These nano-interaction control strategies typically involve the tailoring of material structures either during synthesis or through invasive post-synthesis processing with no opportunity for real-time, remote modulation of intermolecular and/or interparticle forces.

This research focuses on the reversible photo-control of molecular interactions through the introduction of photosensitive molecular structures into the material system. The photo-switchable organic moieties can affect solution properties through surface wetting, ion adsorption, hydrogen bonding, or charge interaction, and when incorporated in polymeric systems through solubility parameter, polymer conformation, and chirality. This new material strategy provides optical actuation of nano-interactions impacting behavior on both the nano- and micro-scales with the potential for impact in directed nanostructure formation, microfluidic rheology, and tribological control. In this section, the identification of molecular groups exhibiting photocontrolled response will be detailed and related to the formation of photosensitive surfactants. Studies performed to investigate the control of surface properties will also be described.

Photo-switchable Organic Moieties and Their Use as Surfactants

There are a large number of studies focusing on the incorporation of photosensitive compounds into surfactant molecules, self-assembled monolayers, membranes, liquid-crystalline materials, polymer matrices and gels, and in directing fluid flow via changes in surface energy [4,5,6,7,8,9,10,11,12,13,14,15,16,17,18,19,20,21,22]. These materials utilize the property of photochromism which can be defined as the reversible change in molecular properties induced by specific wavelength(s) of light. These properties can be thermally reversible or irreversible dependant on the pendant groups around the photochromic centers, and there can be more than two potential photochromic states. Compounds include the variations of azobenzene, fulgides, sterically overcrowded stilbenes, spiropyrans, diarylethenes, salicylideneimines, viologens, and azulenes. The photochromic processes include (cis-trans)

isomerization, photocyclization, photo-induced electron transfer, and keto-tautomerism[23]. For the applications of interest in this work, there are several properties that are desired or must be considered. These include thermal stability against switching, steric requirements for switching, generation of photo-physical effects as surfactant monolayers or polymer components, and rapidity of switching response. The following section considers available work performed on these switching chemistries and their use to impact surface or polymer properties.

Azobenzene compounds have been extensively studied for their impact on the properties of other compounds to which they are incorporated. Azobenzene undergoes photochromism through the conformational change between the benzene rings across a double bond. The trans isomer is generally the thermally stable conformation, but photo-switching causes the cis-isomer to be expressed and the adsorption changes from colorless to red. The dipole moment of the molecule changes from 0.5 to 3.1 Debye during this process, and the increase in polarity leads to greater affinity for polar solvents or other molecular compounds. The transition is thermally reversible with dynamics dependant on the pendant groups of the photochromic compound, and it is also photo-switched back to the trans-isomer by visible light. The addition of azobenzene has created photocontrollable surfactants, Langmuir-Blodgett films, monolayers[24], and liquid crystal compounds[25]. This has led to reversible changes in wetting behavior[26],[27], chiral expression[28], adsorbed surface morphology[29],[30], and reversible gelation or insolubility effects[31],[32],[33]. The switching behavior is sensitive to the solvent conditions and to the packing and intermolecule bonding interactions in the photochromic groups. The steric effects on the pendant groups dictate the ability to switch conformations for azobenzene-urea amphiphiles in Langmuir monolayers based on hydrogen bonding between the groups[34]. Key design considerations for application of azobenzene include the available volume for the molecule to switch, local bonding interactions, and speed of response.

Azobenzene has been applied to polymeric systems and shown the ability to affect solution properties. These properties include solubility[35], viscosity[36],[37], and conductivity. Polystyrene with pendant azobenzene groups have dynamics of property changes under a minute, which is too slow for switching, but adequate for controlling the properties of colloids[38]. In some instances, the cis-isomer is described as forming crosslinking groups in gels[39]. The addition of azobenzene groups in aqueous systems has affected the hydrogen bonding interactions of thermally sensitive polymers, so that reversible switching between the soluble and insoluble forms of poly(N-isopropyl acrylamide) can be performed at room temperature[40],[41]. Polymer phase transitions are used as an *amplification method* to improve the efficiency of the polymer response. Polymer phase transitions are accompanied by changes in conformation, and thereby the property changes. The phase separation process of PNIPAM depends on the balance of the hydrophobic bonds formed with water and the hydrophobic forces between molecules. The dynamics of the change require ~30 minutes for completion to be reached, and an induction period was observed. Based on this published literature, azobenzene derivatives are appropriate for examination within this study.

Spiropyran (SP) based compounds undergo photo-controlled bond scission from a non-polar ring to a zwitterion, and as a resulting, the dipole moment of the molecule increases greatly. Positive spirobenzopyran behavior involves a transition from the closed to open form, whereas negative behavior involves the reverse process. Spiropyrans and their derivatives undergo photochromism through cleavage of the C-O bond of the spiropyran ring. The open form becomes a zwitterion and is called the merocyanine form (MC). The MC form has a strong tendency to associate into aggregates with a stack-like arrangement. When the dipoles are arranged in a parallel (head-to-head) structure, they are termed J-aggregates and the adsorption spectra is shifted to the red. The antiparallel association is termed the H-aggregate and the spectra is shifted to the blue. For certain conditions, switching in a nonpolar solvent can lead to the formation of submicrometer beads with J-aggregate cores and an amorphous exterior. Under an electric field, the colloidal beads form threads along the electric lines of force. Aggregate formation can take place even in a methacrylate polymer and during polymer swelling. Spiropyran compounds are very sensitive to their detailed chemical structure and environment in their photochemistry. “Positive” photochromic behavior occurs when the DES only weakly adsorbs visible light, and “negative”

photochromism in the case of strong adsorption of visible light. UV excitation increases the adsorption of positive photochromics, and decreases it for negative photochromics.

Spiropyran compounds have also been incorporated into surfactants and studied. Some of the benefits of spiropyran include no production of free radicals during switching, they exhibit high cycling lifetime, they show good quantum yield for isomerization, and are biocompatible. They are extremely sensitive to steric effects (i.e. local environment) and should be dilute to allow for the volume change during switching; and the environment strongly affects the photochromism. A polar solvent will stabilize the merocyanine form, so the layer should contain both polar and non-polar regions to maintain switching. The photo-switching reaction was seen to affect surface pressure in Langmuir films and indicated that the volume changes in the molecule lead to stress[42]. Another study suggested the aggregation of MC forms causes hysteresis in the switching behavior of the photochromic molecules[43]. A mixture of spiropyran organosilanes mixed with organosilanes in order to control the surface environment created reversible changes in wetting behavior[44]. A dilute layer of spiropyran was chemisorbed to a flat silica surface by using non-reactive spacer molecules and allowed the SP switching to be sterically unimpeded. Photo-switching to the more polar merocyanine form lowered contact angle in water at pH 5.5 by 11-14º. Water in capillary tubes was seen to rise due to the polarity change, but contact angle hysteresis prevented the water from flowing back down the tube when the light was switched back to visible from UV. Another study found the MC form associated with the substrate surface and therefore did not exhibit significant changes in wettability[45].

Spiropyran has been incorporated into DNA biomolecules to affect the hybridization of DNA[46]. Methyl cellulose has also been derivitized with spiropyran to provide reversible changes in wetting behavior, but the films cast show fatigue after only twenty cycles of switching irradiation[47]. Spiropyran is also considered as a potential material for holographic gratings[48]. Spiropyran compounds are another likely candidate for application, as their polarity change is greater than that of azobenzene, and the MC forms have a tendency to assume aggregated states. However, there is more consideration required for control of the local environment around the molecule to prevent it from becoming exclusively polar through polar solvent coordination.

Other compounds considered include furyl fulgide and diarylethenes. The photochromism of fulgides occurs between one of the colorless open forms (E-form) and the photocyclized, colored form (C-form). A third form (Z-form) can also occur in competition with the E-form, as it is a geometrical isomer, but it is an energy wasting and system complicating process. The colorization mechanism is the photochemical 6π-electrocyclization of the hexatriene moiety. The conformation of fulgides at their ground state influences the quantum yield of photocyclization. Shifts in the electronic wavelengths are controlled by the electron donating power of substituents. Photochromism intrinsically involves their chiral nature. Photochromism is achieved in solutions, polymer films, or glass solids, but in crystals only the surface layers switch. Photochromic phenylthiophene fulgide films were UHV deposited and formed nanostructures[49]. Switching is reversible and fairly uniform with times under a microsecond.

Diarylethenes have been used to form photo-controlled ion complexes[50] and surfaces with switchable wettability[51]. They are also employed as photooptical switches based on changes in refractive index, where the specific derivatives contain fluoro compounds and exhibit thermal stability[52].

Surface Energy Measurement: Theory and Experimentation

Wettability and surface energy calculations are linked by their typical measurement procedure; the determination of contact angle. Through the Young equation, the substrate surface energy can be predicted based on the fluid surface tension and an estimate of the solid-vapor surface energy. The interpretation of the measurement of contact angle is dependant on the method used to model the surface energy, and also upon complications based on solubility of the substrate or interactions between the surface groups and the solvent molecules, as well as the roughness of the surface. In addition, the contact

angle is divided as to whether the drop edge is advancing across the substrate (θ_a), or is receeding as the droplet is pulled back (θ_r). The difference between these two values is considered the contact angle hysteresis, and is a measurement of the affinity of the solvent for the substrate.

The measurements have already been used to characterize the potential use of contact angles to drive fluid flow. The requirement in a switchable surface for moving fluid is that the advancing contact angle in state A is lower than the receding contact angle of state B[53]. By using a gradient of the stimulating agent or field, such conditions can cause fluid flow. Microfluidic applications are perhaps more complicated, as new theoretical treatment of the liquid interface suggests that the surface energy of the liquid-solid interface is different than the treatment used for the surface tension[54].

Attempts to model the surface energy properties of a surface utilize a number of theoretical approaches, none of which achieve complete success and are thus situation-dependant. Whereas the surface tension of liquids is known, there are no accepted definitions of surface energy for solids in the literature, as no theory models interactions perfectly[55]. The applicability of each theory can be appreciated by taking certain guidelines. In Zisman theory, the definition is the surface energy of a solid equals the surface tension of the highest surface tension liquid (real or imaginary) that will completely wet the solid with a contact angle of 0. Zisman theory works best for non-polar surfaces (generally polymers), and fails with even a small polarity to the surface. In Fowkes Theory, the assumption is made that the surface has a dispersive (van der Waals) component and a polar component to surface energy. Two contact angle measurements using different solvents are made. Each liquid must be characterized with dispersive and polar components to surface energy based on testing against a reference surface (typically teflon).

$$\sqrt{\sigma_l^D}\sqrt{\sigma_s^D} + \sqrt{\sigma_l^P}\sqrt{\sigma_s^P} = \frac{\sigma_l(Cos\Theta + 1)}{2} \quad (1)$$

Fowkes equation requires measurement with a polar liquid and a liquid with purely nonpolar components to surface tension. Typically water and diiodomethane are used as polar-containing and purely nonpolar liquids. This theory works well for surfaces with some polarity. It is also used for predictions of adhesive strength, where adhesion is maximized for liquids and surfaces with similar levels of polarity. In van Oss theory, the solid surface energy is separated into the dispersive (D), acid (+) and base (-) components. The acid component specifies interactions like dipole-dipole, induced dipole-dipole, and hydrogen bonding types, and the wetting liquids have a tendency to *donate* electron density (act acidic). The base component characterizes interactions where the solvent has the tendency to *accept* electron density (act basic). Three test liquids are used, a non-polar, an acid dominated polar liquid, and a base dominated polar liquid. This theory is best suited for surfaces with significant polar interactions such as inorganics, organometallics, and surfaces containing ions. However, there is disagreement on a standard solid for characterizing the parameters of liquids.

$$\left(\sqrt{\sigma_l^D}\sqrt{\sigma_s^D} + \sqrt{\sigma_l^-}\sqrt{\sigma_s^+} + \sqrt{\sigma_l^+}\sqrt{\sigma_s^-}\right) = \frac{\sigma_l(Cos\Theta + 1)}{2} \quad (2)$$

The van Oss theory has been applied to the characterization of polymer surfaces as well[56], which suggests that the substituents of the polymer backbone are critical for the surface energy and determination of contact angle. Low surface energy polymers are given by chemistry (CH_2> CH_3> CF_2> CF_3), amorphous structure, roughness (assessed from contact angle hysteresis), nature of the pendant chain, length of pendant chain, nature of the linking moiety, and nature of the polymer backbone. Very large contact angles with polar fluids were found for some fluoropolymer surfaces with rough interfaces. Fluoro-substituted compounds exhibit markedly lower surface energies than the alkyl analogues, and a long fluoro-substituted linking group masks the linking moeity and the polymer backbone.

Photo-switchable compounds have been tested for wettability changes using contact angles. Reversible change was observed in a poly(butyl methacrylate) surface using (2-hydroxyphenyl diphenyl methanol) photochromic compounds (and they reference azobenzene and spiropyran compounds for changes as well)[57]. Exposure causes the film to become highly hydrophobic. Studies have also been

performed with thermally switchable polymer films grown from a surface, where contact angle is switched using temperature[58].

Synthesis of Surface Terminated Photo-Switchable Compounds

Furyl Fulgide

Surface terminated layers of furyl fulgide organic moieties were synthesized for evaluation of wetting changes resulting from optical switching. These photochromic structures were chosen for investigation due to the high efficiency of the photoconversion reaction. They are also known to have wide variability of potential substitution patterns which can be used to alter absorption wavelength and photoefficiency. Furyl fulgide molecules transform from the polar "E" state to the non-polar "C" state during the isomerization reaction. The creation of a furyl fulgide surface was performed by synthesis of a siloxane derivative, followed by the condensation of the siloxane groups to a fused quartz surface. Derivative groups incorporating methyl (1a) and isopropyl (1b) functionality were synthesized. These materials demonstrated photochromic behavior in solution and dry form.

Successfully derivatized furyl fulgide **1a** to furyl fulgimide **2a** via new synthetic protocol, by which hydrolytically sensitive alkoxysilane group is incorporated into fulgimide molecule via condensation of primary amine with fulgide's acid anhydride functionality. Novel fulgimide compound was completely characterized; confirmed that desired optical properties are maintained in solution. Successfully prepared furyl fulgide analogue **1b**. Pursuing derivatization of **1b** to fulgimide **2b** analogous to that defined for compound **1b**.

Evaluation of the appended surface compounds are presented in section 1.5.

Scheme 1: Preparation of benzospiropyran surface modifier.

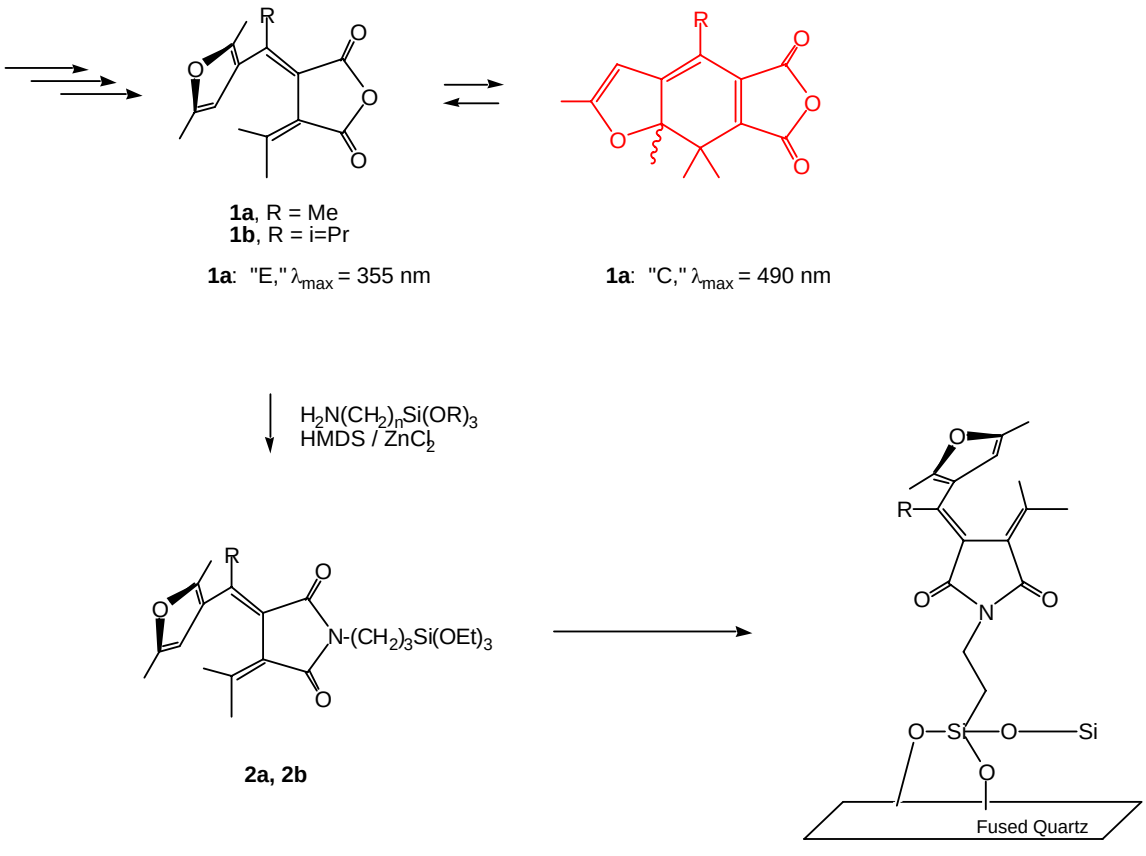

Benzospiropyran

Attempts to purify benzospiropyran containing sol gel monomers proved difficult. So a method was devised to attach a precursor of the dye molecule to a quartz surface and then react that with an α-hydroxybenzaldehyde to generate a surface bound benzospiropyran. In addition to side stepping purification problems, this method could allow us to generate a wide variety of benzospiropyran derivatives from the same common surface by simply changing the aldehyde. The surface modifier was prepared in three steps from 1,3,3-trimethyl-2-methyleneindoline (Scheme 2). The 1,3,3-trimethyl-2-methyleneindoline was initially nitrated with nitric/sulfuric acids. Then the nitro group was then reduced with tin dichloride to give the amino functionalized indoline in 79% yield. The surface modifier was finally prepared by near quantitative reaction of isocyanotopropyltriethoxysilane with the amino indoline.

Scheme 2 Preparation of benzospiropyran surface modifier.

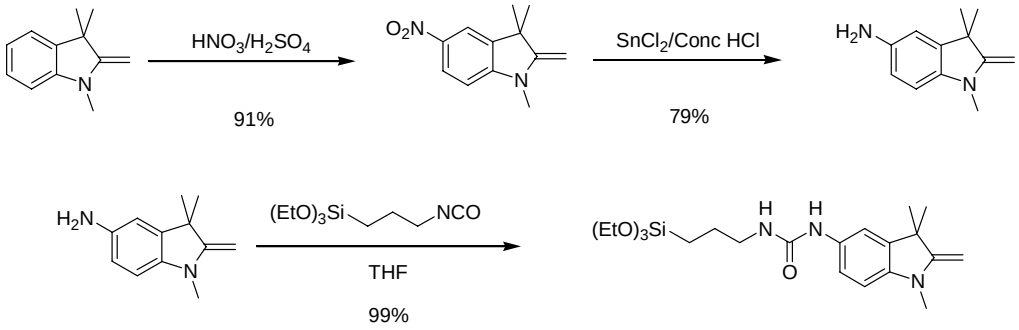

The surface modifier was polymerized by base catalysis in tetrahydrofuran (Scheme 3). The still soluble polymer was then spin coated onto previously cleaned quartz slides. The thin film was baked at 120 ^{o}C for 2 h so that the polymer could react with the free silanols on the quartz for permanent attachment. The surface bound indoline was then reacted 2-hydroxy-4-nitrobenzaldehdye in tetrahydrofuran at 80 ^{o}C to complete the surface modification of quartz with a benzospiropyran dye.

Scheme 3

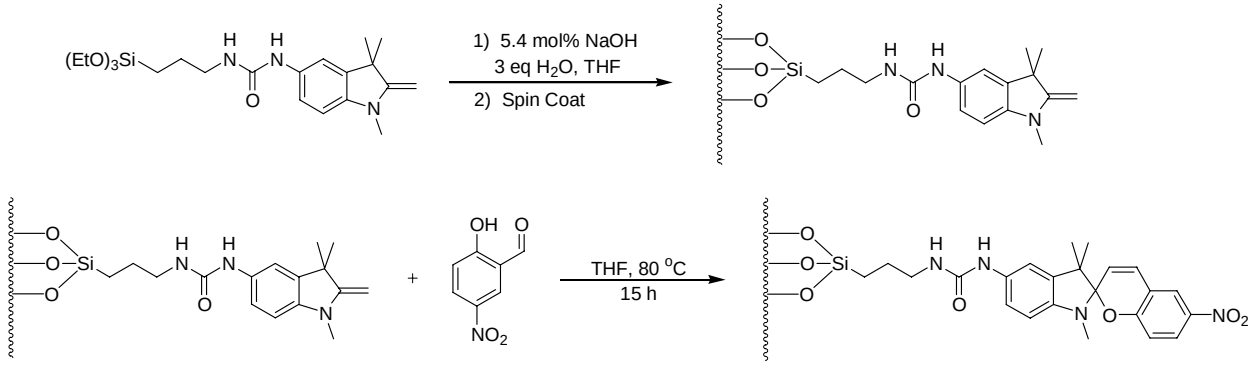

Benzospiropyran formation was confirmed by UV-Vis spectrophotometry. As shown in Figure 1, the coated quartz slide gave absorbance maxima at 325 and 560 nm. These absorbance maximas are consistent with benzospiropyran dyes.

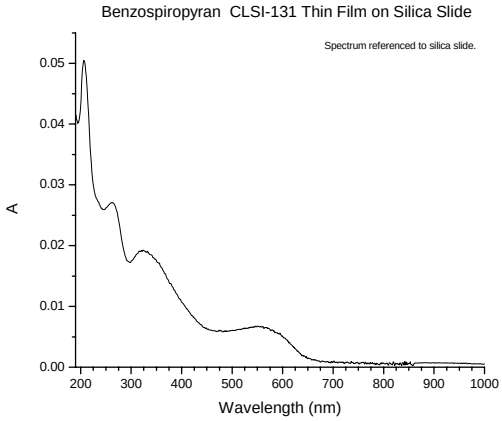

Figure 1 UV-Vis absorbance spectra of the benzospiropyran coated slide

Next, the film was irradiated to test its ability to photo switch (Scheme 4). The slide was irradiated with UV light and allowed to stand in the UV-Vis spectrophotometer to observe the conversion of the zwitterion to the neutral form. The decay was too weak to be observed by UV-Vis

Scheme 4. Photo switching of benzospiropyran

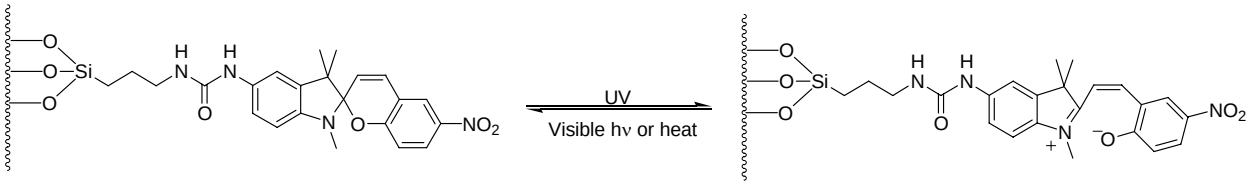

Azobenzene

A monofunctionalized azobenzene monomer was prepared from the reaction of 4-hydroxazobenzene with isocyanotopropyltriethoxysilane in 97% yield (Scheme 5).

Scheme 5

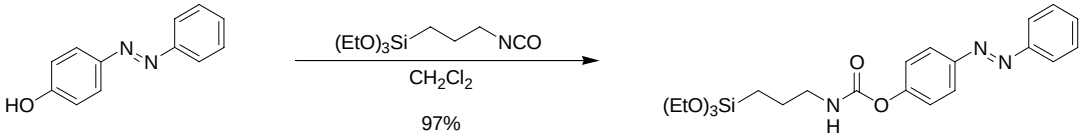

Next the monofuctional azobenzene monomer was polymerized with acid and allowed to stand for 4.5 days (Scheme 6). The solution was then diluted and spun coat onto some previously cleaned quartz slides. The slightly orange film was annealed at 150 ^{o}C for 1.5 h to permanently adhere the film to the quartz surface. The UV-Vis absorption spectra was taken and shown to be consistent with that of an azobenzene.

Scheme 6

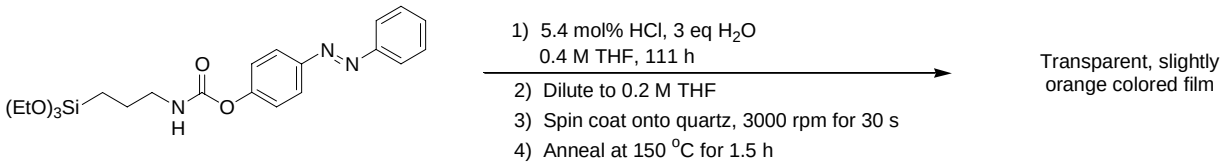

The film was irradiated with 337 nm laser light and then placed in a UV-Vis to monitor the decay of the of the absorption maximum at 315 nm. The decay is representative of the azobenzene switching from a trans to cis conformation. The film was allowed to stand over night and UV-Vis spectrophotometry indicated that molecule had partially reverted back to the lower energy trans conformation.

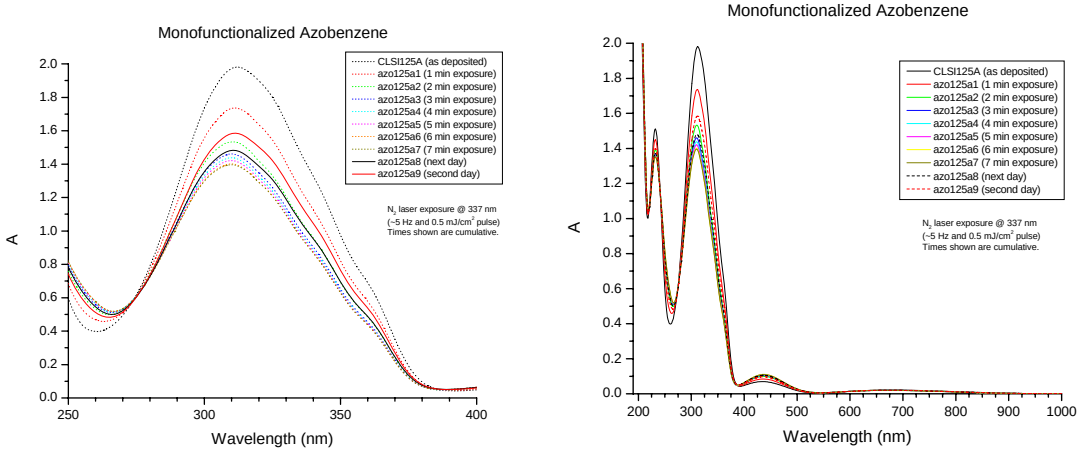

Figure 2 UV-Vis absorbance spectra of the azobenzene coated slide.

Wetting and Contact Angle Measurements

Organic synthesis of the photo-controlled groups that affect behavior is a critical component to the success of this program. We have identified two chemistries that show viability for production of a number of films and structures for the investigation of photo-controlled response. The three original candidates included derivates of furyl fulgide, azobenzene and benzospiropyran. Chemical synthesis of films derivatized for attachment to silica surfaces was successful, and testing proceeded using UV-vis spectroscopy and contact angle measurement. The contact angle information was fitted using the Fowkes equation for the dispersive and polar components of surface energy, and the individual molecules were modeled using a semi-empirical molecular orbital approach.

As can be seen in Table 1, the dispersive component of each surface energy is nearly constant, and the polar component switches by the light exposure. The direction of the change is predictable from the calculation of the individual molecules dipole moment, but the magnitude is lower. The fulgimide structure does not indicate significant changes in surface properties from of exposure, whereas the spiropyran and azobenzene both exhibit a significant alteration of surface properties. These results show these groups can cause behavioral changes in systems with low polar character.

Table 1 Surface energy characterization of photo-switchable groups with molecular orbital calculations of the molecular dipole moment.

	Surface Energy	Disperse Component	Polar Component	Dipole Moment
Fulgimide Open	34.55 mN/m	25.09	9.46	6.663 D
Fulgimide Closed	32.39 mN/m	25.08	7.31	5.866 D
Spiropyran	33.55 mN/m	25.07	8.48	4.422 D
Merocyanine	36.69 mN/m	24.89	11.80	9.652 D
Azobenzene – cis	36.44 mN/m	25.20	11.24	0.841 D
Azobenzene - trans	43.58 mN/m	25.22	21.19	8.842 D

Additional Measurements using Van Oss theory were conducted to characterize the behavior of azobenzene modified films. A monosilanated and disilanated derivative was synthesized and placed on fused silica slides. The contact angle fluids were water, diiodomethane, and formamide, and their dispersive, acid and base components were taken from van Oss' text. Table 2 gives the solution to the contact angle data for the films before and after exposure to UV radiation.

Table 2 Surface energy parameters for azobenzene films using van Oss theory.

Monosilanated	σ^D	σ^+	σ^-
Unexposed	40.08	0.10	1.23
Exposed	40.44	0.07	7.89
Disilanated			
Unexposed	29.1	0.02	7.24
Exposed	29.44	0.95	7.15

The disilanated azobenzene is bound at either group of the molecule, and predictably has very little surface energy change on UV exposure. The monosilanated azobenzene has a large increase in its basic character, which is derived by the exposure of the electron orbital pairs in the trans conformation, and the increase in molecular dipole moment. With these parameters determined, the surface can be compared with liquids of known van Oss properties, and a change in wetting interaction can be predicted. Table 3 provides this modeling using fluids characterized by van Oss.

Table 3 Wetting interaction of azobenzene films from van Oss modeling.

	Pre-exposure	Post-exposure	$\Delta\gamma$
Cyclohexane	-4.69	-7.03	-2.34
Chloroform	2.72	13.51	10.78
Tetrahydrofuran	-12.29	-16.31	-4.02
Diiodomethane	-2.67	-3.83	-1.16
Water	-80.14	-49.41	30.73
Formamide	-24.77	-17.46	7.31
Glycerol	-43.54	-33.54	10.00
Ethylene Glycol	-26.37	-20.52	5.85

A transition from negative to positive interfacial energy is desired for photo-control of wetting characteristics. As the table shows, these azobenzene films can undergo significant shifts in their interfacial energy, but the sign of the calculation for any liquid does not change from positive to negative. This response is required for fluid flow in microchannels for example, and in colloidal aggregation through wetting attraction.

Conclusions

In study of these molecular groups, it was found that the dipole moment of the investigated photo-isomers can create significant changes in polarity, which have the potential to influence the properties of surfaces and colloids. Furyl fulgide was found to have very little change in dipole moment, and was terminated as a research subject. Azobenzene and spiropyran moieties were significant in property changes and have a literature background for influencing the phase behavior of polymers, and they were chosen for additional work and evaluation after being appended on colloidal particles. The contact angle data was modeled using Fowkes and van Oss theory, and showed the potential to characterize the changes in polarity of the prepared films. Comparison of the azobenzene data with surface tension properties of test liquids showed that surface energy changes can be significant, but a transition from wetting to non-wetting was not determined. It is likely that a pure wetting interaction leading to control of colloidal deposition will not be achieved. The route chosen to continue the research is to utilize the influence of photochromic molecules to influence the phase behavior of grafted polymers.

Section 2

Synthesis of Photoswitchable Organic Structures and Applicability to Photo-control of Colloidal Stability

Introduction

Self-assembly is increasingly being investigated for processes utilizing bottom-up approaches to forming novel devices. External fields can be used to align colloidal units to provide an anisotropic material property, or higher resolution than can be achieved using photolithography. Such a system can also be used to build nanostructured materials sequentially and with defined features to provide desired property responses. These approaches employ molecular surface groups which can be switched on or off based on external stimuli. Hydrogen bonding can be overcome through the input of heat both between molecules[59] and in colloids with surface bonded molecular groups[60]. Uniform coverage of colloids with surfactants of this type leads to random agglomeration between groups. Self-assembly can produce intricate structure when the attractive interactions are directional, but to date this has not been achieved at the colloidal scale[61]. There are examples of ordered structures being produced by cycling between swelled and unswelled states for hydrogel materials under the proper solids content conditions[62]. It remains to be seen if this can be achieved with solid colloidal particles.

There are examples in the literature of colloidal materials derivatized with photo-sensitive surface groups such as spirobenzopyran[63,64,65,66,67] and azobenzene[68,69,70]. In non-polar solvents, these colloidal systems exhibit reversible agglomeration/re-dispersion behavior under alternating UV/Vis irradiation. However, while the aggregation occurs spontaneously post UV irradiation, the re-dispersion following visible light or thermal treatment requires an input of ultrasonic energy to disperse formed aggregates. The underlying mechanism behind flocculation appears to be a wetting phenomenon with the particle surfaces becoming more polar post-UV irradiation and displaying preferential attraction towards each other. Since particles are uniformly coated with a photo-active surfactant or a monolayer, the aggregates exhibit random structures. To date, however, it has not been determined whether the aggregation is diffusion or surface reaction controlled. Despite the lack of precise control in formation of aggregate structures, these photo-sensitive colloidal materials have several potential applications. They may allow for the directed deposition of colloidal units in the growth of nanostructures and formation of metastable or unstable crystalline colloidal assemblies. There are also examples of functional colloids being used as valve and pump components for microfluidic networks[71]. Furthermore, it would be interesting to determine if the repeated aggregation and re-dispersion of photo-sensitive particles can be used to improve ordering within colloidal crystal assemblies. In order to carry out crystallization of colloidal particles in concentrated state, however, a better understanding and control over the aggregation mechanism, volume expansion between the photo-switched states and particle diffusion are required. While photo-active monolayer surfactants used previously ([65,66,67]) exhibit a strong surface wettability change, they do not display an ability to undergo volume changes. Therefore, once aggregated, colloids bearing these monolayers require the input of ultrasonic energy in addition to the visible irradiation (or heat treatment) for re-dispersion. Using surface appended polymer networks should overcome this limitation as a reversible swelling behavior between switched states would aid the re-dispersion process. In fact, a common thermo-sensitive polymer (poly N-isopropyl acrylamide) has demonstrated such a force profile response[72]. In its swollen state the polymer layer induced repulsive interactions between colloidal surfaces, while in the collapsed state attraction was found. This proves that polymer layers can be used to impart reversible and fully repulsive interactions between colloidal particles. The ability to fabricate such a reversible system responsive to the light stimuli and characterized by a high fatigue resistance has not yet been realized.

The addition of photochromic molecules to polymeric systems often resulted in alteration of the material properties including viscosity changes, phase transformations, and optical characteristics. While most of the studies involved fabrication of thin photo-sensitive films for optical data storage applications,[,,,23] photo-responsive polymer solutions were also developed. For example, azobenzene derivatization of polyamides led to the control of polymer conformational changes through photochemistry[73]. Irie and coworkers studied extensively the solution phase behavior of polymers containing photochromic molecules[35,36,37,38,39,40,41]. It was found that effect of photochromic molecules is amplified near a phase transition. While these investigations were focused on determining polymer solution properties, there have been only a limited number of publications dealing with photo-sensitive polymer brushes chemically attached (*i.e.*, grafted) onto flat surfaces[74,75,76,77,78] and even less literature dealing with such modification of colloidal particles[79]. It is important to have the photo-sensitive polymer molecules permanently attached to the surface through covalent bonds as abrasive processing of colloidal particles is often employed in various applications and during material purification (*e.g.*, prolonged ultrasound treatment, solvent changes from polar to non-polar medium and vice versa, temperature cycling and abrupt pH changes). It should be mentioned here that although photochromic behavior of polymer brushes has not been extensively researched in the past, there have been some studies dealing with functional polymer shell-solid core colloids influenced though temperature, pH or salt concentration changes[80,81,82,83,84,85,86,87,88]. Moreover, numerous studies have focused on covalent attachment and growth of polymer layers from solid surfaces and colloidal particles.

The sections below describe the synthesis of surface-modified photo-sensitive colloidal particles and their characterization. Planar surfaces were studied to examine contact angle response, cycling phenomena, and optical properties. Derivatives of each photochromic moiety were syntheisized and are described for their wetting behavior in sequence. Initial colloidal efforts were directed at monolayer formation based on the results reported for flat surfaces. Later work concentrated on polymeric shell-silica core architectures incorporating photo-sensitive molecules.

Photoswitchable coatings containing in-chain azobenzene

Monolayer coatings

An attempt has been made to attach organic molecules containing photoactive azobenzene groups onto oxidized silicone surfaces. The goal sought after is the ability to predictably and reproducibly graft these molecules to colloidal silica particles. It is not merely enough, however, to have these photoactive compounds attached firmly to the surface. The main requirement for these molecular monolayers is to alter wettability behavior of the underlying substrate upon exposure to UV or visible light. This in turn, is not a trivial task, as the molecules need to be well ordered in the monolayer and yet possess enough freedom to undergo the light induced trans-cis isomerization.

Scheme 7

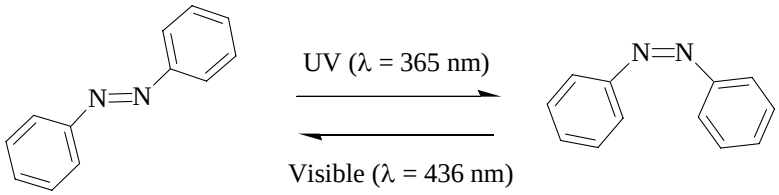

Several recent studies demonstrate the feasibility of this approach applied to flat silica surfaces (,[89],[90],[91],[92],[93]). The light induced wettability changes quantified by the water contact angle measurements in the range from 2º to 9º were reported in these investigations. Here, an attempt is made to modify some of the published protocols in order to allow coating of dispersed colloidal particles with the photoactive azobenzene derivatives using a relatively simple procedure. Current efforts also concentrate on

increasing the wettability changes upon UV or visible irradiation beyond the maximum 9º contact angle change (unless otherwise noted the phase 'contact angle' refers to the measured water contract angle) reported in the literature.

Two approaches for fixing azobenzene containing compounds onto the silica surfaces were investigated: 1) direct reaction of tri-ethoxysilane modified azobenzene molecules with the surface, and 2) attachment of azobenzene molecules to an amine terminated self-assembled monolayer (SAM). These two routes are illustrated below:

Scheme 8

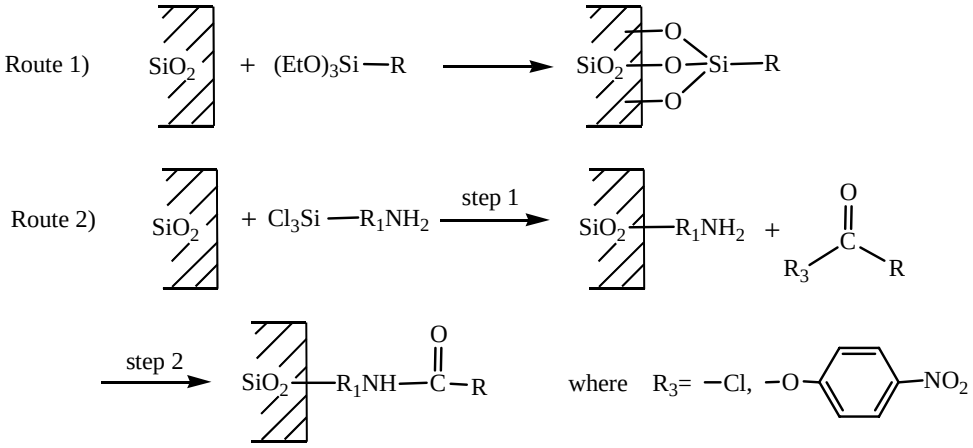

Here, -R denotes azobenzene functionality, while $-R_1$ represents an alkyl group. In particular, the following reaction was carried out according to route 1:

Scheme 9

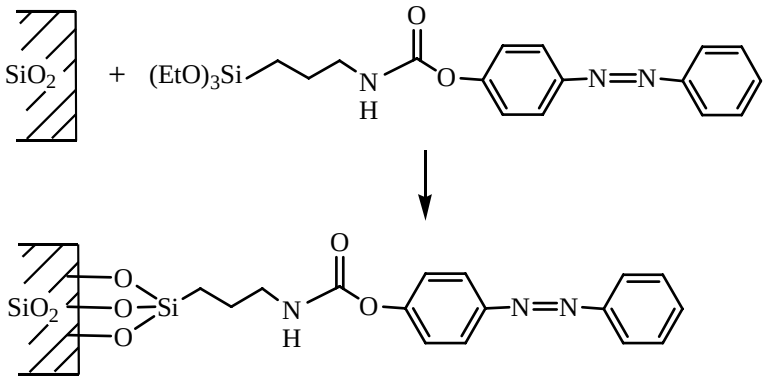

When the tri-ethoxysilane azobenzene molecules were spin coated onto the surface from THF solution containing HCl catalyst and the sample was cured in the oven at 130ºC for 1.5 hours afterward, the formed coating demonstrated photoswitchability. Specifically, water advancing contact angle decreased from 94.5±2.9º to 79.4±1.4º (15.1º change) upon UV irradiation. However, the procedure was not reproducible as second and third samples gave a change of only 4º and 6º, respectively. Moreover, the curing step requires the silica surface to be dried, which would be difficult to carry out with silica colloids. In order to circumvent the curing step, this reaction was carried out in anhydrous toluene heated to 70-80ºC for 24 hours with the tri-ethoxysilane azobenzene molecules at concentration of 50 mM. While the compound appeared to graft to the surface as evidenced by the contact angle change before and

after the reaction (*i.e.*, the advancing contact angle increased from 47.9±1.6º to 69.5±1.3), no photoactivity was detected.

Due to difficulty in reliably controlling the deposition of tri-ethoxy silane compounds, several reactions were carried out according to route 2 illustrated in Scheme 8 above. The first step in this approach is to form an amine-terminated monolayer on the silica surface. While few different methods were tried to this end ([94],[95],[96]), the procedure described by Vogler *et al.* ([97],[98]), later by Heise *et al.* ([99],[100]) and others ([101]) gave the most reliable results. It involves formation of bromine terminated SAM using tri-chlorosilane compounds, followed by conversion of the Br head group to azide. Finally, the N_3 group is reduced to an amine with lithium aluminum hydride (LAH) according to the procedure shown below:

Scheme 10

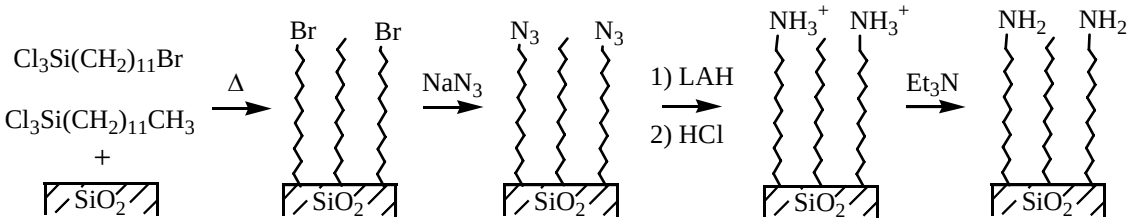

By modifying the relative concentrations of methyl and bromo terminated tri-chlorosilanes in the initial reaction mixture it is possible to control the density of amine groups on the surface. This in turn, changes the surface wettability as illustrated in Table 4 below.

Table 4 Effect of initial reaction mixture composition on the surface wettability of -NH_2 terminated SAM.

sample	*initial mixture composition*	*advancing contact angle*[*]	*receding contact angle*[*]
a	$Cl_3Si(CH_2)_{11}Br$ 100%	80.5 ± 0.9º	41.2 ± 1.9º
b	$Cl_3Si(CH_2)_{11}Br$ 25% $Cl_3Si(CH_2)_{11}CH_3$ 75%	96.2 ± 0.9º	71.5 ± 2.5º
c	$Cl_3Si(CH_2)_{11}Br$ 25% $Cl_3Si(CH_2)_7CH_3$ 75%	80.6 ± 1.6º	46.2 ± 3.3º
d	$Cl_3Si(CH_2)_{11}Br$ 75% $Cl_3Si(CH_2)_7CH_3$ 25%	80.6 ± 1.1º	47.3 ± 4.3º

[*] The contact angle measurements were performed on freshly formed SAMs. When the samples were left to stand in air, the measured contact angles decreased due to hydration of amine headgroups by ambient moisture. In the extreme case of storing the amine SAMs under water for 7 days the advancing contact angles fell to 69.1 ± 3.2º and 83.9 ± 2.3º for samples #1 and #2, respectively.

It is important to notice that when $Cl_3Si(CH_2)_{11}CH_3$ was used to lower the density of amine groups on the surface, the contact angle changed significantly with reaction mixture composition. The effect was negligible, however, when a shorter alkyl chain, $Cl_3Si(CH_2)_7CH_3$, was employed for the same purpose. Not surprisingly, the groups at the outermost boundary of the SAM control its surface properties.

Wettability changes quantified by the contact angle measurements also offer an easy way of monitoring reaction progress. Table 5 below exemplifies this concept applied to the formation of $–NH_2$ terminated SAM from the initial reaction mixture comprised of 25% $Cl_3Si(CH_2)_{11}Br$ and 75% $Cl_3Si(CH_2)_{11}CH_3$. In this particular case, the X-ray photoelectron spectroscopy (XPS) confirmed the presence of nitrogen on the surface with C/N ratio of 43. Thus, approximately 27% of molecules comprising the SAM bear $–NH_2$ terminal groups.

Table 5 Wettability changes associated with various reaction steps leading to the formation of $-NH_2$ terminated SAM from the initial reaction mixture comprised of 25% $Cl_3Si(CH_2)_{11}Br$ and 75% $Cl_3Si(CH_2)_{11}CH_3$.

step #	*SAM headgroup*	*advancing contact angle*[*]	*receding contact angle*[*]
1	-Br	102.2 ± 1.7º	71.8 ± 4.8º
2	$-N_3$	101.2 ± 1.4º	83.5 ± 3.3º
3	$-NH_3^+Cl^-$	90.3 ± 2.1º	63.7 ± 1.5º
4	$-NH_2$	96.2 ± 0.9º	71.5 ± 2.5º

[*] The contact angle measurements were performed on freshly formed SAMs.

While very good results were obtained using flat surfaces, attempts to coat silica particles with $-NH_2$ terminated SAM according to Scheme 10 were unsuccessful. Specifically, the LAH reduction of $-N_3$ groups generated large quantities of aluminum salts resulting in aggregation of the colloidal suspension. Furthermore, it proved very difficult to separate the silica particles from these weakly dissociating aluminum compounds. In the end, an alternative route to the formation of $-NH_2$ terminated SAM was designed. It is shown in the Scheme 11.

Scheme 11

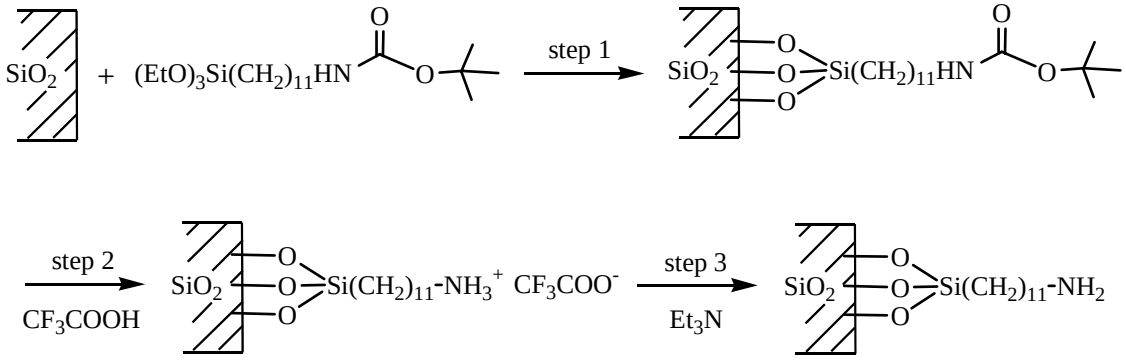

The reaction progress quantified by contact angle measurements is reported Table 6 for an oxidized silicone wafer. As can be seen, the final contact angle is the same as for 100% NH_2 SAM generated using Scheme 10 (compare sample 1 in Table 4 with step 3 in Table 6). Moreover, exposure to water decreased the advancing contact angle by approximately the same amount for both samples (*i.e.*, the advancing contact angle on hydrated surfaces was 69.1 ± 3.2º and 73.5 ± 2.0º for the two samples, which is significantly lower than the 80.5 ± 1.0º measured on dehydrated SAMs). Finally, the reactivity of NH_2 SAMs formed according to either Scheme 10 or Scheme 11 towards acid chloride functionalized azobenzene compounds was essentially identical as will be shown later. Therefore, because Scheme 11 can be applied to the processing of colloidal particles and due to much shorter preparation time, it is the preferred method of NH_2 SAM formation.

In the case of Scheme 11 reactions, it was also found that a different pretreatment of the substrates did not have a bearing on the final wettability behavior of the formed amine coating. In particular, the same contact angles were obtained for the SAMs deposited on an oxidized silicone wafer: 1) treated with 'pirana'[*] solution, 2) treated with 'pirana' solution followed by 2 minute soak in 1.0 M NaOH, 3) treated with 'pirana' solution followed by 1.0 M NaOH and 1.0 M HCl soak for 2 minutes each, and 4) dried under vacuum at 180ºC for 3h, followed by 2 minute sonication in dry toluene.

[*] H_2SO_4: H_2O_2 solution mixed in the ratio 4:1 by volume.

Table 6 Wettability changes associated with various reaction steps leading to the formation of 100% –NH_2 terminated SAM according to Scheme 11.

step #	*SAM head group*	*advancing contact angle*[*]	*receding contact angle*[*]
1	-t-butyl	84.6 ± 0.9º	64.6 ± 1.7º
2	$-NH_3^+CF_3COO^-$	63.2 ± 1.4º	29.5 ± 4.1º
3	$-NH_2$	80.6 ± 1.0º	42.2 ± 2.8º

[*] The contact angle measurements were performed on freshly formed SAMs. When $-NH_2$ SAM was exposed to water for 1 hour, the advancing contact angle decreased to 73.5 ± 2.0º.

Successful attachment of an azobenzene containing compound to NH_2 derivatized silica surface was achieved following a modified protocol of Siewierski *et al.*() depicted in Scheme 12. Instead of carrying out the reaction in benzene and utilizing dry pyridine as a proton scavenger (the original procedure), the coupling was performed in dry toluene containing DMAP (4-dimethyl aminopyridine). This latter procedure not only avoided highly air-sensitive pyridine, but yielded more reproducible results.

Scheme 12

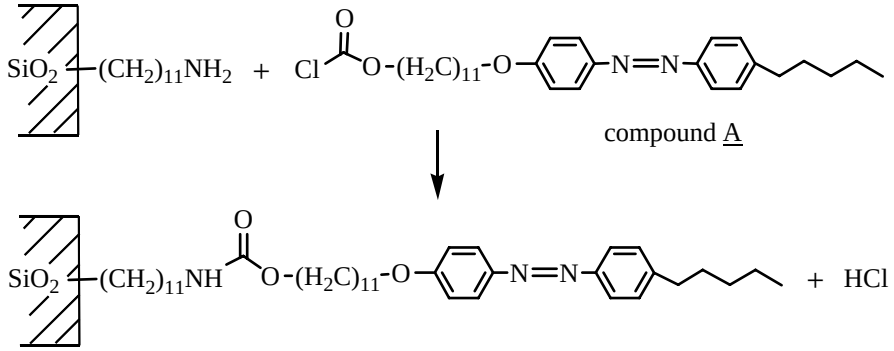

The contact angle measurements before and after coupling compound A to various NH_2 containing SAMs according to Scheme 12 are presented in Table 7. Clearly, there is a significant increase in the advancing contact angle upon attachment of the azobenzene molecules. Moreover, the formed monolayers exhibit wettability changes upon exposure to the alternating UV and visible irradiation as demonstrated by the advancing contact angle measurements. (It was found that receding contact angle changes upon UV irradiation were erratic and typically within the measurement error.)

The largest decrease in measured contact angle upon UV irradiation occurred with azobenzene molecules grafted onto 100% NH_2 SAMs (*i.e.*, average of 8.4º based on 6 different samples with the measurement carried out on 10 different spots per sample). This change corresponds very well with $\Delta\theta_{UV} = 9^\circ$ reported by Siewierski *et al.* () for the same system. It should be noted here that almost identical $\Delta\theta_{UV}$ switches were recorded for azobenzene molecules coupled to 100% NH_2 SAMs prepared by either Scheme 10 or 11 (*i.e.*, $\Delta\theta_{UV} = 8.7^\circ$ for SAM prepared by Scheme 10 and $\Delta\theta_{UV} = 8.0^\circ$ for SAM prepared by Scheme 11). This further justifies the use of Scheme 11 in preparing high quality amine monolayers on silica surfaces.

As can be seen from the data presented in Table 7, much better results with respect to the UV light induced wettability changes were obtained when C_{12} alkane chains were used instead of C_8 hydrocarbons in the mixed NH_2/ CH_3 SAM formulations. This is most likely due to the lower degree of order and more flexibility enjoyed by molecules in the SAM formed from $Cl_3Si(CH_2)_8CH_3$. Furthermore, the fact that $\Delta\theta_{UV}$ values are lower for azobenzene molecules grafted onto the mixed NH_2/CH_3 SAMs compared with the 100% $-NH_2$ terminated surfaces stresses the requirement for tightly

packed and well-ordered azobenzene monolayers, if good photo-activated wettability changes are to be expected.

Table 7 Contact angle measurements on various –NH_2 SAMs reacted with azobenzene compound A according to Scheme 12. Changes in the contact angle upon UV and visible light exposure following the coupling are also reported.

smpl.	*initial SAM*	θ_{SAM} [A]	$\theta_{rnx.}$ [B]	θ_{UV} [C]	θ_{VIS} [D]	$\Delta\theta_{UV}$ [E]
a	100% -NH_2 (via Scheme 4) [F]	77.4 ± 0.9º	90.4 ± 0.9º	81.0 ± 0.7º	89.7 ± 1.0º	8.7º
b	100% -NH_2 (via Scheme 5) [G]	79.5 ± 1.9º	91.0 ± 1.3º	82.1 ± 0.9º	90.1 ± 1.6º	8.0º
c	25%/75% -NH_2/ -C_{12} [H]	85.9 ± 0.9º	92.7 ± 1.2º	85.5 ± 0.9º	91.8 ± 0.9º	6.3º
d	25%/75% -NH_2/ -C_8 [I]	80.6 ± 1.6º	84.4 ± 0.5º	81.9 ± 0.5º	[J]	2.5º
e	75%/25% -NH_2/ -C_8 [K]	81.9 ± 1.4º	86.4 ± 1.0º	82.2 ± 1.2º	86.1 ± 1.2º	3.9º

[A] Advancing contact angle on the initial –NH_2 SAM before reaction. Because samples were stored in air for up 2 days prior to the measurement, contact angles may be lower than values reported in Table 1 due to the hydration of surface amino groups.

[B] Advancing contact angle on the surface after the reaction with the azobenzene compound.

[C] Advancing contact angle on the surface after the reaction and exposure to UV light (20 minute irradiation with 200W Hg lamp equipped with 300-400 nm band pass filter).

[D] Advancing contact angle on the surface after the reaction, exposure to UV light and 24 hours under ambient laboratory conditions (samples exposed to laboratory light). It was found that receding contact angle changes upon UV irradiation were erratic and typically within measurement error (*i.e.*, within 2-3º).

[E] Advancing contact angle change upon UV light exposure.

[F] SAM formed from $Cl_3Si(CH_2)_{11}Br$ according to Scheme 10.

[G] SAM formed from $(EtO)_3Si(CH_2)_{11}NHCOOt$-But according to Scheme 11.

[H] SAM formed using 25% $Cl_3Si(CH_2)_{11}Br$ and 75% $Cl_3Si(CH_2)_{11}CH_3$ according to Scheme 10.

[I] SAM formed using 25% $Cl_3Si(CH_2)_{11}Br$ and 75% $Cl_3Si(CH_2)_8CH_3$ according to Scheme 10.

[J] Sample was damaged prior to the measurement.

[K] SAM formed using 75% $Cl_3Si(CH_2)_{11}Br$ and 25% $Cl_3Si(CH_2)_8CH_3$ according to Scheme 10.

Another interesting aspect of these azobenzene monolayers is the reversibility of the photo-induced 'trans-cis' isomerization (see Scheme 7), which translates into reversible wettability changes. Figure 3 below demonstrates this effect for the SAM prepared via Scheme 12 subjected to 5 cycles of alternating UV and visible irradiation. The wettability changes were followed with contact angle measurements and indicate good reproducibility.

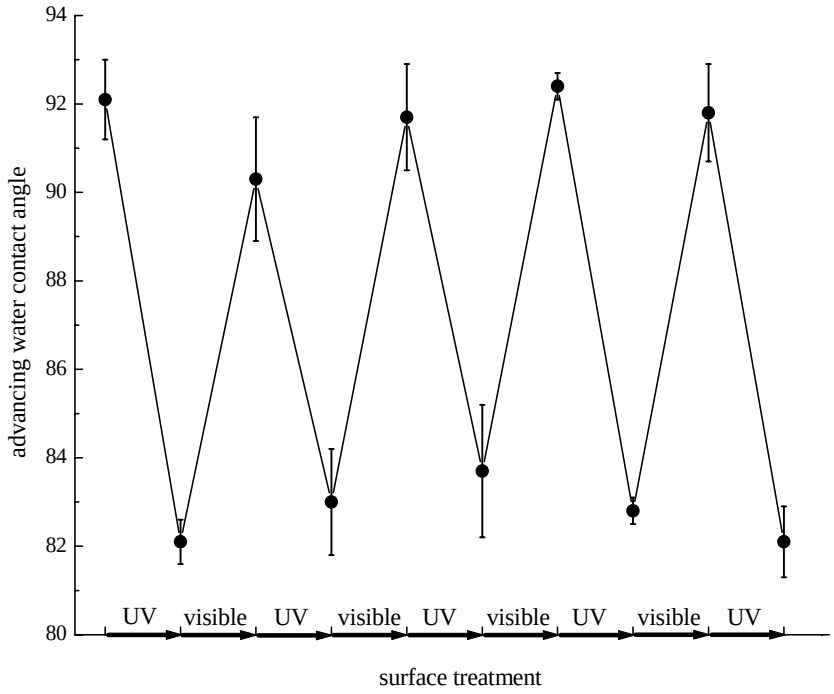

Figure 3 Light-induced advancing water contact angle change on azobenzene derivatized 100% -NH_2 SAM (the 100% -NH_2 SAM was prepared according to Scheme 11, with the azobenzene monolayer coupled via Scheme 12). The UV irradiation was accomplished using 200W Hg lamp equipped with 300-400 nm band pass filter and was carried out for 20-30 minutes. Following the UV treatment, the surface (stored in N_2) was allowed to equilibrate under N_2 atmosphere exposed to ambient light for 24 hours.

It was a goal of subsequent experiments to increase $\Delta\theta_{UV}$ for photo-active monolayers beyond the 8.4º already attained. To this end, a fluorinated derivative of compound A has been synthesized and coupled to the silica surface. The specific reaction between this new fluorinated azo-benzene derivative (compound B) and NH_2 terminated silica surface is depicted in Scheme 13 below, while Table 8 summarized the obtained results.

Scheme 13

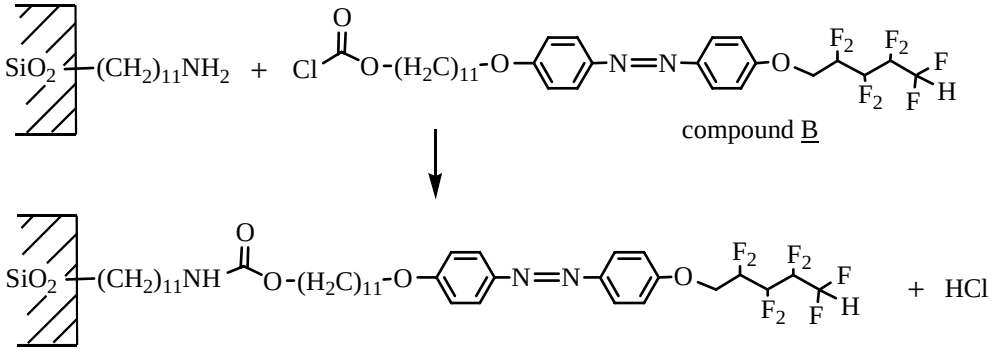

Table 8 Contact angle measurements on 100% –NH_2 SAMs (formed via Scheme 11) reacted with azobenzene compounds A and B according to Schemes 12 and 13, respectively. Also reported in the table is a result for a mixed monolayer formed from a 1:1 mixture of compounds A and B.

smpl.	*reaction mixture composition*	θ_{UV} [A]	θ_{VIS} [B]	$\Delta\theta_{UV}$ [C]
a	100% compound A	82.1 ± 0.9º	90.1 ± 1.6º	8.9º
b	100% compound B	83.0 ± 0.6º	88.1 ± 1.2º	5.1º
c	1:1 compound A:B	80.6 ± 1.2º	86.2 ± 0.8º	5.6º

[A] Advancing contact angle on the surface after the reaction and exposure to UV light (20 minute irradiation with 200W Hg lamp equipped with 300-400 nm band pass filter).

[B] Advancing contact angle on the surface after the reaction, exposure to UV light and 24 hours under ambient laboratory conditions (samples exposed to laboratory light). It was found that receding contact angle changes upon UV irradiation were erratic and typically within measurement error (*i.e.*, within 2-3º).

[C] Advancing contact angle change upon UV light exposure.

As can be seen from Table 8, incorporating fluorinated terminal groups into the azobenzene monolayer actually decreased the contact angle change upon UV irradiation. This could be caused by a worse packing of bulkier molecules and a less ordered SAM.

In a slightly different set of experiments a di-azo dye (compound C in Scheme 14) has been employed. With two azobenzene groups per molecule, the UV induced conformational change in a monolayer should cause greater disordering leading to a greater $\Delta\theta_{UV}$ values. Unfortunately, coupling reactions using activated ester, acid, and acid chloride derivatives of compound C under various reaction conditions did not provide any evidence of attachment to the aminated silica surfaces. The contact angle of 100% NH_2 SAM was essentially the same before and after the reaction and the allegedly formed azobenzene monolayers did not exhibit wettability changes upon exposure to alternating UV and visible light.

Scheme 14

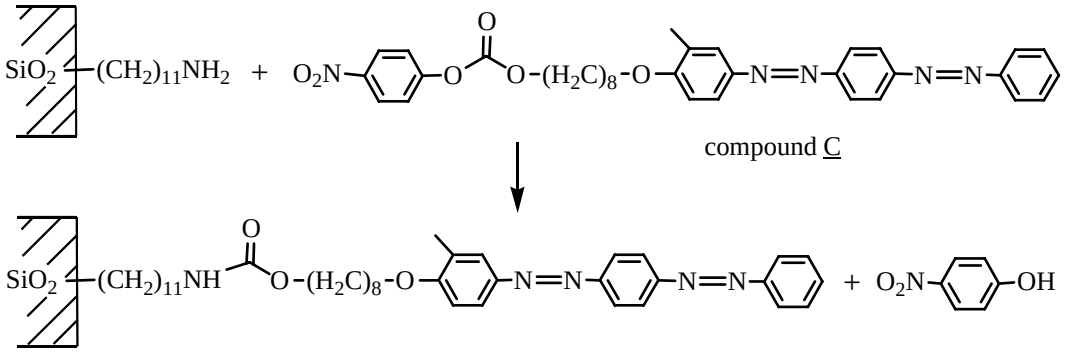

Next, an attempt to synthesize a monolayer comprised of cyclic azobenzene molecules on NH_2 SAMs has been made (see Scheme 15). When in the 'trans' conformation, the azobenzene group should lie down flat resulting in highly hydrophobic surface. After UV irradiation with the azobenzene group in 'cis' conformation the molecule would 'stand up' exposing more polar nitrogen atoms to yield a more hydrophobic surface and possibly $\Delta\theta_{UV} > 9º$.

Scheme 15

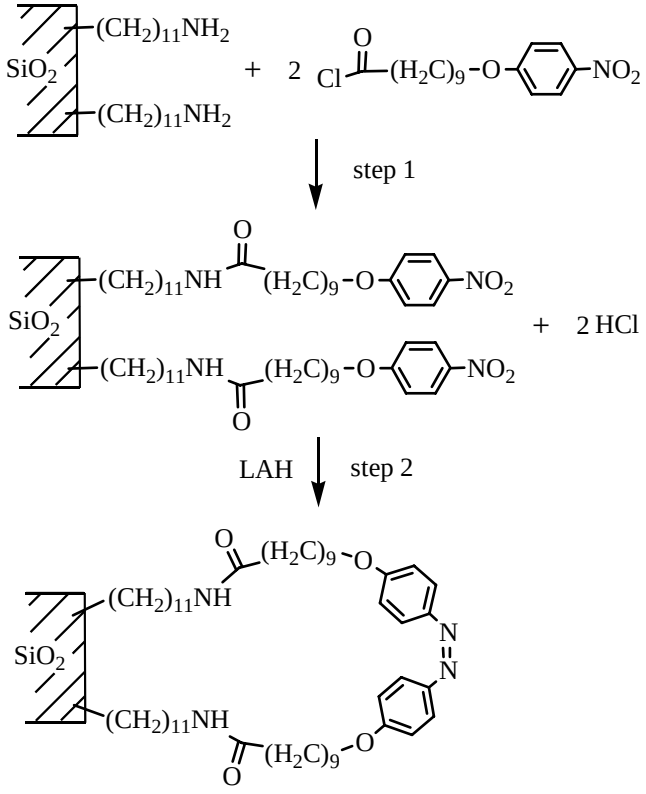

While contact angle changes indicated successful step 1 (*i.e.*, attachment of nitrobenzene precursors to the surface amino groups), the LAH reduction in step 2 did not yield anticipated result (*i.e.*, there was no contact angle change after the reaction and surface did not alter its wettability upon UV/Vis light irradiation).

It should be commented here that while azobenzene monolayers are fairly stable, they may slowly undergo oxidation reactions in air and storage in dry N_2 is recommended. Caution should also be exercised when cleaning these delicate coatings. Soaking in triethylamine (Et_3N) for any period of time lowered the measured contact angles irreversibly (typically by ≈ 4º-6º) and diminished $\Delta\theta_{UV}$. Sonicating the azobenzene SAMs in various solvents (*e.g.*, toluene, methanol, ethanol) also irreversibly lowered the contact angle, although to a smaller degree than Et_3N treatment (typically by ≈ 2º-5º). Similarly, using a Q-tip soaked with CH_2Cl_2 to clean off dust or other particulate from the azobenzene film surface was found to occasionally lower the contact angle (typically by ≈ 2º). Therefore, the recommended cleaning method is to rinse the sample with solvent (*e.g.*, toluene, CH_2Cl_2) followed by drying in a stream of dry and filtered N_2. Note that due to abovementioned concerns (especially the fact that sonication lowers $\Delta\theta_{UV}$) it may prove difficult to apply these azobenzene coatings to colloidal particles.

Azobenzene Polymeric coatings

Finally, attempts have been made to graft polymer chains containing in-chain azobenzene groups onto NH_2 derivatized silica surfaces according to Scheme 16. The idea was to reversibly alternate the thickness of these polymer films using UV and visible light. While NMR data indicated polymer formation in the bulk, attachment of these polymer molecules onto silica substrates proved to be unsuccessful. Similarly, polymerizations with a more reactive di-acid chloride linker (Scheme 17) did not produce grafted polymers. A possible reason for failed attachment of the azobenzene polymer to the

surface-bound NH_2 monolayers could be the very poor polymer solubility (*i.e.*, solubility in THF, DMF, toluene, and CH_2Cl_2 was marginal). Due to the π-stacking of adjacent azobenzene groups, the formed polymer may exhibit liquid-crystalline properties and its poor solubility even in typically good polymer solvents could be expected. To overcome this problem, a synthesis of a less symmetric and more sterically hindered azobenzene monomer was attempted (monomers 1 & 2 in Scheme 18). However, after initial trials synthesized these monomers in yields lower than 10%, the route was abandoned.

Scheme 16

1) Monomer preparation

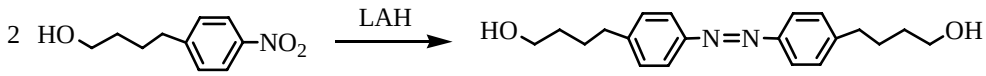

2) Polymerization

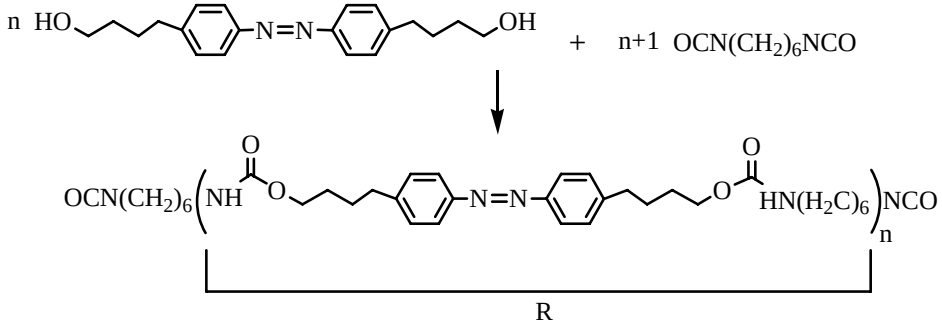

3) Attachement to $-NH_2$ SAM

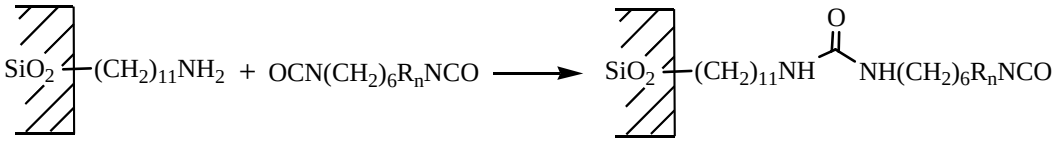

4) Quenching

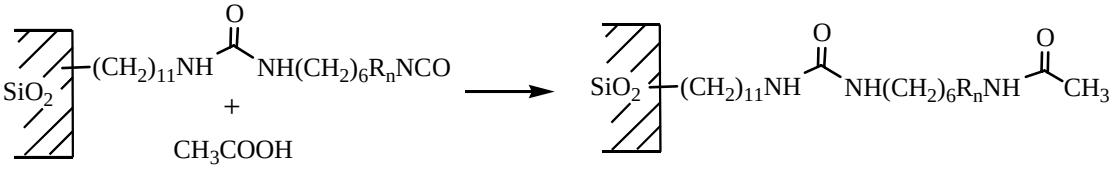

Scheme 17

2b) Polymerization

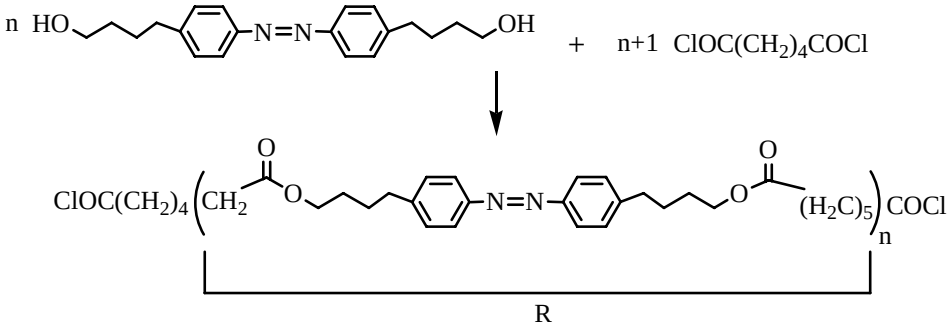

3b) Attachement to $-NH_2$ SAM

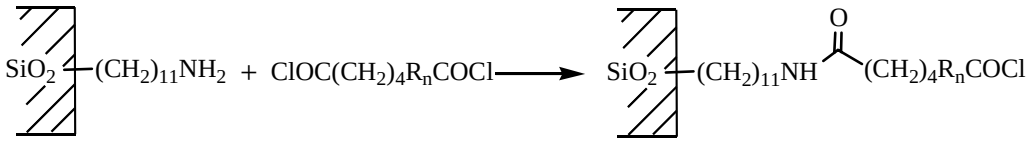

4b) Quenching

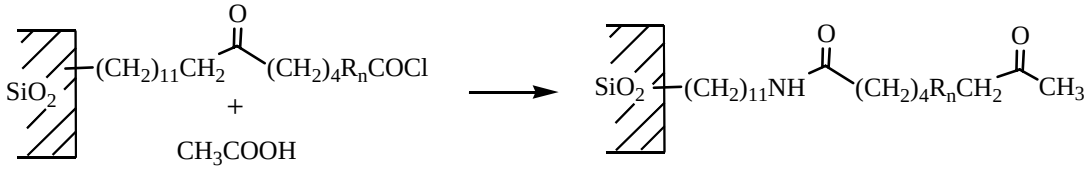

Scheme 18

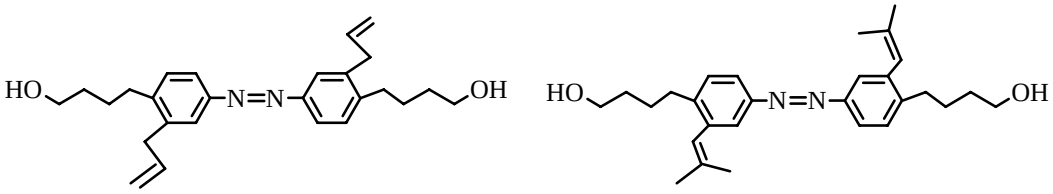

monomer 1 monomer 2

Synthesis and Response of Reversible Photo-dispersable Colloidal Particles based on the Azobenzene system

Monolayer coatings

Following a successful azobenzene monolayer deposition on flat silica substrates, colloidal silica particles (Fuso Chemical's SP03B type silica characterized by 284 nm diameter monodisperse spherical particles) were functionalized with 100% NH_2 SAM according to Scheme 11 and afterwards reacted with azobenzene compound A (Scheme 12). After the reaction and extensive washing with CH_2Cl_2 via centerfugation/decantation (7 cycles) the particles appeared yellow and well dispersed. The UV-Vis absorbance spectra of these azobenzene modified silica particles confirmed successful attachment of compound A as shown in Figure 4.

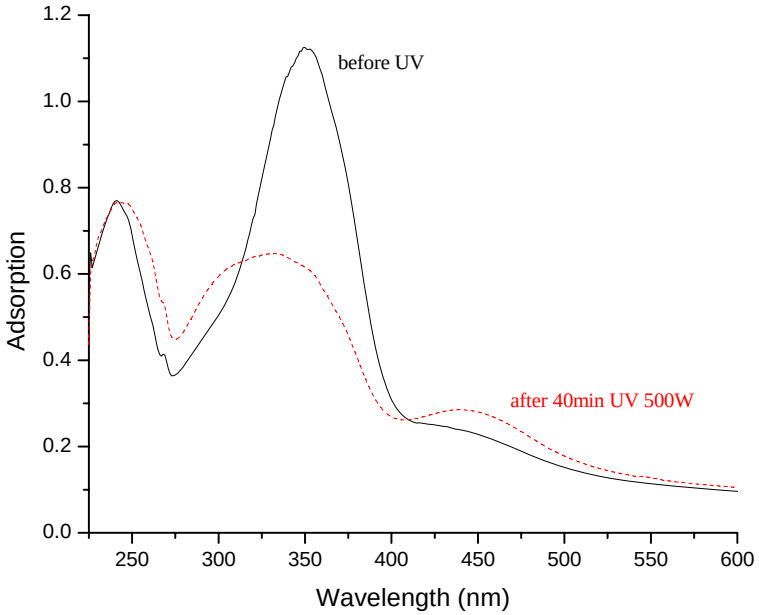

Figure 4 UV-Vis absorbance spectra of amine functionalized 284 nm silica particles with azobenzene monolayer before and after UV irradiation in CH_2Cl_2 (The UV irradiation was accomplished using 500W Xe/Hg lamp equipped with 300-400 nm band pass filter and was carried out for 40 minutes.)

Just as in the case of azobenzene films spin coated onto the silica surface (compare Figure 2), the adsorption maximum at $\lambda \approx 350$ nm decreased markedly, while simultaneously the maximum at $\lambda \approx 440$ nm increased upon UV irradiation as a result of the 'trans' to 'cis' isomerization.

When these azobenzene modified particles were dispersed in non-polar solvents such as cyclohexane or toluene, aggregation and sedimentation ensued. However, subsequent UV irradiation aimed at increasing the surface polarity by 'trans' to 'cis' isomerization accelerated this process (Figure 5). The UV enhanced aggregation was reversible after visible light irradiation and subsequent sonication to disperse the flocculated dispersion. Following this procedure the particles aggregated with the rate similar to that before UV treatment. Similar results have been reported by Ueda *et. al.* (68) in the case of silica particles bearing adsorbed calix[4] resorcinarene molecules with azobenzene groups. They suggested that the UV enhanced aggregation was caused by attractive interparticle forces due to less favorable interaction between particle surfaces and the non-polar solvent molecules.

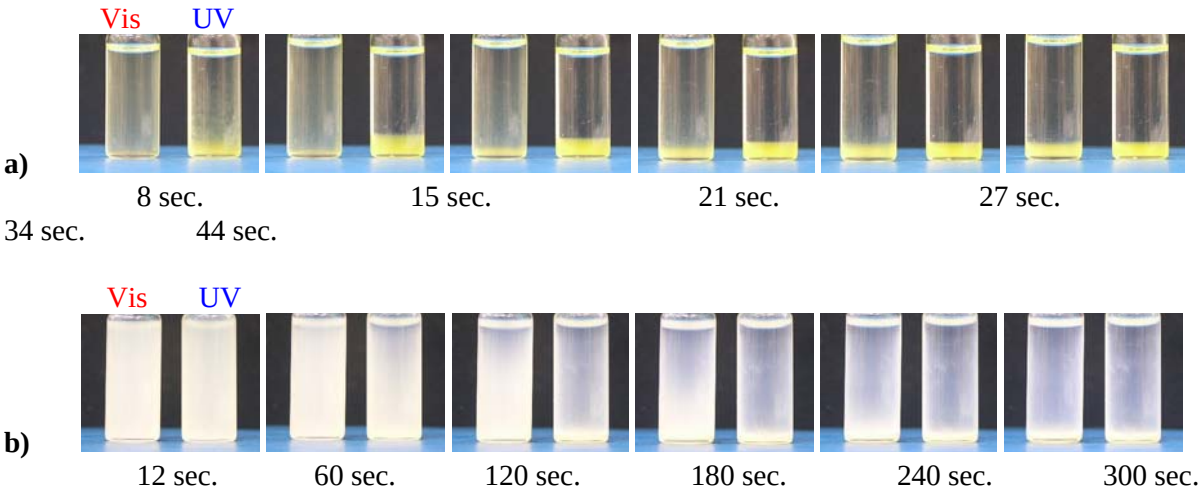

Figure 5 Aggregation/sedimentation behavior of 927 nm diameter silica particles modified with azobenzene monolayer (Compound A in Scheme 12) and dispersed in a) **cyclohaxane, or** b) **toluene. The vial on the left has been irradiated with visible light (> 450 nm) for 15 min. prior to the measurement. Similarly, the vial on the right has been treated with UV light (365 nm) for the same amount of time.**

Attempts have been made to create a border-line solvent mixture in which the particles would aggregate only upon UV irradiation. While only a few systems were investigated (*i.e.*, CCl_4/dodecane, CCl_4/cyclohexane, octane/butanol) at various solvent ratios, in all cases the particles either aggregated to some extent without UV exposure or remained dispersed regardless of UV or Vis irradiation. This result suggests that for the solvent systems investigated, the polarity change due to 'trans' to 'cis' isomerism within an azobenzene monolayer is not sufficient to cause aggregation of an otherwise stable dispersion.

2.2.2 Polymeric coatings

After unsuccessful condensation polymerization reactions aimed at growing azobenzene polymers from flat silica surfaces (section 1.6), another approach was adopted for silica colloids. In this case, acyclic diene metathesis polymerization (ADMET) was carried out using Grubbs' catalyst (Scheme 19). The NMR data indicated polymer formation in the bulk as well as on the colloids. However, there was also a significant amount of monomer physisorbed to the particle surfaces even after extensive washing with THF, $CHCl_3$, and toluene (*e.g.*, typically 4 sedimentation/decantation cycles in each solvent). Subsequent treatment with trifluoroacetic acid (TFA) and triethylamine (Et_3N) followed by 4 more $CHCl_3$ washes helped to remove the attached monomer. While the NMR spectra indicated presence of the surface-bound polymer, TEM micrographs indicated very thin (thickness, $h = 7.6 \pm 0.8$ nm), non-uniform coatings (Figure 8). Moreover, the azobenzene-polymer coated particles were highly aggregated in all solvents used for their dispersion (*i.e.*, THF, toluene, CH_2Cl_2 and $CHCl_3$) suggesting either particle-particle cross-linking or unfavorable solvent-polymer interactions.

Under ambient laboratory conditions (*i.e.*, under visible light illumination) and within non-polar solvents, the azobenzene chromophores are expected to be in their 'trans' conformation. The UV irradiation causing 'trans' to 'cis' isomerization would then increase polarity of colloidal particle surfaces causing aggregation. But because the polymeric azobenzene shell-silica core particles developed here remain aggregated in non-polar solvents, the photo-induced aggregation was not achievable in this case.

Scheme 19

1) Initiator attachement to $-NH_2$ SAM

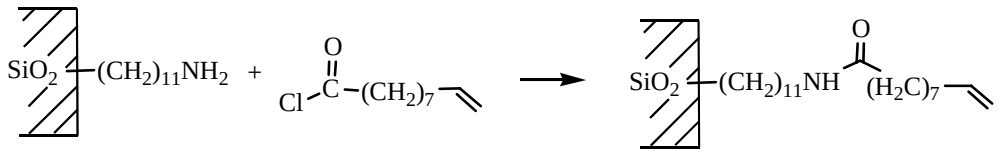

2) Monomer preparation

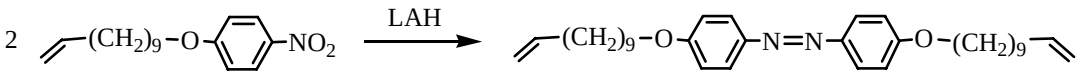

3) Surface polymerization

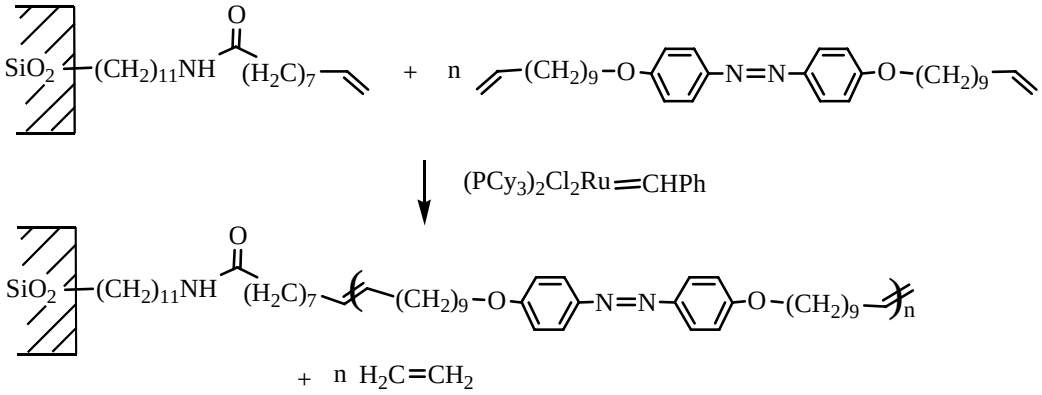

where Cy = cyclohexyl and Ph = phenyl groups

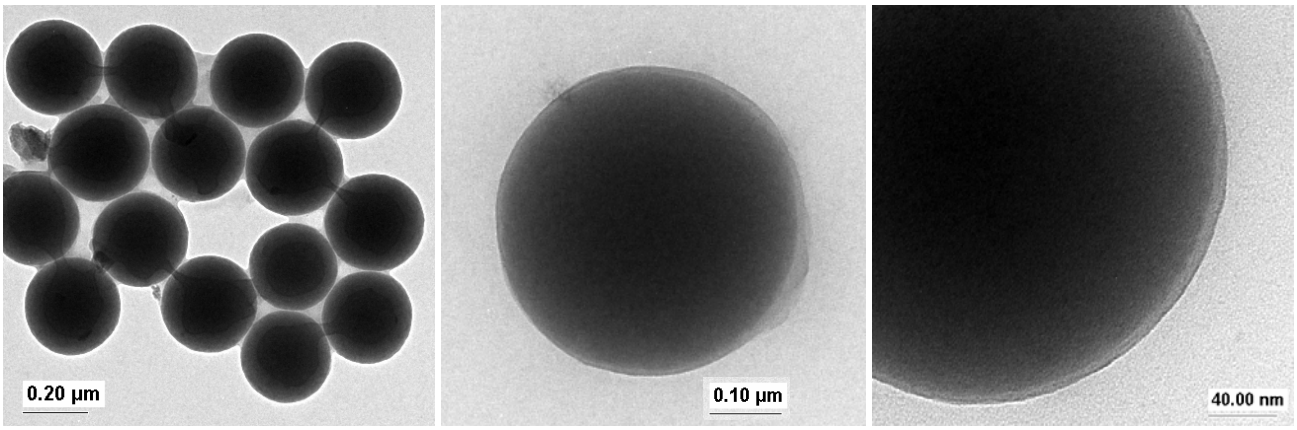

Figure 6 TEM micrographs of 284 nm silica core particles modified with azobenzene polymer shell according to Scheme 19. The polymer coating is relatively thin at 7.6±0.8 nm.

Photoswitchable surface coatings containing spirobenzopyran chromophores

Monolayer coatings

Analogous to the case of azobenzene monolayers described above, the grafting of spirobenzopyran (SP) chromophores onto the silica surfaces was also performed. Recent literature on the subject suggests that water contact angle on smooth SP-coated substrates can be reversibly modulated by as much as 11-15° by successive UV and visible light irradiation (,[102],[103]). In the case of rough, super-hydrophobic surfaces, the effect is further amplified and light-induced contact angle changes up to 23° have been observed (103). This wettability change results from SP molecule isomerization from a relatively non-polar 'closed' form to a significantly more polar, 'open', merocyanine (MC) form:

Scheme 20

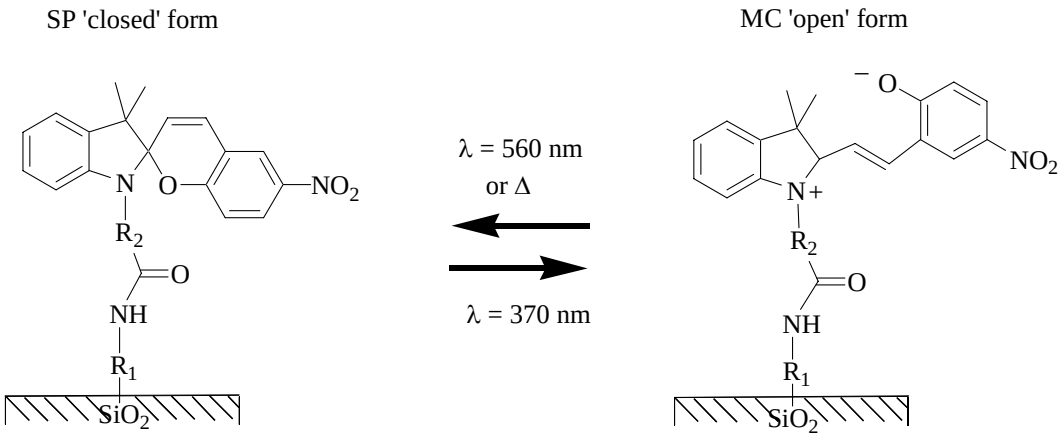

The R_1 and R_2 groups are typically alkyl chains containing 3-18 carbon atoms.

In addition to the significant wettability change, other physical properties of SP films have been reversibly modulated thorough the SP to MC isomerization. For example, Polymeropoulos and Mobius observed a 2-3 fold increase in the area per SP molecule at an air-water interface upon its conversion into MC form ([104]). Similarly, Hyashida *et al.* reported reversible thickness change for evaporated SP films comprised of model SP compounds shown in Scheme 21 below ([105],[106]).

Scheme 21

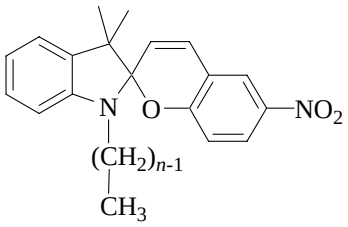

SP-*n*, *n* = 1,6,7,8,12,18

The authors observed the largest thickness change (from 2μm to 6μm upon UV irradiation) for SP-7, while no film swelling was found with SP-1, SP-12, and SP-18 compounds. This was explained as SP-7 molecule having an ideal geometry allowing a relatively unhindered SP-MC isomerization (*i.e.*, shorter alkyl spacers hinder the ring-opening reaction), while at the same time transmitting enough stress to cause

a micro-deformation. The longer alkyl spacers absorb most of the generated stress. Structure changes in Langmuir and Langmuir-Blodgett films containing spirobenzopyran molecules (,[107],[108],[109],[110],[111]) were also attributed to the SP-MC isomerization and the subsequent J-aggregate* formation ([112],[113]). In the case of SP surfactants, their surface activity and self-assembly could be controlled reversibly ([114],[115]). Finally, reversible control of electrochemical processes ([116]) and photoconduction ([117]) and electrical double layer force ([118]) were achieved in SP monolayer assemblies.

In order to graft SP molecules onto SiO_2 surface, the following coupling reaction between a spyrobenzopyran carboxylic acid derivative (SP acid) and an amine terminated alkyl SAM was carried out according to the procedure reported in ref. 44 (see Scheme 22 below).

Scheme 22

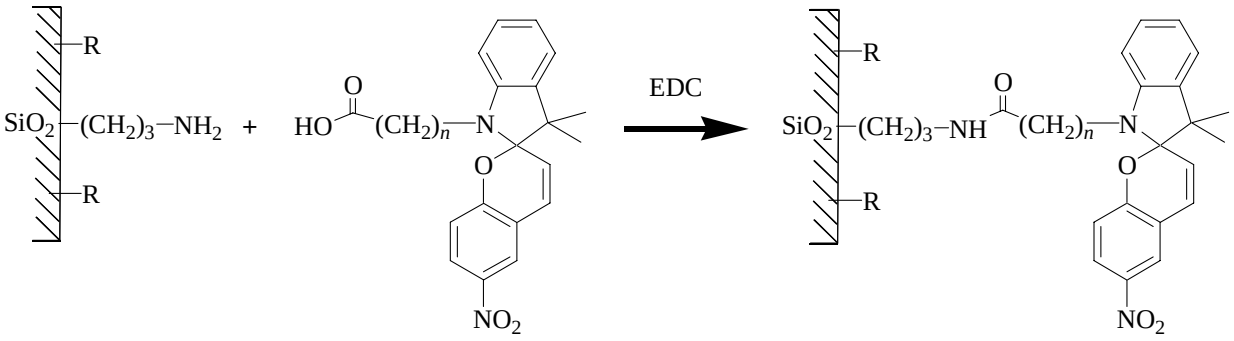

SP acid

The coupling was accomplished using 1-ethyl-3-(3-(dimethylamino)-propyl)carbodiimide (EDC) in ethanolic solution of SP acid having $n = 10$. Moreover, two types of aminated surfaces were used in the reaction: (1) substrates derivatized solely with an aminopropyltriethoxysilane (ATES), and (2) substrates treated first with a tert-butylchlorodiphenylsilane (TBDS) and then with ATES. In both cases the SP acid was grafted successfully as evidenced by a pronounced difference in the water contact angle before and after the reaction (see Table 9). However, the wettability of these SP monolayers changed only slightly upon successive UV and visible light irradiation. This is in marked contrast to the data of Rosario *et al.* () and Koide *et al.* () for analogous monolayers having the SP moiety linked to the surface by a shorter alkyl chain (*i.e.*, $n = 3$ in Scheme 22). Specifically, Rosario *et al.* report $\Delta\theta_{Adv}$ † as large as 14° for SP coatings deposited onto silica surfaces treated first with TBDS and then ATES. For surfaces derivatized using only ATES, the same authors report $\Delta\theta_{Adv} = 7°$, while reference 102 lists $\Delta\theta = 15°$. (Koide *et al.* did not specify whether this value refers to the advancing, receding or static contact angle measurement.)

It should be mentioned here that $\Delta\theta_{Adv}$ diminished after the first cycle of alternating visible/UV light irradiation (see Table 9). This was also the case with the data presented in reference 44 and suggests photo-bleaching, roughening, or another dynamic process within the monolayer.

---

* J-aggregates (Scheibe aggregates) are characterized by a very narrow red-shifted absorption band and a narrow fluorescence band with a small Stokes shift due to the formation of a delocalized excitonic state among the densely packed molecules (113). These aggregates have been reported for many merocyanine dyes and their formation is usually critically dependent on the structure and orientation of the merocyanine molecules within the layer (112).

† $\Delta\theta_{Adv}$ represents the change in an advancing water contact angle upon successive UV and visible light irradiation.

Table 9 Contact angle measurements on various –NH_2 SAMs reacted with SP acid according to Scheme 1.7-3. Changes in the contact angle upon UV and visible light exposure following the coupling are also reported.

smpl.	*monolayer* [A]	*treatment* [B]	*SP acid* [C]	θ_{Adv} [D]	θ_{Rec} [E]	$\Delta\theta_{Adv}$ [F]	$\Delta\theta_{Rec}$ [G]
1a	ATES	—	—	54.6 ± 2.4º	32.2 ± 2.1º	—	—
1b	ATES+SP	Vis	*n* = 10	86.6 ± 1.7º	45.6 ± 3.6º	0.7	3.6
1c	ATES+SP	UV	*n* = 10	85.9 ± 1.5º	42.0 ± 2.8º		
2a	TBDS	—	—	93.5 ± 1.3º	36.1 ± 1.2º	—	—
2b	TBDS+ATES	—	—	54.9 ± 2.3º	31.1 ± 1.5º	—	—
2c	TBDS+ATES+SP	Vis	*n* = 10	88.0 ± 1.7º	49.3 ± 2.4º	3.7	8.3
2d	TBDS+ATES+SP	UV	*n* = 10	84.3 ± 1.7º	41.0 ± 2.0º		
2e	TBDS+ATES+SP	Vis (2)	*n* = 10	88.3 ± 1.5º	49.7 ± 1.2º	1.5	5.7
2f	TBDS+ATES+SP	UV (2)	*n* = 10	86.8 ± 1.6º	44.0 ± 3.5º		
3a [H]	ATES+SP	Vis	*n* = 3	77 ± 3º	—	7	—
3b [H]	ATES+SP	UV	*n* = 3	70 ± 3º	—		
3c [H]	ATES+SP	Vis (2)	*n* = 3	75 ± 6º	—	4	—
3d [H]	ATES+SP	UV (2)	*n* = 3	71 ± 6º	—		
4a [H]	TBDS+ATES+SP	Vis	*n* = 3	74 ± 3º	—	14	—
4b [H]	TBDS+ATES+SP	UV	*n* = 3	60 ± 3º	—		
4c [H]	TBDS+ATES+SP	Vis (2)	*n* = 3	71 ± 3º	—	12	—
4d [H]	TBDS+ATES+SP	UV (2)	*n* = 3	59 ± 7º	—		

[A] Silica surface derivatized with aminopropyltriethoxysilane (ATES), tert-butylchlorodiphenylsilane (TBDS), SP acid, or combination of these reagents. For example, 'TBDS+ATES+SP' represents a surface treated first with TBDS, then with ATES, and finally reacted with SP acid according to Scheme 22.
[B] Denotes either visible (Vis) or UV light irradiation prior to and during the measurement.
[C] Specific SP acid molecule employed in the monolayer formation according to Scheme 22.
[D, E] The measured advancing and receding water contact angle.
[F, G] Changes in θ_{Adv} and θ_{Rec} following the change in surface treatment from visible to UV irradiation.
[H] Data from Rosario *et al.* (44), Figure 5.

In summary, for SP molecules suitably distributed within a monolayer and with proper choice of an alkyl linker joining the SP chromophore to the underlying surface, large wettability changes may be expected in response to the light stimulus. The reported $\Delta\theta$ values ([44,102]) are higher than for the azobenzene monolayers discussed earlier. However, the SP films exhibit noticeable degradation of photo-response even after a single Vis/UV cycle; effect which is absent in the case of azobenzene coatings (*i.e.*, compare data in Table 9 with Figure 3).

Polymeric coatings

Further research was directed at polymeric matrices in an attempt to increase the density of SP chromophores on a surface and hoping to overcome the degradation of photo-responsiveness observed with the monolayer coatings. The major aim was to controllably grow surface grafted polymeric films incorporating chemically bound SP molecules.

While a fairly comprehensive literature can be found on SP homopolymer and SP co-polymer coatings, only a handful of studies describe chemically grafted SP polymer films ([74,77,78]). Meanwhile, most of these citations describe synthesis and behavior of SP homopolymers and co-polymers in solution ([119,120,121,122,123,124,125,126,127,128,129,130,131,132,133,134,135,136,137,138,139,140]), within Langmuir and Langmuir-Blodgett films ([141,142,143]), in the bulk ([144,145,146,147,148,149]), in liquid crystalline phases ([150,151,152,153,154,155]), in membranes ([156,157,158]), within thin films ([48,129,144,159,160,161,162,163,164,165,166]), and as a composite of organic/inorganic gels, sols and resins ([167,168,169,170]). In addition, free SP molecules (*i.e.*, not chemically attached to the polymeric backbone) have been widely used as dopants in polymeric films ([171,172,173,174,175,176,177,178,179,180,181]), membranes ([182,183,184,185,186,187,188]), liquid crystalline phases

([189]), in the bulk polymer matrix ([190], [191], [192], [193], [194], [195], [196], [197], [198], [199], [200]), in Langmuir and Langmuir-Blodgett films (,[201],[202],[203]), onto fibers ([204]), colloids ([205]), and as a composite of organic/inorganic gels, sols and resins ([206], [207], [208], [209]). Finally, a good overview of SP-based polymeric materials can be found in several reviews treating photochromic/photoresponsive polymers ([15,16,17,18,19,22,210], [211]).

The grafting of SP homo- and co-polymer onto silica surfaces was carried out utilizing the approach similar to that reported by Park *et al.* (). In the first step, a spyrobenzopyran-substituted methyl methacrylate monomer (SPMMA) was synthesized according to Scheme 23. A modified procedure of Raymo and Giordani ([212]) has been adopted in forming the SP-alcohol (Steps 1 & 2 in Scheme 23), while Mitsunobu-type reaction ([213],[214],[215]) was used to couple methacrylic acid with the alcohol functionality (Step 3 in Scheme 23). In this way, the coupling reaction was performed under relatively mild conditions. (References [74,78,216] describe the synthesis of SPMMA carried out with methacryloyl chloride in the presence of pyridine.)

Scheme 23

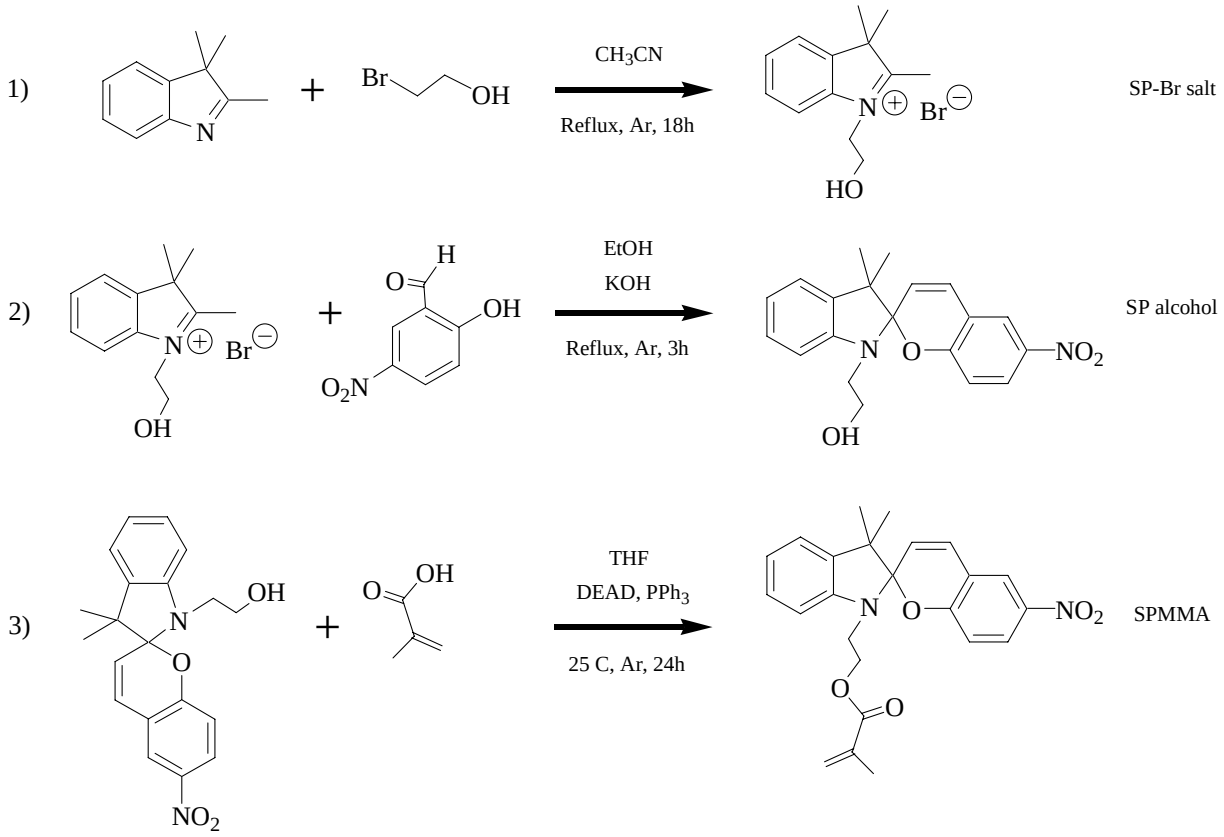

Next, silica surfaces were modified with an initiator (Step 1 in Scheme 24) according to the protocol of Matyjaszewski *et al.* ([217]). Finally, a controlled growth of SPMMA homopolymers and SPMMA-co-methyl methacrylate (MMA) random copolymers was performed using atom transfer radical polymerization (ATRP) as described in ref. 217 (Step 2 in Scheme 24).

Scheme 24

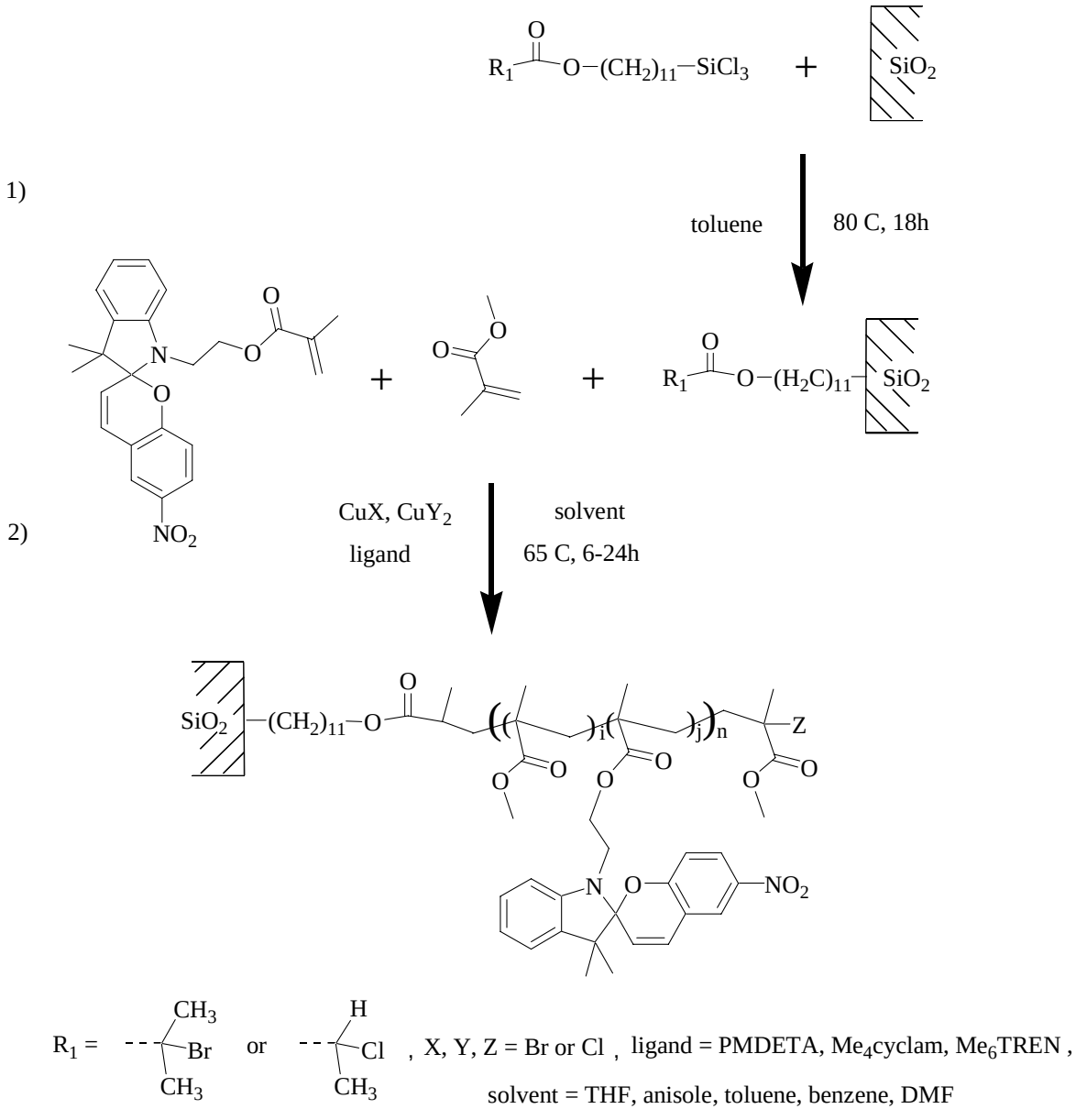

In the Scheme 1.7-5, PMDETA = N,N,N',N",N"-pentamethyldiethylenetriamine, Me_4cyclam = 1,4,8,11-tetraaza-1,4,8,11-tetramethylcyclotetradecane , Me_6TREN = tris[2-(dimethylamino) ethyl]amine, THF = tetrahydrofuran, and DMF = N,N-dimethylformamide. Indices i and j represent the relative number of MMA and SPMMA monomers, while index n stands for the degree of polymerization. To within the experimental error, the ratio i/j was found to mirror composition of the initial reaction mixture.

It should be mentioned here that the use of metal-catalyzed 'living' radical polymerization such as the ATRP process (for excellent reviews on the topic see refs. [218], [219], [220], [221], [222,223]) is preferred to the more conventional 2,2'-azobisisobutyronitrile (AIBN) catalyzed reactions employed for example by Park *et al.* (). This is because a better control over the reaction progress and the polymer layer thickness can be realized in the former case. Moreover, ATRP is a "grafting-from" polymerization technique performed under mild conditions (*i.e.*, temperatures often < 100°C), applicable to a wide range of vinyl monomers

(*e.g.*, styrenes, methyl methacrylates, acrylates, vinylpyridines, acrylonitriles, acrylamides) and preserving end-functionalization (*i.e.*, allowing for block co-polymerization). There are also a few more control variables available, such as the choice of metal catalyst (*e.g.*, Cu, Ni, Rh, Re, Pt, *etc.*), coordinating ligand (*e.g.*, PMDETA, Me_6TREN, Me_4cyclam, *etc.*), type of initiator (*e.g.*, haloalkanes, allyl halides, haloesters, sulfonyl halides, *etc.*), and the presence/absence of inhibitor (*e.g.*, $CuCl_2$, $CuBr_2$, *etc.*) allowing for the better optimization of reaction conditions during the 'living' polymerization process.

A typical ATRP polymerization reaction starts with a homolytic cleavage of a surface-bound initiator molecule (*e.g.*, benzyl chloride, sulfonyl chloride, ethyl 2-bromopropionate, azo-type compounds, *etc*.218) and a subsequent chain growth from the activated initiator radical (see Scheme 25 for an example of PMMA polymerization from (2-bromo-2-methyl)priopionyloxy type initiator using CuBr catalyst). During an early stage of monomer addition the growing radical is deactivated by a halogen atom abstraction from a catalytic transition-metal complex undergoing reversible reduction. This 'dormant' chain end can then be re-activated by the same transition metal-complex undergoing reversible oxidation and further chain growth proceeds until another deactivation event. Because reversible deactivation is fast compared to the monomer addition (*i.e.*, chain growth) all polymer chains are expected to grow with the same rate, which results in a narrow polydispersity of the final polymer layer (*i.e.*, $M_w/M_n<1.1$). The key factors for successful ATRP reactions are the low concentration of the radical intermediates (*i.e.*, active chains) at a given time and their fast but reversible transformation into the dormant species before undergoing successive addition of monomers. If the former condition is not met, chain termination occurs resulting in low conversions and thin polymer layers. If on the other hand, monomer addition is faster than transformation into the dormant species, the polymers exhibit high polydispersity and uncontrolled reaction ensues. Maintaining a proper equilibrium between dormant and active polymer chains requires a careful choice of the initiator, solvent and especially the transition-metal complex employed at suitable concentrations. Typically, these variables need to be investigated for each system before successful ATRP reaction can be achieved. In the case of surface initiated polymerization (*e.g.*, reaction from plain silicone wafers, colloidal particles, micron-sized beads) supplying a sufficient amount of deactivating species (*e.g.*, Cu(II)Br_2 in Scheme 24) becomes of paramount importance to provide reversible deactivation of chains during propagation ([224],[225]). Specifically, the concentration of Cu(II) in the range 10^{-3} mol/L is needed for a well controlled process (,[226]). Because amount of spontaneously generated deactivating specie formed by homolytic cleavage of the surface-bound initiator is typically much lower than this, two approaches were developed to correct the problem. In the first, the 'sacrificial' initiator was added to the solution ([227],[228]). The activation of these 'free' initiator molecules and the subsequent termination reactions of growing polymer chains formed a sufficient amount of the deactivator. One issue with this approach is that extensive cleaning of the surface-bound polymer brushes is required in order to remove the free polymer. The second approach relied on direct addition of the deactivating specie (*e.g.*, Cu(II)Br_2) to the reaction mixture (). Finally, it should be mentioned that true ATRP processes yield linear chain growth rates based on time and monomer conversion. Non-linear growth indicates the presence of termination reactions (retarded chain growth), or cross-linking (in the case of growth enhancement).

In the case of SPMMA-co-MMA films with 20% SP content, it was possible to grow polymer layers up to 50 nm thick using the ATRP polymerization method described in Schemes 24 and 25. With SPMMA homopolymer coatings, however, 10 nm films were obtained. A detailed study of varying reaction conditions (*e.g.*, different initiator SAMs, halogens, ligands, and solvents) to affect the polymer layer thickness was carried out with silica colloids in the place of silica coverslips/wafers, detailed later in this report. Similarly, spectroscopic analyses and aggregation/re-dispersion studies are also presented. Here, changes in the surface wettability after the polymerization reaction and upon subsequent exposure of the polymeric coatings to UV irradiation were examined. The results are illustrated in Figures 7 and 8 for the SPMMA and SPMMA-co-MAA (20% SP content) films, respectively, while Table 10 provides a concise summary.

Scheme 25

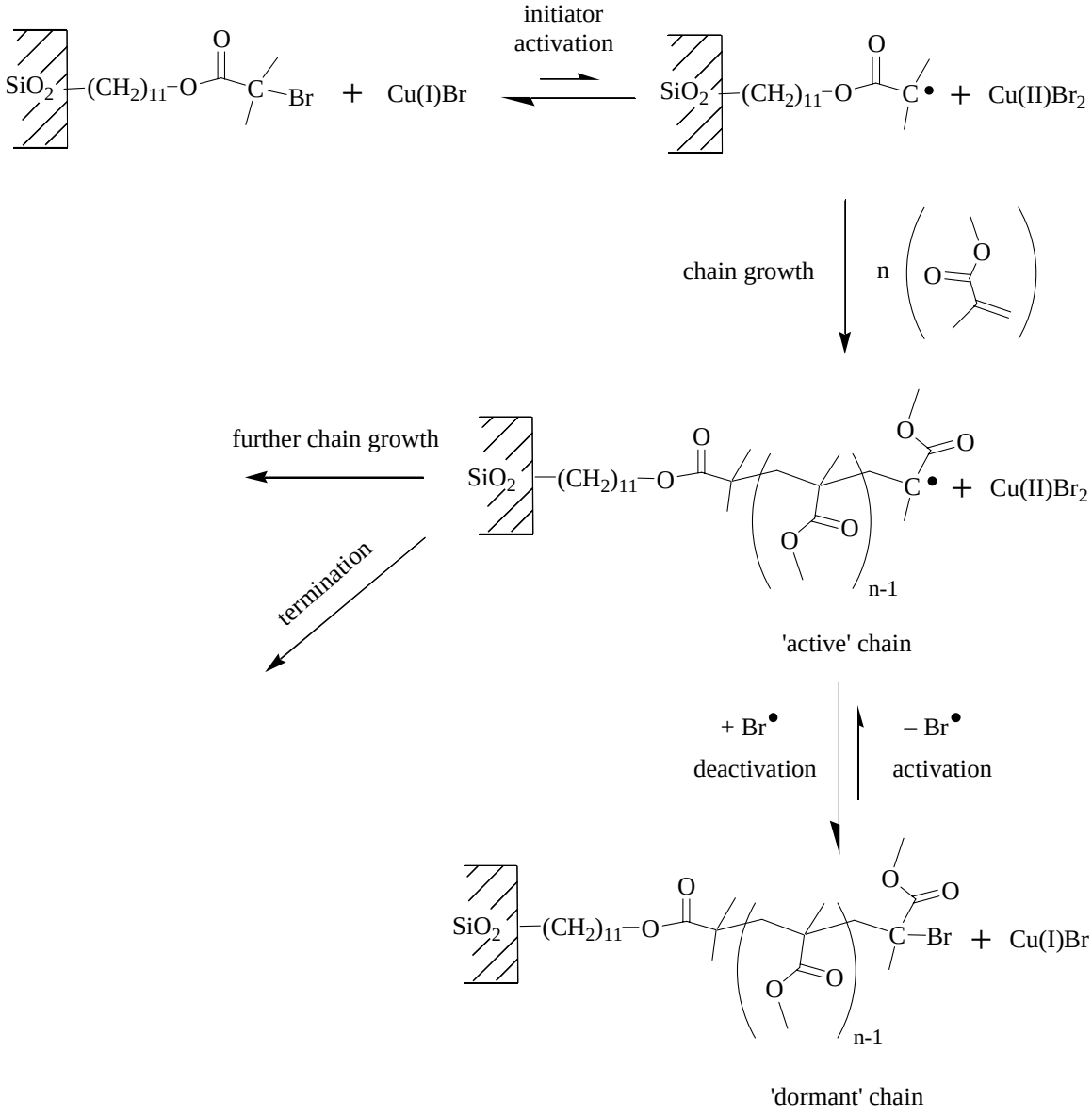
initiator
activation
SiO2
(CH2)11
O
C
Br
Cu(I)Br
Cu(II)Br2
chain growth
n
further chain growth
termination
n-1
'active' chain
+ Br•
deactivation
– Br•
activation
'dormant' chain

Table 10 Contact angle measurements for SPMMA homopolymer and SPMMA-co-MMA copolymer (20% SP content) films on silica surfaces modified with (2-bromo-2-methyl)priopionyloxy initiator SAMs according to Scheme 24. Changes in the contact angle upon UV light exposure are also reported.

smpl.	*coating* [A]	*treatment* [B]	θ_{Adv} [C]	θ_{Rec} [D]
1	initiator SAM	—	94.0 ± 1.1º	63.8 ± 3.2º
2a	SPMMA	—	85.4 ± 2.2º	58.8 ± 6.1º
2b	SPMMA	UV	83.3 ± 1.7º	44.2 ± 4.2º
2c	SPMMA	60°C, 24h	91.9 ± 58.8º	58.8 ± 1.6º
3a	SPMMA-co-MAA/20% SP	—	78.2 ± 1.3º	56.7 ± 2.8º
3b	SPMMA-co-MAA/20% SP	UV	76.2 ± 1.3º	44.6 ± 1.9º
3c	SPMMA-co-MAA/20% SP	60°C, 24h	79.7 ± 1.3º	55.8 ± 3.1º

[A] Silica surface derivatized with (11-(2-bromo-2-methyl)priopionyloxy)undecyl-trichlorosilane (initiator SAM), initiator SAM + SPMMA homopolymer (SPMMA), or initiator SAM + SPMMA-co-MAA copolymer containing 20% SP molecules (SPMMA-co-MAA/20% SP).

[B] Denotes either UV light irradiation or storage in the 60°C oven for 24h prior to the measurement.

[C,D,] The measured advancing and receding water contact angle. In the case of SPMMA film, data from two different surfaces with 9 measurements/sample was averaged. For the SPMMA-co-MAA/20% SP coating, results reported here represent an average of 7 samples with 9 measurements/sample. Only data for the first cycle of UV irradiation and the subsequent thermal treatment are given.

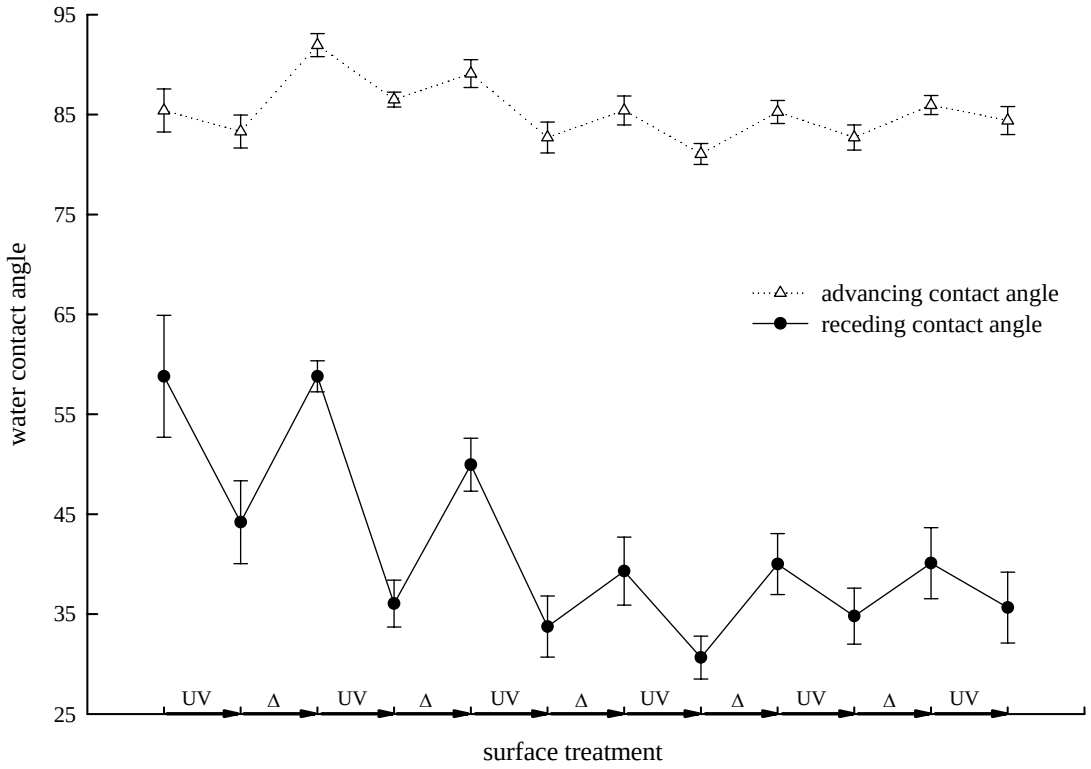

Figure 7 Light-induced water contact angle change for SPMMA polymeric film on a silica surface (see Scheme 24). The UV irradiation was carried out for 5-10 minutes using a hand held UV lamp operating at λ = 366 nm. Following UV treatment, the surface was allowed to equilibrate at 60°C for 24 hours (abbreviated 'Δ' in the figure). Data reported here represents an average over 2 substrates with 9 measurements per substrate.

As can be seen, the advancing water contact angle does not change significantly with the surface treatment (*i.e.*, $\Delta\theta_{Adv}$ = 16º). In contrast, $\Delta\theta_{Rec}$ values as large as 22º were recorded for the SPMMA coating, although the film responsiveness deteriorated significantly after 3 UV/Δ cycles (Figure 7). Similarly, SPMMA-co-MAA (20% SP content) coating gave $\Delta\theta_{Rec}$ = 9.4±1.5º (averaged over 6 UV/Δ cycles), while its responsiveness to the light stimuli was not compromised even after 6 UV irradiation/thermal recovery cycles (Figure 8). It should be pointed out that following UV treatment, the samples could be returned to their original state by either visible light irradiation or storage in the dark at ambient temperature. However, the MC ring closure reaction (see Scheme 20) and possible J-aggregate conversion under those conditions proved to be relatively slow (typically 24-60 hours). Meanwhile only 12-24 hours were required for this recovery process at 60ºC.

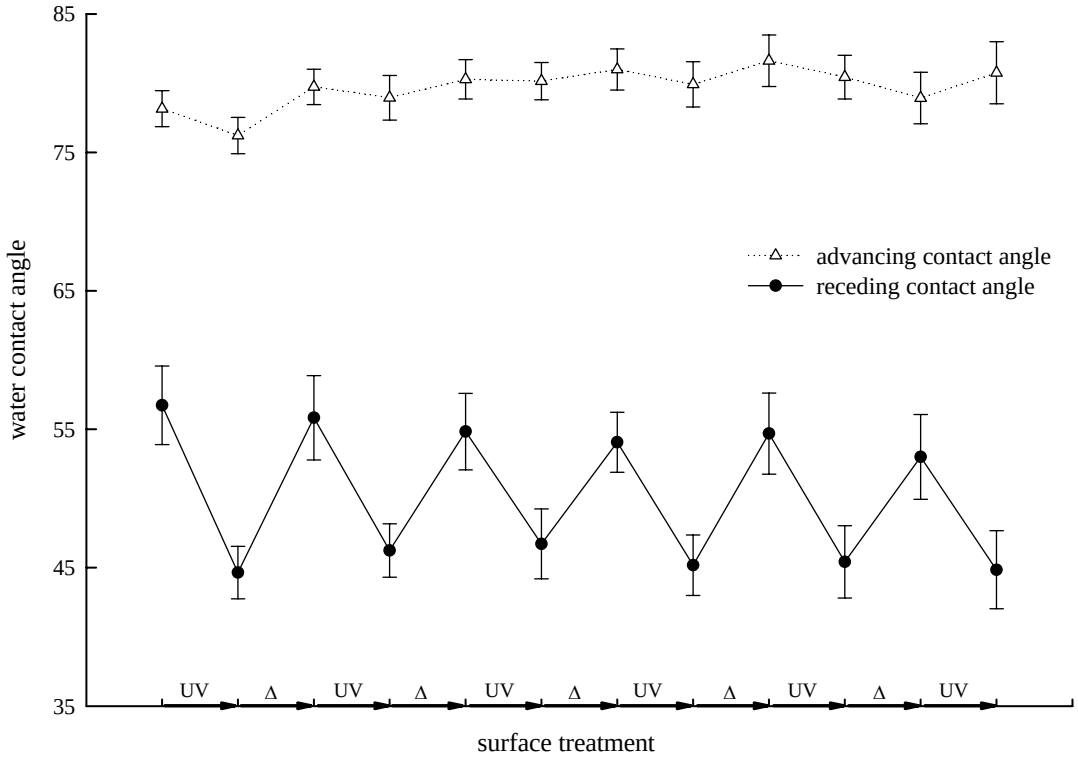

Figure 8 Light-induced water contact angle change for SPMMA-co-MAA (20% SP content) polymeric film on a silica surface (see Scheme 24). The UV irradiation was carried out for 5-10 minutes using a hand held UV lamp operating at λ = 366 nm. Following UV treatment, the surface was allowed to equilibrate at 60°C for 24 hours (abbreviated 'Δ' in the figure). Data reported here represents an average over 6 substrates with 9 measurements per substrate.

For comparison, Negishi *et al.* reported contact angle change of 10.5º (*i.e.*, from 90º to 79.5º upon UV irradiation) in the case SPMMA homopolymer coating ([159,229]). Likewise, Higuchi *et al.* () observed $\Delta\theta$=11±1º with SPMMA-co-MMA copolymer films (*i.e.*, 66º before and 55º after UV exposure). In another study, Hayashida *et al.* () found $\Delta\theta$ = 0 - 25º depending on the type of SP molecule doped into PMMA film. When a SP-*n* compound containing a very short alkyl chain (*i.e.*, *n* = 1 in Scheme 21) was used, the contact angle did not change upon the UV treatment. Moderate to large $\Delta\theta$ were observed, however, with intermediate and long alkyl chains. Specifically, PMMA films with 27 mol% of SP-7 gave $\Delta\theta$ = 10º, while 25 mol% of SP-12 and 22 mol% of SP-18 resulted in $\Delta\theta$ = 21º and 24º, respectively. Furthermore, $\Delta\theta$ values increased monotonically with SP molecule content in the PMMA matrix. It was

also discovered that significant film wettability changes upon UV light exposure occurred only with films containing at least 5 mol% of SP chromophores and only when microcrystals formed within these coatings.

In summary, the SPMMA homopolymer and SPMMA-co-MMA brushes grown from silica surfaces utilizing a robust and controllable ATRP process were found to display reversible wettability changes upon UV light exposure. Compared to the same process in solution, the MC to SP conversion within dry films was extremely retarded (*i.e*, it was necessary to incubate the surfaces at 60ºC for reasonable reaction rates.) Finally, while SPMMA-co-MMA film exhibited reversible wettability changes even after 6 UV/thermal treatment cycles, the SPMMA homopolymer coating showed signs of fatigue after just 2-3 cycles. The loss of responsiveness in this latter case could be caused by MC isomerization into optically inactive species trapped within the rigid polymer matrix, J-aggregation of MC units, or other photo-bleaching processes affecting to proximal chromophores.

Experimental

Scheme 23:

General: Alkylation of 2,3,3-trimethyl-3-H-indole with 2-bromoethanol afforded SP-Br salt. Reaction of SP-Br salt with 2-hydroxy-5-nitrobenzaldehyde in the ethanolic KOH gave the spirobenzopyran alcohol derivative (SP alcohol). Treatment of SP alcohol with methacrylic acid in the presence of diethyl azodicarboxylate and triphenylphosphine resulted in the spiropyran methyl methacrylate monomer (SPMMA).

1'-(2-hydroxyethyl)-3',3'-dimethyl-6-nitrospiro(2H-1-benzopyran-2,2'-indoline) (SP alcohol): A solution of 2,3,3-trimethyl-3-H-indole (31.9g, 200mmol) and 2-bromoethanol (31.2g, 250mmol) in acetonitrile (160mL) was refluxed under Ar for 18h. After cooling down, the solvent was removed under reduced pressure. Next, 2-hydroxy-5-nitrobenzaldehyde (35.4g, 212mmol) was added to the residue along with ethanol (250mL) and the mixture was stirred until the solids dissolved. Ethanolic solution of KOH (12.4g, 215mmol in 100mL of ethanol) was then added and the mixture was refluxed under Ar for 3h. After cooling to room temperature, the crystalline solid was filtered and washed with cold ethanol (50mL). Purification using a silica gel column afforded 49.3g (140mmol) of purple crystalline solid in 70% yield.

1'-(2-methacryloxyethyl)-3',3'-dimethyl-6-nitrospiro(2H-1-benzopyran-2,2'-indoline) (SPMMA): A solution of SP alcohol (15.0g, 42.6mmol) and triphenylphosphine (20.1g, 76.7mmol) in tetrahydrofuran (640mL) was cooled to 0°C under Ar. Diethylazodicarboxylate (13.2g, 75.8mmol) was then added and the mixture stirred for 10min. Following the addition of methacrylic acid (6.6g, 75.8mmol) and after removal of cooling, the solution was stirred for 24h at room temperature. The solvent was dried using a rotary evaporator and the product passed through the silica gel column to remove oxyphosphonium salts. The crude product (21.9g) was re-crystalized from hexanes to give 14.8g (35.1mmol) of pale green crystals in 82.5% yield.

Scheme 24:

General: Haloester initiators with trichlorosilane functionality were synthesized according to ref. 217. These were then reacted with silica substrates to give chemisorbed self-assembled monolayers. The atom transfer radical polymerization of SPMMA and methyl methacrylate from these modified surfaces in the presence of CuCl or CuBr catalyst, $CuCl_2$ or $CuBr_2$ inhibitor and a suitable ligand was then carried out in a given solvent.

undecen-1-yl 2-bromo-2-methylpropionate and *(11-(2-bromo-2-methyl)priopionyloxy)undecyl-trichlorosilane*: procedure in ref. 217 was followed.

undecen-1-yl 2-chloropropionate: To the solution of 10-undecen-1-ol (17.0g, 100mmol) and pyridine (8.4g, 106mmol) in THF (125mL) under Ar was added dropwise 2-chloropriopionyl chloride (12.7g, 100mmol). The mixture was stirred under Ar for 24h at ambient temperature. The solvent was dried using a rotary evaporator and the product dissolved in hexanes (300mL). Following two washes with 2M HCl and then two more with H_2O the organic layer was dried over $NaSO_4$ and filtered. Removal of the solvent under reduced pressure gave 25.1g (96.4mmol) of yellowish oil in 96.4% yield.

(11-(2-chloro)priopionyloxy)undecyl-trichlorosilane: To neat undecen-1-yl 2-chloropropionate (24.6g, 95mmol) added trichlorosilane (33.5g, 247mmol) and H_2PtCl_6 catalyst (110mg) previously dissolved in ethanol (2mL) and ethyl acetate (2mL) solution. The mixture was stirred at room temperature under Ar for 18h. After adding hexanes (25mL) the product was dried over $NaSO_4$ and filtered through a plug of silica gel to remove the catalyst. Following the removal of solvent under reduced pressure the product was purified by vacuum distillation (100-110°C at 4.5×10^{-2} mm Hg).

Initiator SAMs on silica substrates: Either fused silica coverslips (2.5cm × 2.5cm squares) or silicon (100) wafers (also cut into 2.5cm × 2.5cm squares) were cleaned in a hot pirana solution (70 parts H_2SO_4 to 30 parts H_2O_2 by volume) for 3h, followed by UV/O_3 treatment for 20min. The substrates were then moved to a drybox and submerged into a solution of 1mL of the trichlorosilane (either (11-(2-bromo-2-methyl)priopionyloxy)undecyl-trichlorosilane or (11-(2-chloro)priopionyloxy)undecyl-trichlorosilane was used depending on the desired SAM functionality) in 140mL of dry toluene. The samples were soaked in this solution for 18h at room temperature before 10min ultrasound cleaning in dry toluene, dry THF, and finally CH_2Cl_2.

Polymerization: The reactions were carried out in an O_2 free glovebox under anhydrous conditions. Typically, 5-10 silica substrates containing either (2-bromo-2-methyl)priopionyloxy or (2-chloro)priopionyloxy initiator SAM were mounted into a custsom design teflon holder. These samples were then immersed into a monomer/catalyst/solvent mixture kept in a glass jar (for typical mixture composition see the two examples described below). After sealing tightly with a screw-top lid, the container was placed in a thermostated oil bath kept at 65°C and the reaction was allowed to proceed for 6-24h. Upon removal from the solution, samples were immediately transferred into anhydrous THF and cleaned under ultrasound for 15min. This cleaning procedure was repeated in dry toluene and then again in CH_2Cl_2. When not in use, the samples were kept under anhydrous toluene in a drybox.

SPMMA homopolymer films: Glass jar was filled with SPMMA (3.42g, 8.12mmol) and THF (3.5mL) and the contents stirred until solids dissolved (0.5-1h). A catalyst solution containing CuBr (26mg, 0.18mmol), $CuBr_2$ (1.2mg, 0.0055mmol), PMDETA (0.14mL, 0.68mmol), and THF (0.1mL) was then added. After stirring for 1-2min, the holder containing 2 silica substrates modified with the initiator SAM was submerged in this mixture.

SPMMA-co-MMA random copolymer films containing 20% SP: Contents of the glass jar filled with SPMMA (16.0g, 38.0mmol), MMA (15.2g, 152mmol), and THF (4mL) were stirred until SPMMA monomer dissolved completely. To this a catalyst solution comprised of CuBr (163mg, 0.73mmol) and $CuCl_2$ (4.86mg, 0.035mmol) dissolved in PMDETA (0.90mL, 4.31mmol) and THF (0.37mL) was added and the mixture stirred for 1-2min. Following the removal of stirring, the holder containing 7 silica substrates modified with the initiator SAM was immersed in this polymerization mixture.

Synthesis and Response of Reversible Photo-dispersable Colloidal Particles based on the Spirobenzopyran System

Monolayer coatings

Few successful attempts to deposit SP chromophores onto colloidal particle surfaces were described in the past ([63,64,65,66,67]). Most recently, Taguchi *et al.* incorporated SP dye into vesicles encapsulating iron oxide cores to create a novel photoresponsive magnetic system (). The authors observed photo-induced vesicle aggregation even without any supporting media such as solvents or polymer matrices. As a result, the magnetization value of the vesicle cast films was increased by UV light irradiation in the solid state and at room temperature. Sugiyama *et al.* introduced a spirooxazine moiety onto the surface of poly(methyl methacrylate) microspheres and reported a photoresponsive adsorption of bovine serum albumin (BSA) onto these modified particles (). Finally, in a series of publications, Ichimura *et al.* demonstrated photocontrolled aggregation of colloidal silica modified with chemisorbed SP monolayers ([65,66,67]). In their initial study (), the authors coupled a spirobenzopyran carboxylic acid derivative bearing decamethylene spacer to an amine monolayer fixed on 150 nm diameter silica particles (see Scheme 22 for an analogous coupling reaction). The density of grafted SP chromophores was estimated at 1.6 nm^2/molecule and the particles exhibited normal photochromism in cyclohexane, carbon tetrachloride (CCl_4), chloroform ($CHCl_3$), and ethylene glycol. Meanwhile, untethered SP molecules have shown reverse photochromism in ethylene glycol (*i.e.*, MC was the stable form in the dark and could be bleached with UV irradiation) and normal behavior in the other three solvents. Moreover, free SP molecules in cyclohexane and CCl_4 displayed two peaks in their UV/Vis spectra with the peak at longer wavelength assigned to SP_nMC molecular aggregates. In the case of SP modified colloids, on the other hand, only one peak was found suggesting no intimate molecular interaction for the MC units. Particle dispersions in CCl_4 were stable in the dark, but flocculated upon UV exposure. Furthermore, the blue/violet colored sediment had porous structure suggesting loose aggregate formation. This photocontrolled aggregation behavior was observed only in CCl_4 (the particles flocculated in cyclohexane and stayed well dispersed in chloroform regardless of the treatment) and is due to an increase in surface polarity of the colloids following the UV triggered SP to MC conversion.

Mechanistically, the change in surface polarity causes abrupt reduction of the interaction between less polar SP units and non-polar solvent molecules giving rise to an attractive force between the colloids. Thus, the ionic interaction of MC moieties on the surface brings about flocculation and sedimentation (). This explanation was confirmed when lecithin (*i.e.*, naturally occurring amphiphilic compound with zwitterionic character) added to the UV irradiated particles in CCl_4 prevented flocculation. In a later study, Ichimura *et al.* () examined the effect of elongating the methylene spacer linking the SP chromophore to the silica surface (*i.e.*, increasing *n* in Scheme 22 from 2 to 10). They noted an increase in the thermal decoloration rate for particles modified with SP-10 vs. those containing SP-2, due to the larger mobility enjoyed by SP chromophores in the former case. Moreover, dispersion of SP modified colloids in polar solvents such as ethylene glycol yielded single first-order decay of photoformed MC because of efficient solvation assuring a homogenous microenvironment on the particle surface. On the contrary, the non-polar solvents (*e.g.*, cyclohexane, CCl_4) were found to force the MC moiety to distribute into a heterogenous microenvironment with variant polarity bringing about the bimodal first-order kinetics of the MC thermal decoloration process.

Here, the attachment of SP carboxylic acid derivative (*i.e.*, $n = 10$ in Scheme 22) to the surface of aminated silica colloids was performed following the protocol described in the literature ([44,66]). As evidenced by a color change of the particulate suspension upon UV irradiation (*i.e.*, the color changed from pale yellow to blue/purple), the coupling reaction was successful. However, contrary to the results of Ichimura *et al.* () the SP modified 284 nm diameter particles did not display photocontrolled aggregation behavior in pure CCl_4 solvent (*i.e.*, dispersions were equally flocculated before and after λ = 366 nm light exposure). Instead, UV induced aggregation was observed in a mixed solvent system

containing CCl_4 and $CHCl_3$ in a 1:6 volumetric ratio. In $CHCl_3$, only a slight flocculation of the otherwise stable dispersion was observed following UV irradiation, while in CH_2Cl_2 the suspension remained stable regardless of the treatment. Since the photo-controlled flocculation process took place in a slightly more polar medium than for the analogous system investigated by Ichimura *et al.* (), the SP monolayers prepared here are characterized by larger polarity. This could be due to a higher density of unreacted amine groups or simply greater water content on the silica surfaces.

While particle aggregates precipitated by UV exposure in $CCl_4/CHCl_3$ (6:1 by volume) dispersions could be readily redispersed by a subsequent visible light irradiation (λ = 520 nm) and ultrasonication, a significant loss of responsiveness was observed even after 2 flocculation/redispersion cycles (*i.e.*, flocs quickly reformed even post visible light and ultrasound treatment). Several factors could contribute to this: MC isomerization into optically inactive species, molecular rearrangement on the surface exposing more polar amine groups to the solvent, or monolayer degradation.

Polymer coatings

Following a successful ATRP polymerization of SPMMA and SP-co-MMA brushes from flat silica surfaces, the same approach was adopted for silica colloids. This was done to increase the density of SP chromophores on a surface and overcome the degradation of photo-responsiveness observed with the monolayer coatings. Furthermore, reversible, light induced swelling was observed with these types of polymeric brushes in certain solvents. Specifically, Imanishi *et al*. reported reversible, photo-controlled permeability change of a glass membrane filter (nominal pore size = 5 μm) modified with SP-co-MMA films (). In toluene, the solvent permeation rate was increased by approx. 6% upon UV irradiation indicating a decrease in the polymer brush thickness from 45 nm to 15 nm. The original permeability was recovered post visible light treatment. In DMF, on the other hand, no change in solvent permeation rate was found following UV exposure with the polymer layer thickness remaining constant at 55 nm. Earlier, Imanishi *et al*. observed a similar behavior for SPMMA-co-AM (AM represents acrylamide) grafted onto PTFE membrane (). The permeation of H_2O/methanol (1:9 by volume) solvent mixture could be reversibly increased by approx. 20% by exposing the membrane to UV light. Thus, compared to the SP photo-responsive monolayers the appended polymer networks add the benefit of reversible swelling behavior between switched states. This volume expansion functionality might aid the re-dispersion process of flocculated photo-responsive colloids.

The grafting/growing of polymer brushes containing SP chromophores from colloidal particles has not been attempted before, while only a limited number of studies dealt with SP molecules chemisorbed onto polymeric particles (). Furthermore, only a handful of reports describe grafting of SP copolymers from solid surfaces ([74,75,76,77,78]). Extensive literature can be found on SP homo- and co-polymers however (see polymeric coatings system above), while several recent investigations describe polymer brushes grown from nano- and micron- sized particles using the ATRP method ([221,230, 231, 232, 233, 234, 235, 236, 237, 238, 239, 240, 241, 242, 243]). Based on the data presented in these studies, a robust ATRP method for growing well defined SPMMA homopolymer and SPMMA-co-MMA copolymer brushes from silica colloids has been designed. Particularly, the same procedure applied to flat silica substrates was followed (*i.e.*, Scheme 24) yielding uniform, spherical polymer layers up to 80 nm thick. Some examples of these core-shell composite particles are illustrated in Figure 9.

In the course of manufacturing the silica-*graft*-(SPMMA-co-MMA) colloids, polymerization conditions have been adjusted from batch to batch in order to produce particles with the thickest layers. These efforts are summarized in Table 11.

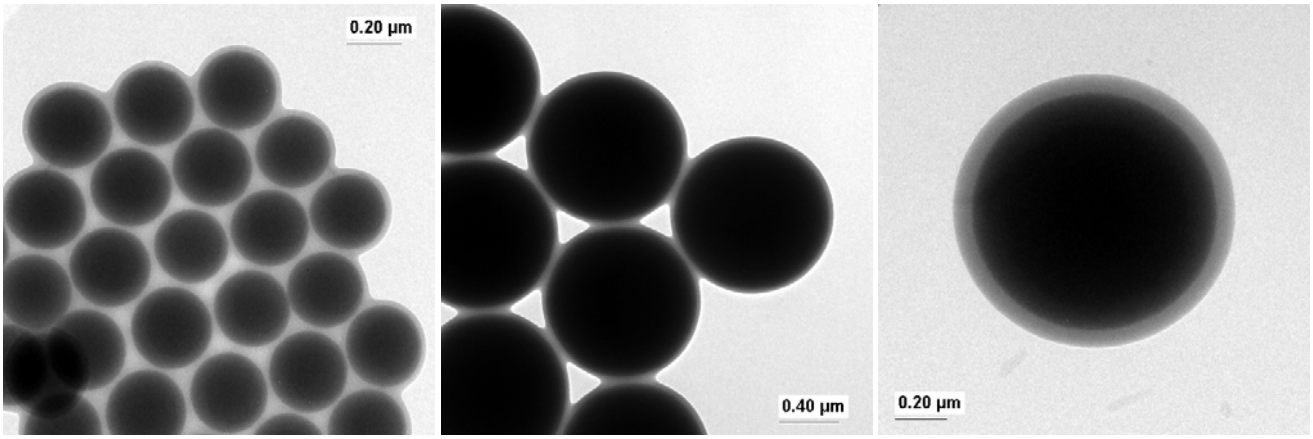

a **b** **c**

Figure 9 TEM micrographs of silica core particles modified with grafted SPMMA-co-MMA shells according to Scheme 24. (a) 283 nm silica colloids with 19.4±5.5 nm thick SPMMA-co-MMA (10% SP content) shells from batch PC3-25; (b) 927 nm silica colloids with 21.2±2.7 nm thick SPMMA-co-MMA (15% SP content) shells from batch PC3-144; (b) 927 nm silica colloid with 76.3±4.8 nm thick SPMMA-co-MMA (20% SP content) shell from batch PC5-153.

Table 11 The effect of different reaction conditions on SPMMA-co-MMA brush thickness, *h*. The polymerization from 284 nm and 927 nm diameter silica colloids were carried out according to Scheme 24.

batch	*init.* [A]	*SP %* [B]	*solvent* [C]	*ligand* [D]	*[ligand]* [E]	*[mono]* [F]	*X*	*[CuX]* [G]	*Y*	*[CuY$_2$]* [H]	*h (nm)*
effect of SPMMA content											
3-25	Br	10	THF	PMDETA	1.6×10^{-2}	4.2	Br	8.2×10^{-3}	—	—	19.4 ± 5.5
3-144	Br	15	THF	PMDETA	7.4×10^{-2}	3.5	Br	3.7×10^{-2}	—	—	21.2 ± 2.7
4-81a	Br	20	THF	PMDETA	2.7×10^{-2}	3.4	Br	1.5×10^{-2}	—	—	26.2 ± 1.2
effect of adding CuY_2 inhibitor											
4-81a	Br	20	THF	PMDETA	2.7×10^{-2}	3.4	Br	1.5×10^{-2}	—	—	26.2 ± 1.2
4-81b	Br	20	THF	PMDETA	2.7×10^{-2}	3.4	Br	1.5×10^{-2}	Br	4.0×10^{-4}	25.5 ± 1.2
3-144	Br	15	THF	PMDETA	7.4×10^{-2}	3.5	Br	3.7×10^{-2}	—	—	21.2 ± 2.7
3-145	Br	15	THF	PMDETA	7.4×10^{-2}	3.5	Br	3.7×10^{-2}	Br	4.9×10^{-4}	22.6 ± 2.1
effect of adding free initiator, ethyl-2-bromoisobutyrate											
4-81a	Br	20	THF	PMDETA	2.7×10^{-2}	3.4	Br	1.5×10^{-2}	—	—	26.2 ± 1.2
4-81c [I]	Br	20	THF	PMDETA	2.7×10^{-2}	3.4	Br	1.5×10^{-2}	—	—	29.4 ± 4.3
effect of initiator surface coverage											
4-56 [J]	Br	20	anisole	PMDETA	1.1×10^{-2}	2.1	Br	1.1×10^{-2}	—	—	13.3 ± 1.8
4-27 [J]	Br	20	anisole	PMDETA	1.1×10^{-2}	2.2	Br	1.1×10^{-2}	—	—	16.6 ± 1.7
effect of solvent											
4-27	Br	20	anisole	PMDETA	1.1×10^{-2}	2.2	Br	1.1×10^{-2}	—	—	16.6 ± 1.7
3-79	Br	20	THF	PMDETA	2.1×10^{-2}	2.6	Br	1.1×10^{-2}	—	—	25.8 ± 3.0
effect of adding H_2O											
4-81a	Br	20	THF	PMDETA	2.7×10^{-2}	3.4	Br	1.5×10^{-2}	—	—	26.2 ± 1.2
4-81d [K]	Br	20	THF	PMDETA	2.7×10^{-2}	3.4	Br	1.5×10^{-2}	—	—	10.8 ± 4.6
effect of ligand concentration											
5-137c	Cl	20	THF	PMDETA	7.8×10^{-2}	3.8	Br	2.1×10^{-2}	Cl	6.3×10^{-4}	75.8 ± 2.6
5-145a	Cl	20	THF	PMDETA	3.2×10^{-3}	3.8	Br	2.1×10^{-2}	Cl	6.3×10^{-4}	79.5 ± 2.6
effect of different ligands											
5-145a	Cl	20	THF	PMDETA	3.2×10^{-2}	3.8	Br	2.1×10^{-2}	Cl	6.3×10^{-4}	79.5 ± 2.6
5-145b	Cl	20	THF	Me_4cyclam	3.2×10^{-2}	3.8	Br	2.1×10^{-2}	Cl	6.3×10^{-4}	73.8 ± 6.0
5-145c	Cl	20	THF	Me_6TREN	3.2×10^{-2}	3.8	Br	2.1×10^{-2}	Cl	6.3×10^{-4}	32.7 ± 1.7
effect of different inititators and halogens in catalytic system											
4-98	Br	20	THF	PMDETA	8.6×10^{-2}	3.8	Br	1.6×10^{-2}	Br	4.9×10^{-4}	24.9 ± 2.6
5-137d	Br	20	THF	PMDETA	7.8×10^{-2}	3.8	Cl	2.1×10^{-2}	Cl	6.3×10^{-4}	34.2 ± 3.3
5-137b	Cl	20	THF	PMDETA	7.8×10^{-2}	3.8	Cl	2.1×10^{-2}	Br	6.3×10^{-4}	50.3 ± 1.7
5-55	Cl	20	THF	PMDETA	7.8×10^{-2}	3.8	Br	2.1×10^{-2}	Br	6.3×10^{-4}	55.5 ± 2.3
5-137a	Cl	20	THF	PMDETA	7.8×10^{-2}	3.8	Cl	2.1×10^{-2}	Cl	6.3×10^{-4}	57.8 ± 1.3
5-137c	Cl	20	THF	PMDETA	7.8×10^{-2}	3.8	Br	2.1×10^{-2}	Cl	6.3×10^{-4}	75.8 ± 2.6

[A] Type of initiator monolayer chemisorbed onto the colloidal silica surface: "Br" stands for (11-(2-bromo-2-methyl) priopionyloxy)undecyl-trichlorosilane, while "Cl" denotes (11-(2-chloro)priopionyloxy)undecyl-trichlorosilane.

[B] Content of SPMMA in SPMMA-co-MMA polymer brush expressed as molar fraction.

[C] Solvent used during the polymerization reaction. THF = tetrahydrofuran, DMF = N,N-dimethylformamide

[D] Type of ligand utilized. See Scheme 1.7-5 for explanation of PMDETA, Me_4cyclam, Me_6TREN abbreviations.

[E] Total monomer concentration, [SPMMA] + [MMA] expressed in mol/l.

[F] Ligand concentration expressed in mol/l.

[G] CuBr (X = Br) or CuCl (X = Cl) catalyst concentration expressed in mol/l.

[H] $CuBr_2$ (Y = Br) or $CuCl_2$ (Y = Cl) inhibitor concentration expressed in mol/l.

[I] Free, initiator, ethyl-2-bromoisobutyrate was added such that [free initiator] = 2.3×10^{-3} mol/l.

[J] In the case of batch 4-56, the initiator SAM was comprised of 80% decyltrichlorosilane and 20% (11-(2-bromo-2-methyl) priopionyloxy)undecyl-trichlorosilane, while batch 4-27 contained 100% of the latter.

[K] Added 3.1×10^{-3} mol/l of water to the polymerization solution.

Although polymer shells with 10%, 15%, 25% and 100% SP content were also prepared, most of the work was aimed at optimizing the synthesis of SPMMA-co-MMA (20% SP content) brushes. This was motivated by the work of Irie *et al.* (), who reported the largest viscosity change for benzene solutions of SPMMA-co-MMA copolymers characterized by 11-27% SP content. Thus, the biggest photo-controlled response can be expected of polymer brushes with approx. 19% SPMMA mol fraction.

As can be seen from Table 11 (entries 1-3), increasing the SP content in the brush yielded thicker layers. There is, however, a practical limit to this approach associated with the limited solubility of SPMMA. For example, monomer concentration of only 0.98 mol/l was achievable in the case of SPMMA homopolymer (*i.e.*, 100% SP content) THF solution resulting in coating 10.1 ± 1.4 nm thick. It should be mentioned here that composition of polymer brushes (*i.e.*, SPMMA/MMA ratio) mirrored the composition of polymerization solutions according to the NMR analysis. The same result was reported by Park *et al.* in the case of free SPMMA-co-MMA polymers ().

It is also apparent from the data presented above that addition of $CuBr_2$ inhibitor and free initiator along with a marked increase in the ligand concentration in excess of what is required to complex the Cu catalyst have marginal effect on the brush thickness. Meanwhile, the change of solvent, complexing ligand, type of initiator and its coverage, use of different halogen atoms, and addition of water all affect the polymer coating thickness significantly. Specifically, the addition of polar H_2O (entries 15-16 in Table 9) facilitates the ring-opening isomerization of SP molecules simultaneously stabilizing the MC form. As a result, larger MC molecules are incorporated less efficiently into the growing polymer chain, while their more polar nature may lead to undesired termination reactions and a loss of catalytic activity. Thus, much thinner polymer brushes are obtained in the presence of water. The use of anisole, a slightly less polar solvent (*i.e.*, $\varepsilon_{anisole} = 4.3$ vs. $\varepsilon_{THF} = 7.4$, where ε stands for dielectric constant) also resulted in diminished polymer layers (entries 12-13 in Table 11). Similarly, *h* was reduced upon decreasing initiator surface coverage (entries 10-11 in Table 11). This is due to a smaller number of active chains, so that their overall termination occurs sooner. Moreover, almost twofold increase in the polymer layer thickness was observed when (2-chloro)priopionyloxy type initiator was used instead of the (2-bromo-2-methyl)priopionyloxy monolayer (see entries 21-26 in Table 11). Such a drastic change can be attributed to a slower activation of the chlorine based initiator yielding low amounts of the radical intermediates. With a smaller concentration of activated species (*i.e.*, initiator radicals and active chain ends) the chain termination reactions are less likely to occur and layer growth proceeds to a larger extent. From Table 11, it is also clear that for thickest polymer brushes it is best to use a mixed catalyst/inhibitor system, $CuBr/CuCl_2$ (see entries 21-26), along with PMDETA as the complexing ligand (entries 18-20). In summary, optimization of reaction conditions allowed for the growth of SPMMA-co-MMA brushes up to 80 nm thick.

The kinetics of the polymerization reaction are summarized in Figure 10 for the case of SPMMA-co-MMA (20% SP content) brushes grown from (2-bromo-2-methyl)priopionyloxy type initiator SAM using CuBr/PMDETA catalyst complex and free initiator (*i.e.*, ethyl-2-bromoisobutyrate) dissolved in THF. While generally the reactions were performed at 60-65°C (this is true of all the data presented in Table 11), in this case, the reaction was carried out at 25°C to aid the sampling process. The specific polymerization conditions are summarized in Figure 10 caption.

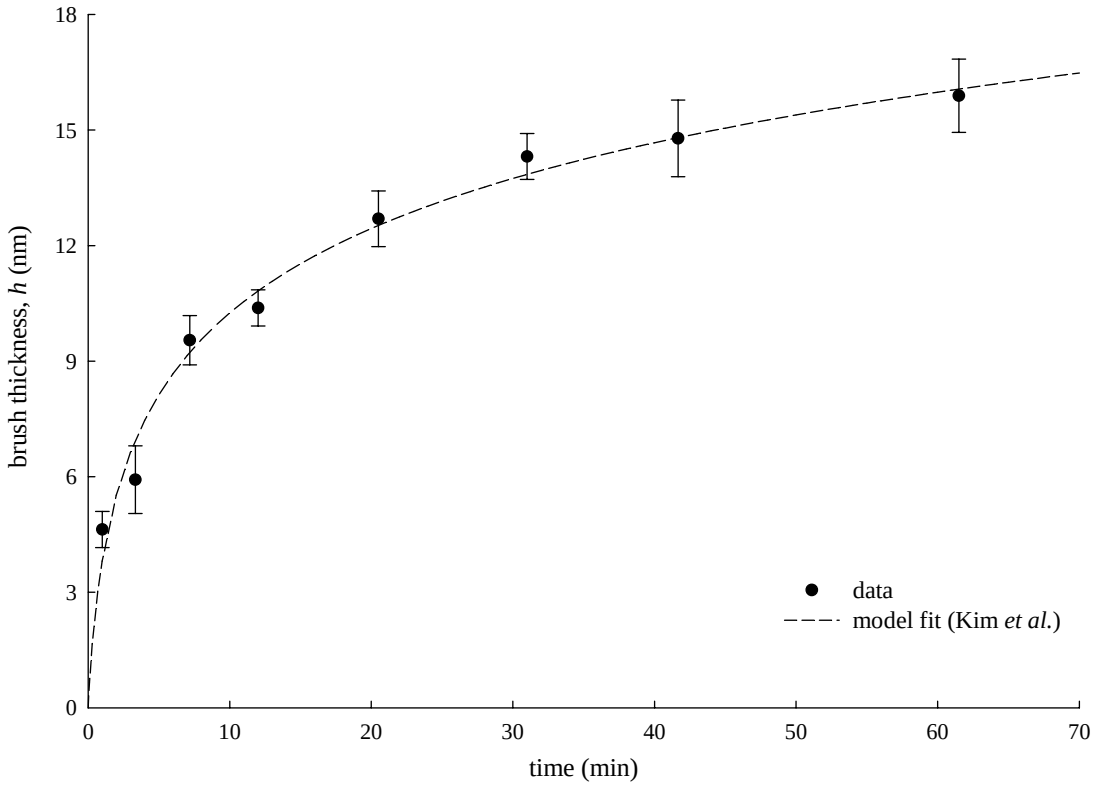

Figure 10 Thickness of SPMMA-co-MMA (20% SP content) brush measured by TEM vs. reaction time. The polymer layers were grown from 927 nm diameter silica colloids modified with (11-(2-bromo-2-methyl) priopionyloxy)undecyl-trichlorosilane. Reaction conditions were as follows: [monomer] = 3.8, [CuBr] = 2.3×10^{-2}, [PMDETA] = 8.6×10^{-2}, [ethyl-2-bromoisobutyrate] = 2.3×10^{-2} (all concentrations expressed in mol/l), solvent = THF, reaction temp. = 25°C. Vertical error bars in the figure represent standard deviation from 25 measurements on different particles. The dashed line through the data is a fit to the model of Kim *et al.* ([244]).

While true ATRP processes yield linear chain elongation rates, the data above corresponds to retarded and non-linear layer growth indicating the presence of termination reactions. To account for the loss of growing chains during surface-initiated polymerization Kim *et al.* employed the following simple model (244):

$$\frac{d[A]}{dt} = -k_1[A]^2 \tag{3}$$

$$\frac{dh}{dt} = k_2[A] \tag{4}$$

$$h = (k_2/k_1)\ln(1 + k_1[A]_0 t) \tag{5}$$

where $[A]$ and $[A]_0$ represent concentration of active chains in both dormant and radical states at any given time t and the initial concentration of active initiator functionalities, respectively. In the first equation it is assumed that the loss of active chains is second order in surface concentration (*i.e.*, chain termination by recombination) with a rate constant k_1. Meanwhile, ATRP process implies a linear layer thickness growth with respect to the number of active chains, hence Eq. 4. The Eq. 5 follows from

integration of Eq. 3, substitution of the resultant expression for [*A*] into Eq. 4 and integrating again. As can be seen from Figure 10, this model fits data very well with parameters k_2/k_1 = 3.27±0.24, $k_1[A]_0$ = 2.21±0.63 and Chi squared statistic equal to 0.379.

Photochromism

UV/Vis spectroscopy was used to characterize photochromic behavior of the silica-polymer composite particles dispersed in different solvents.

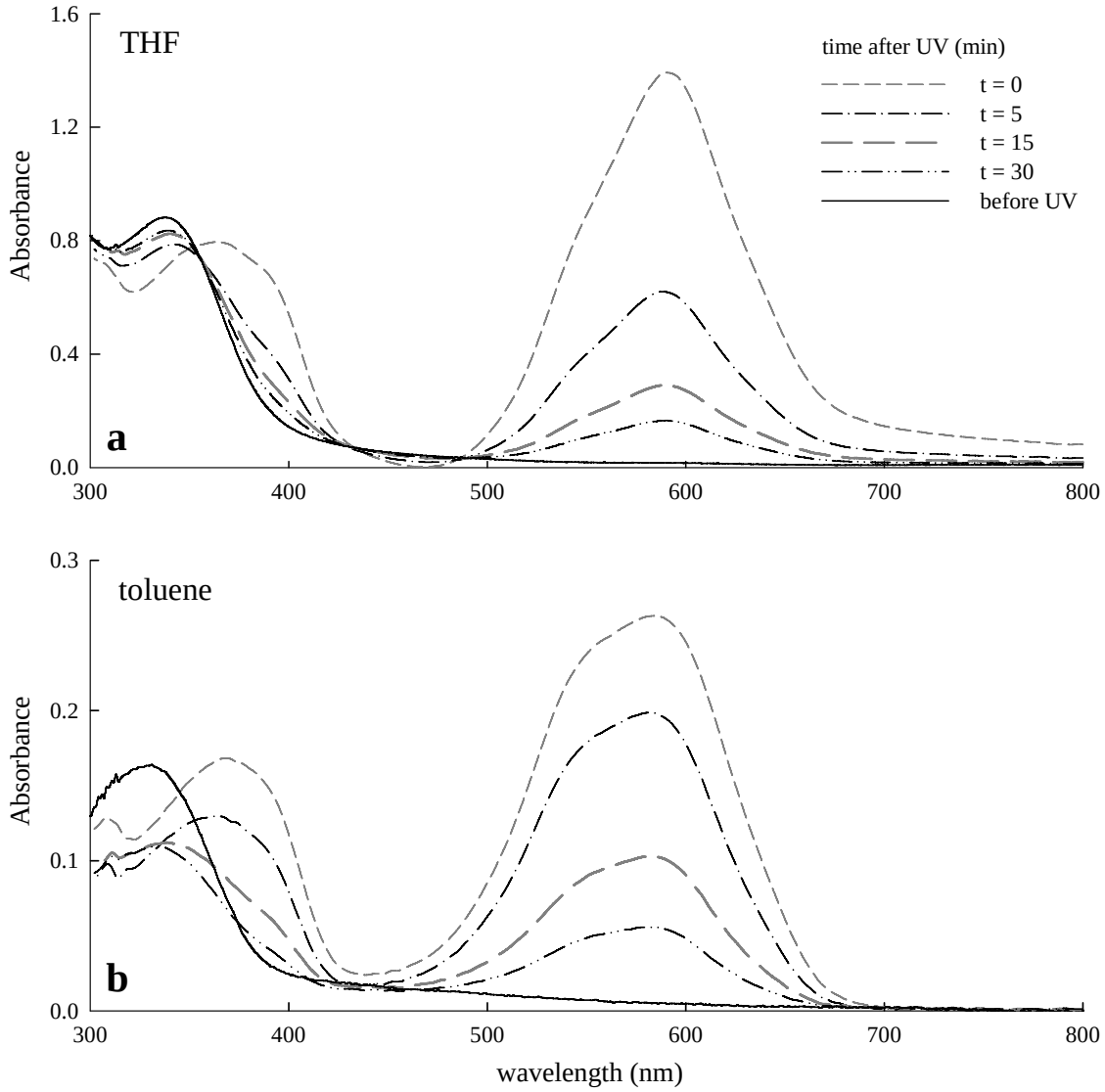

Figure 11 UV/Vis absorption spectra for 0.035% v/v (0.079% wt/wt) dispersions of 927 nm silica core particles with 24.9 nm thick SPMMA-co-MMA shells in (a) THF, and (b) toluene following UV irradiation. For the specific conditions employed in the surface initiated polymerization see entry 21 (*i.e.*, batch 4-98) in Table 9. While THF suspensions were well dispersed, in toluene the particles aggregated following UV treatment. A cell with the optical length of 1 cm was used.

Figure 11 illustrates spectra for 927 nm silica core particles with 24.9 nm thick SPMMA-co-MMA shells dispersed in THF and toluene. It should be mentioned that while colloids dispersed well in THF, aggregation was observed in toluene following UV light exposure. Because of this fact, the toluene data cannot be treated quantitatively to estimate, for example, a concentration of SP chromophores on particle surface. Nonetheless features such as peak positions and MC to SP conversion kinetics following the UV treatment (*i.e.*, the rate of peak absorption decrease) can be deduced accurately.

Examination of Figure 11 yields valuable information as to the microenvironment of SP chromophores in the polymer matrix. Thus, UV irradiation of polymer brushes in THF generated λ_{max} at 589 nm with a small shoulder at λ_{shldr} = 550 nm, while the half-width of this absorption band was $\Delta\lambda_{1/2}$ = 100 nm. In the case of toluene solvent, λ_{max} was blue shifted to 582 nm and a more pronounced shoulder was observed at λ_{shldr} = 545 nm. Moreover, $\Delta\lambda_{1/2}$ = 110 nm and a slower MC to SP thermal relaxation (*i.e.*, rate of absorption fading at λ_{max}) were recorded in toluene. In both solvents, however, the MC to SP conversion process was non-linear. Similar results were observed with free polyphosphazene polymers containing spiropyran units dissolved into THF and THF/toluene mixtures (). The main peak around λ = 580-590 nm can be ascribed to the open merocyanines in the trans form about the double bond ([119,121,122,123]), while the shoulder at λ = 540-560 nm is most likely due to the formation of SP-MC dimers or MC_n molecular aggregates ([123,124,161]). Interestingly, formation of higher order molecular aggregates of the type $(SP\text{-}MC)_n$ ($n > 1$) and $SP_m\text{-}MC_n$ ($m + n > 2$) associated with the absorption in λ = 600-640 nm range ([122,123,161]) was not observed here. The fact that upon changing solvents from THF to toluene λ_{max} was blue shifted, $\Delta\lambda_{1/2}$ increased, and MC $\rightarrow$ SP thermal relaxation rate decreased indicate that MC moieties are in a more polar microenvironment when the polymer brush is solvated by the less polar toluene solvent ([245]). Albeit counterintuitive, this observation helps to expose the mechanism associated with light induced conformational changes of the SPMMA-co-MMA copolymers. Particularly, poly(methyl methacrylate) ester side groups compete with the solvent molecules for solvation of the photogenerated polar merocyanines ([119,123]). In the case of polar solvents such as THF, the MC moieties are well stabilized by the solvent molecules and no conformational changes occur. Meanwhile, in non-polar solvents such as toluene the MC zwitterions are better stabilized by ester side groups of PMMA chain precipitating a conformational change. This concept is schematically illustrated in Scheme 27.

Scheme 27

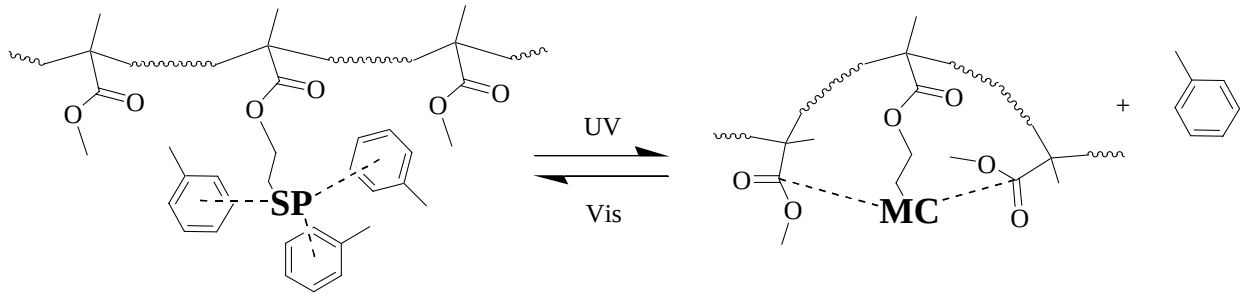

In the past, the photoinduced conformational transformations of SP copolymers have been used to control volume changes in thin films ([74,78]), polymer solubility ([122,123,125,126,127,128]), and solution viscosity ([119,129,130,131,132,246]). Here, this process has been employed to photocontrol dispersibility of colloidal particles.

Conclusions

A comprehensive synthetic investigation aimed at the covalent attachment of azobenzene and spirobenzopyran chromophores onto colloidal silica surfaces has been performed. Successful formation of monolayer coatings allowed photo-actuation of surface wettability. However, derivatization of nano- and micro-particles with such photoactive monolayers did not yield robust, photo-responsive colloidal systems. In the case of azobenzene, there was no response to the light stimulus, while the responsiveness of spirobenzopyran modified colloids was erratic and rapidly degraded with successive UV/Vis irradiation cycles. In an attempt to resolve these issues, azobenzene and spirobenzopyran molecules were chemically incorporated into polymeric matrices grafted from the colloidal silica surfaces. The polymeric brushes modified with azobenzene were thin (h < 10 nm), irregular, and very difficult to separate from physisorbed polymer also formed in polymerization solution. Moreover, the azobenzene-polymer coated particles were highly aggregated in a variety of solvents used for their dispersion. The spirobenzopyran homopolymer and copolymer brushes were successfully prepared via an atom transfer radical polymerization from flat silica surfaces and initiator-modified colloidal particles. Both, the poly(spirobenzopyran methyl methacrylate) and the spirobenzopyran methyl methacrylate-co-methyl methacrylate copolymer coatings were homogenous and well cleaned from the residual catalyst or free polymer by Soxhlet extraction or simple solvent washing. Furthermore, SPMMA and SP-co-MMA modified colloids exhibited excellent dispersibility in good PMMA polymer solvents such as THF and anisole. Optimization of ATRP reaction conditions yielded polymer brushes up to 80 nm thick, while the photochromic behavior of SP molecules was similar to that reported in the case of free polymers.

Section 3

Photophysical Effects between Spirobenzopyran-Methylmethacrylate Functionalized Colloidal Particles

Introduction

In the prior section, the synthesis of photo-controlled colloidal particles was detailed. The system providing the best ease of use and study was the 20% spirobenzopyran methyl methacrylate – 80% methylmethacrylate (SPMMA-co-MMA, 20% SP) copolymer system, with polymers grown by an atom transfer radical polymerization process (ATRP) on silica particles functionalized with grafted initiators. These particles in toluene show reversible states of colloidal stability. This section provides the observations taken to characterize the resulting photo-physical phenomena between the colloids in the two photo-controlled molecular states. These studies include visual observations, sedimentation studies performed using turbidity measurements as a function of time, and observation of rheological response during switching through viscosity changes in a concentrated suspension of particles.

Experimental

Silica colloids were derivatized with spiropyran doped polymer layers of MMA according to the procedures described in Section 2. Both 284 nm and 927 nm particles were derivatized in this way. Visual observations of aggregation were taken using a laboratory UV lamp source, in the long wave mode. Particle suspensions were manually agitated and dried on glass substrates for scanning electron microscopy examination of the particle structure before and after exposure to UV light sources.

Sedimentation was followed using a Hach turbidimeter as a function of time. Parameters varied in the test included solvent (toluene, benzene and o-xylene) and exposure to UV light.

Viscosity measurements were performed using a Thermo Haake RS300 rheometer, and a custom stage designed to allow for exposure of the bottom plate to optically controlled wavelengths of light. Specifically, the parallel spindle and plate components (plate diameter = 35 mm and a gap width of 0.02 mm) were used for the measurements. The lower plate was a fused silica plate mounted to a stage over a 45 degree optical mirror. The mirror was used to direct light from a 200 W Hg lamp (Oriel) with appropriately chosen filters (*i.e.*, $\lambda = 365 \pm 10$ nm bandpass filter for the UV irradiation and $\lambda > 475$ nm cutoff filter for the visible light exposure) to control the exposure wavelengths. The flat plate spindle was used because it was found that the sample of particles in toluene were not homogeneously switched using a 1° cone (with a gap spacing of 0.052 mm). The flat plate was tested at numerous gap spacings from 52 to 20 microns in order to insure that the particles were not attenuating the light over the sample length. This was observed visually after separation of the plates. Drying was a particular problem in the toluene system. Various configurations of bonding a teflon solvent trap were attempted until a measurement was achieved in which viscosity was unchanged with time.

Results and Discussion

Photocontrol of colloidal stability

Light driven conformational and polarity changes in SPMMA-co-MMA copolymer brushes grafted onto silica core particles have been utilized to influence the aggregation and sedimentation behavior of colloids dispersed in non-polar solvents. Figure 12 illustrates such phase transition following UV irradiation of 927 nm silica core particles modified with 24.9 nm thick SPMMA-co-MMA shells dispersed in toluene. Complementary SEM pictures of the dried particles treated with visible and UV light are shown in Figure 13.

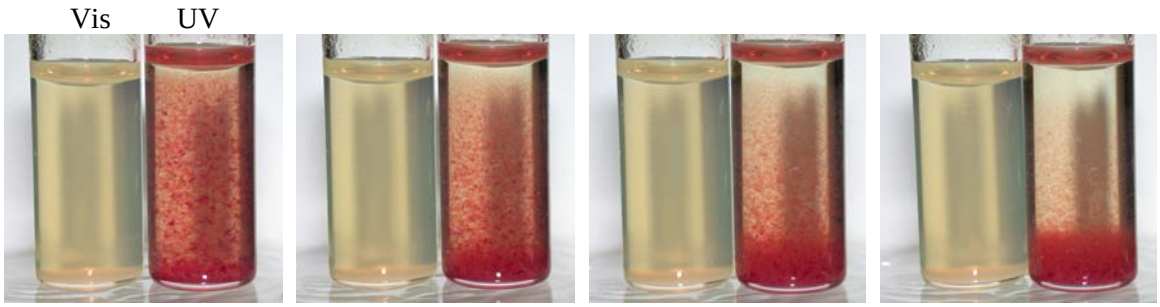

Figure 12 Aggregation/sedimentation behavior of 927 nm silica core particles modified with 24.9 nm thick SPMMA-co-MMA (20% SP content) shells and dispersed in toluene. For the specific conditions employed in the surface initiated polymerization see entry 21 in Table 11. The vial on the left has been irradiated with visible light (> 450 nm) for 10 min. prior to the measurement. Similarly, the vial on the right has been treated with UV light (365 nm) for the same amount of time. Both vials have been mixed for 10-15 sec. and sedimentation time was measured following this treatment.

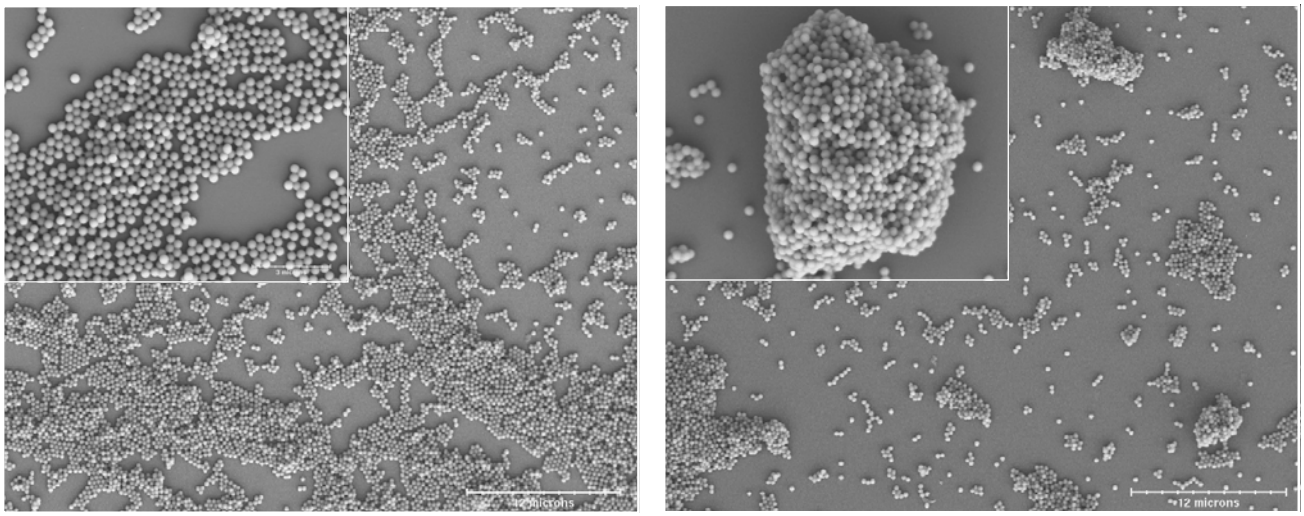

a **b**

Figure 13 SEM micrographs of 284 nm silica core particles modified with 26.2 nm thick SPMMA-co-MMA (20% SP content) shells after dispersion in toluene and (a) visible light irradiation, or (b) UV light exposure. For the specific conditions employed in the surface initiated polymerization see entry 8 in Table 11, while for the treatment of toluene dispersions see Figure 12 caption. The samples were withdrawn 5 min. after light irradiation and immediately dried on graphite support. Inserts in the figures show close-ups of the dried films.

As can be seen from Figure 12, colloidal particles modified with SPMMA-co-MMA brushes and dispersed in toluene aggregate and sediment following UV light exposure. Stable dispersions were recovered following irradiation with visible light ($\lambda > 450$ nm) and short sonication (< 1 min), although vigorous shaking was sufficient at times. Instead of visible light treatment, heating a sample (15-30 min. at 60°C) or leaving it in darkness for more than 3 hours followed by gentle sonication or vigorous shaking also produced stable suspensions. This photocontrolled aggregation behavior was observed in benzene and o-xylene as well. The particles flocculated slower and to a lesser degree in benzene, while o-xylene

dispersions were unstable even before the UV light treatment. In this both cases, however, a notable enhancement of sedimentation rate was recorded.

The SEM photomicrographs in Figure 13 show obvious differences in the dried particle structure. In the colloidally stable case (no UV exposure), the particles have sedimented into monolayers in which a low degree of hexagonal close packing can be seen, with a significant number of flaws, and higher layers do not appear structured. Some studies of opal formation show that a drying front moving across a substrate can sweep particles into ordered networks, and this phenomenon may be causing the modest hexagonal packing visible in these SEM pictures. In contrast, particles exposed to UV light have a distribution of low agglomerate number particles or singlets, and large, unstructured particle aggregates. The large aggregates will undoubtedly sediment rapidly as visually observed, but it is also clear that the singlets were present in solution and were not incorporated into the aggregates. This suggests that the mechanism of particle aggregation may be more complex than a simple non-wetting condition in the photo-modulated co-polymer layer.

The most likely explaination for the UV induced flocculation is a significant polarity increase of the colloidal particle surfaces in contact with the border-line solvent. Specifically, decrease of the polymer-solvent interactions by generation of polar pendant groups markedly reduced the solubility of polymer brushes in non-polar medium causing the observed aggregation (). It should be mentioned that while MC-SP and MC-MC molecular coupling reactions accompany SP to MC isomerization (Section 2), it is unlikely that these very weak associations could bring about the phase transition. The presence of the singlet particles in the UV switched samples may relate to the kinetics of aggregation and diffusion of particles to growing nuclei. As the singlets appear stable, there may be either a kinetic window for aggregation between particles (as SP units are photo-switched), or the particles may adhere to the substrate and are therefore not pulled into the aggregates during sample preparation. Additional studies of sedimentation structure are presented in Section 4.

Sedimentation of particles in solvent series and in each photo-switched state

A series of sedimentation experiments was conducted to examine the role of the solvent polarity in controlling the transition from a colloidally stable to unstable state based on photo-switching of the spirobenzopyran moieties. In addition to toluene, the particles were dispersed into p-xylene, o-xylene, cyclohexane, benzene, anisole and THF. Rapid flocculation was observed in p-xylene and cyclohexane under both visible and UV light. On the contrary, anisole suspensions remained stable regardless of the treatment. In THF, toluene, benzene and o-xylene, UV irradiation enhanced colloidal aggregation and sedimentation rates. This behavior is illustrated in Figure 14 with the absorbance of 0.5% v/v colloidal dispersions plotted against time. The 927 nm silica core particles with 24.9 nm thick SPMMA-co-MMA (20% SP content) copolymer shells were used in these experiments. Prior to each measurement, dispersions were sonicated for 2 min and then additionally mixed by hand for 2 min following 15 min exposure to UV or visible light. The absorbance was recorded at a distance of 32 mm from the bottom of a 75 mm tall cylindrical cell (cell volume = 30 ml) using a Hach 2100AN turbidimeter equipped with a $\lambda > 740$ nm optical cutoff filter. The beam diameter was 6 mm. Samples were carefully removed from and replaced into the cell compartment every 15-20 min to be treated with UV or visible irradiation for a period of 1 min. Special care was taken to conduct all measurements in the same fashion. As can be seen from the Figure 14, a modest sedimentation rate enhancement was observed in the case of THF and o-xylene dispersions (*i.e.*, sedimentation was ≈1.1× faster in THF and ≈6× faster in o-xylene). However, while the particles remained well stabilized in more polar THF, they were strongly aggregated in non-polar o-xylene. The strongest photo-activated flocculation response was recorded in toluene and benzene, although sedimentation rate post UV exposure increased more in the former case (*i.e.*, sedimentation was ≈16× faster in benzene and ≈335× faster in o-xylene). This data reinforces the explanation given in the previous section that the UV induced flocculation is caused by a significant polarity increase of the colloidal particle surfaces in contact with the border-line solvent.

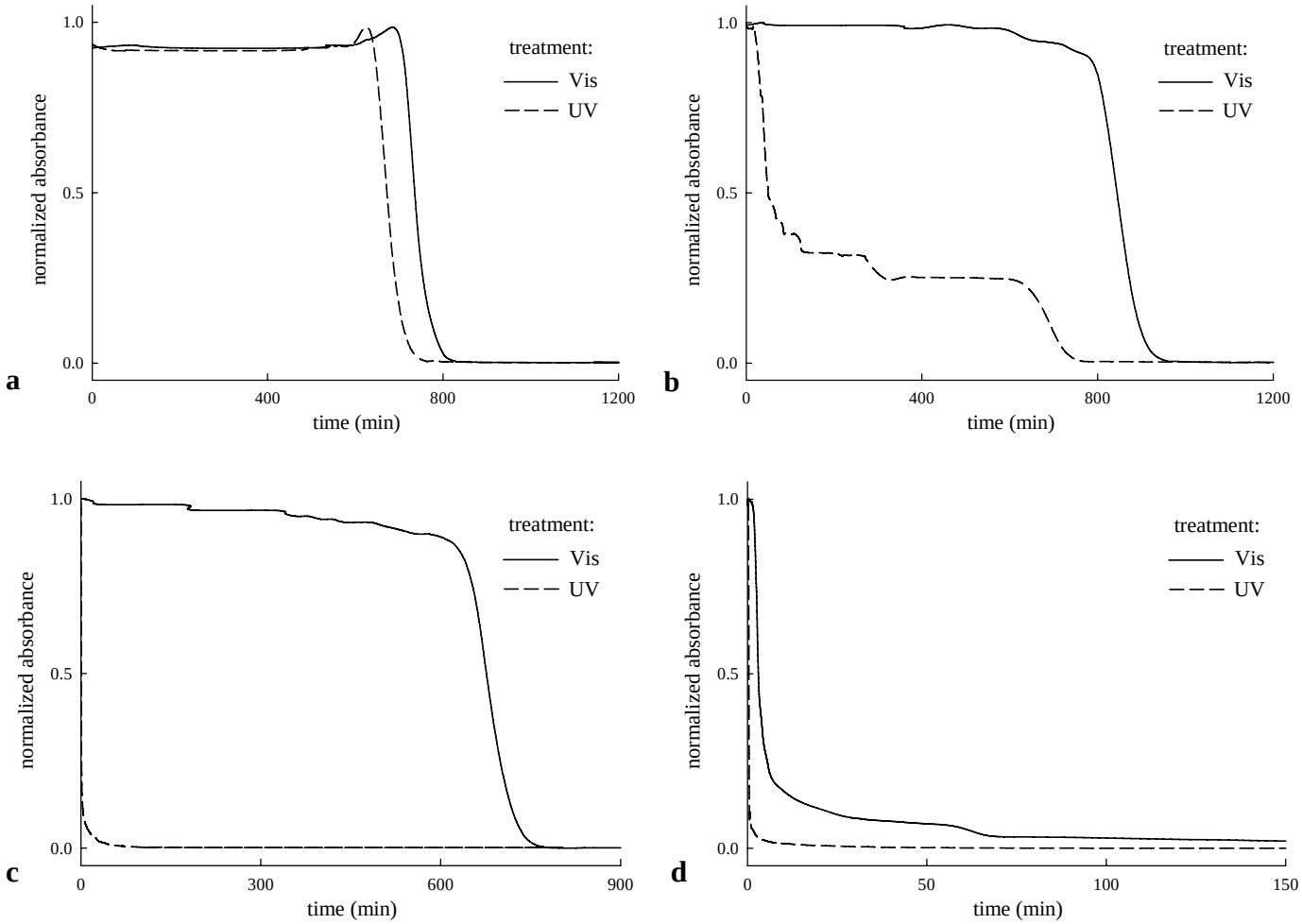

Figure 14 Sedimentation behavior of 927 nm silica core particles modified with 24.9 nm thick SPMMA-co-MMA (20% SP content) shells and dispersed in (a) THF, (b) benzene, (c) toluene, and (d) o-xylene. Prior to each measurement, 0.5% v/v dispersions were sonicated for 2 min and then additionally mixed by hand for 2 min following 15 min exposure to UV or visible light. The absorbance was recorded at a distance of 32 mm from the bottom of a 75 mm tall cylindrical cell (cell volume = 30 ml) using a Hatch 2100AN turbidimeter equipped with a $\lambda > 740$ nm optical cutoff filter. The beam diameter was 6mm. Samples were carefully removed from and replaced into the cell compartment every 15-20 min to be treated with UV or visible irradiation for a period of 1 min.

Photocontrolled rheological behavior

The modification of particle-particle interactions in concentrated dispersion can dramatically alter its rheological properties. Here, the reversible photocontrol of particle attractions (*i.e.*, attractive interactions are 'turned on' upon UV light exposure and 'turned off' following visible light irradiation, or thermal relaxation) translates into a reversible viscosity change of the colloids modified with SP-co-MMA polymer brushes and dispersed into non-polar medium. Figure 14 illustrates such a control for 927 nm core silica particles with 24.9 nm thick SP-co-MMA (20% SP content) shells dispersed in toluene at a concentration of approx. 30% v/v. The experimental details are given in the figure caption.

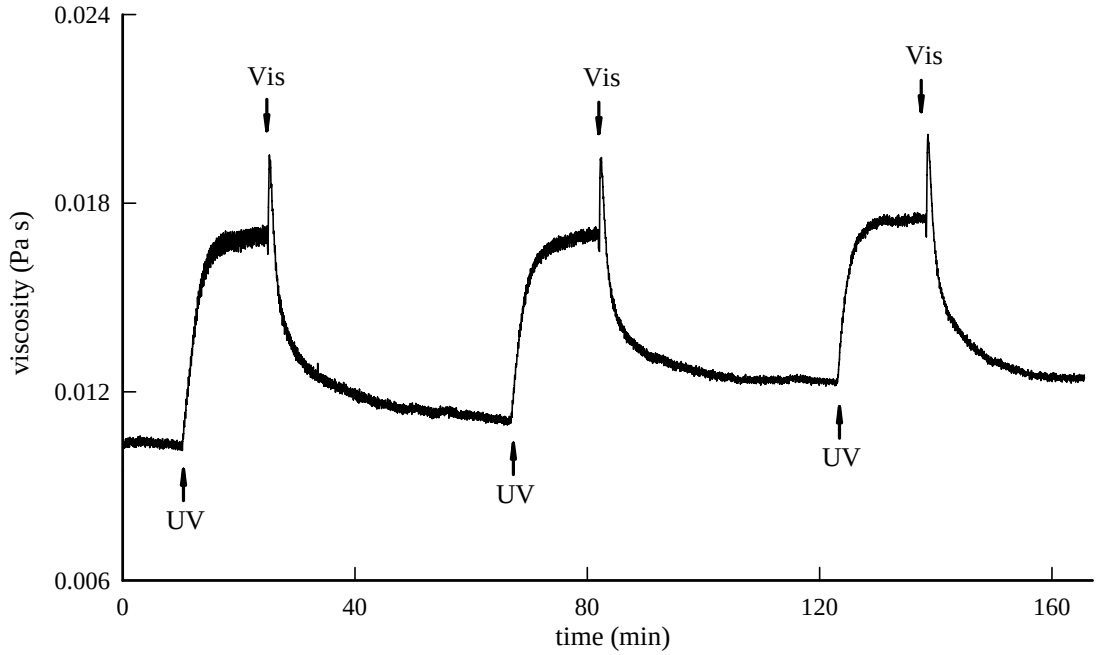

Figure 15 Photocontrol of suspension viscosity for 927 nm silica core particles modified with 24.9 nm thick SPMMA-co-MMA (20% SP content) shells dispersed in toluene at ≈30% v/v. For the specific conditions employed in the surface initiated polymerization see entry 21 in Table 11. The viscosity vs. time measurement was performed on a RheoStress 300 instrument (Thermo Haake) with a parallel plate geometry (plate diameter = 35 mm) and a gap width of 0.02 mm. The applied shear rate was $\dot{\gamma}$ = 1200 s^{-1}. The UV and visible light irradiation of the sample were carried out through the bottom, immobile plate using a custom-made attachment also equipped with a solvent trap. A 200 W Hg lamp (Oriel) was utilized for sample irradiation with appropriately chosen filters (*i.e.*, λ = 365±10 nm bandpass filter for the UV irradiation and λ > 475 nm cutoff filter for the visible light exposure).

In this case, the suspension viscosity (η) could be reversibly modulated by approx. 50% (*i.e.*, on average the viscosity increased from 0.011 Pa*s to 0.017 Pa*s upon the UV treatment) through successive sample irradiation with UV and visible light. As can be seen from the figure, the first cycle of UV/Vis treatment yields slightly larger viscosity change than later cycles. This was true of most samples investigated and might indicate that the initial network structure formed under equilibrium conditions differs from the one formed during shearing and visible light exposure. In the following 3-6 cycles, the observed viscosity changes (Δη) were approximately constant and η typically returned to its baseline value. At longer times, however, sample fatigue became apparent with η steadily increasing after each successive UV/Vis cycle. This could be attributed to drying effects, particle sedimentation or formation of strongly bound aggregates, which could not be broken at the employed shear rates. Moreover, it was found that cycling time could be reduced significantly by using a stronger light source (*e.g.*, 500 W Xe(Hg) lamp), reducing the plate-plate gap width, or decreasing particle concentration in the suspension. These observations suggest that the rate controlling step for viscosity modulation in the present system is the penetration of light through opaque colloidal dispersion.

The reversible viscosity changes observed here differ mechanistically from the analogous phenomenon reported for the SP-co-MMA copolymer solutions ([119,123,130,131,132,246]). In the former case, the particle-particle attractions drive the colloidal phase transition and ultimately cause the viscosity to *increase* upon UV irradiation. In the case of polymer solutions, the viscosity is *reduced* following UV treatment due to the polymer chain conformational change (*i.e.*, shrinkage).

Conclusions

A silica colloidal system demonstrates reversible photo-controlled agglomeration in toluene, through the grafting of spirobenzopyran methylmethacrylate polymer layers. The photo-induced aggregation is reversible, with the requirement of agitation to redisperse the colloids after aggregation. A large number of cycles can be used with reproducable results in this system. The system demonstrates interesting agglomeration behavior with high sensitivity to solvent polarity. Particle systems have photo-sensitive rheological responses, which are limited by the opacity and optical attenuation of the particle system. The rheological response of the suspension is related to the aggregation events between colloidal particles, and is opposite to the response of a polymeric solution. The material system presented here shows photo-physical effects with the potential to provide remote patterning of particles, directed deposition of particles in micro-fluidic networks, and the development of non-close packed particle architectures (leading to unique optical phenomena).

Section 4

Aggregation and Structure of Photo-Controlled Colloidal Particles

Abstract

Silica particles were derivatized using atom transfer radical polymerization to synthesize surface layers of poly(methyl methacrylate containing 20% spirobenzopyran). The aggregation and sedimentation behavior of the polymer-modified silica particles in toluene were studied using confocal microscopy. Additional studies were performed with these particles in a flow cell configuration. The behavior of the particles under visible light and after exposure to UV light was examined. The UV stimulation causes the particles to aggregate in toluene, and the structure of the sedimented layers of the aggregates was characterized. Patterning of a sedimented layer was possible using sequential exposures of UV and visible light. Reversible aggregation and dispersion was not observed. The UV exposed particles require the input of additional energy to become disperse, and reversible "melting" of an aggregate was not possible in this system. Preferential adhesion was observed between patterned vs. unexposed substrate areas in the flow cell configuration with a specificity factor up to 10.8.

Introduction

Self-assembled colloidal systems are of commercial interest for the potential fabrication of low cost photonic lattices. Photonic crystals possess the ability to forbid photon transport for certain bands of frequencies regardless of polarization and propagation direction. This, in turn, leads to the potential for a complete photonic band gap. Due to this property, photonic crystals are desired for many applications. For example, silicon is being used as the dielectric material in the optical-communications industry. More specifically, these crystals are being used to transfer information faster and more efficiently through optic fibers at different optical wavelengths, a method known as dense wavelength division multiplexing (DWDM). Photonic crystals are also being used to make narrow-line width lasers that are also used in optical-communication devices.

There are two primary classes of colloidal structures which that are ordered in nature, and they are distinguished by their formation mechanism. The first class is termed a colloidal crystal array (CCA), and is formed from particles having strong electrostatic repulsion in extensively deionized water[247]. These particles assume an ordered structure separated by relatively large interparticle separations, and the structure is fixed by the reaction of an organic monomer to form a gel (example: polyacrylamide). These materials can be deformed using mechanical stress and have shown control over the bandgap wavelength based on the deformation[248]. The second class is termed a photonic lattice (PL) and is formed by a dilute suspension of monodisperse colloids which crystallize during the concentration of the particles. The modes of concentrating particles include sedimentation, centrifugation, electrostatics, capillary action at a drying interface, and forced filtration. Ultrasonic vibration is also employed to assist the crystallization process in some cases. In either route, the primary obstacle to formation of high quality materials is the uncontrolled presence of defects. These defects affect the photonic structure, and control over the placement, quantity, and orientation of defects is a significant achievement in formation of device quality photonic materials. Methods to control the formation of colloidal crystal arrays require a transition in the volume fraction of particles within a kinetic processing window. Rapid coagulation/concentration of particles leads to an amorphous structure, and extremely slow coagulation promotes multiple crystal nucleation events and a high defect density.

In this study, particles have been derivatized with polymers containing photo-switchable organic moieties which create a large change in dipole moment. Exposure to UV light causes the particles to aggregate rapidly in toluene and sediment quickly. These particles are monodisperse and have the

potential to form ordered structures. By study of the aggregation of these particles and their sedimentation structure, the potential for formation of photonic lattices which can undergo the formation of controlled defects or removal of these imperfections via "zone refining" can be tested.

Background

This section is being included to provide an understanding of the formation of ordered colloidal networks that produce an optical response. Colloidal crystals are used to achieve either two or three-dimensional lattices out of a variety of materials, which is attractive to researchers. There are three main types of particles that are found in colloidal crystals: organic particles (i.e. polystyrene latex microspheres, emulsion droplets), inorganics (i.e. TiO_2, SiO_2, metals), and biomolecules (i.e. proteins, protein-lipid complexes, DNA). Different particles are used depending on the application of the colloidal and photonic crystal. An important property for successful crystallization is monodispersity of the colloids. Their size distribution must vary by less than 5%, and the particles must be spherical and stable to aggregation at close approach. Colloidal crystal systems also assume nearly the most thermodynamically stable form possible; the FCC lattice. However, stacking faults are a common problem that can lead to random close packed structures or hexagonally close packed structures. There are very few examples of other crystal structures that have been formed, but using separate populations of particle sizes allows for the AB_2 and AB_{13} structures to be formed.

The crystallization process is thermodynamic in nature, and in these particle systems it is dominated by entropy. Phase diagrams for particle systems have been calculated based on the interaction between two spheres, such as a hard sphere system (no interaction beyond hard wall repulsion) and short range attraction (van der Waals association). In hard sphere systems, particle interactions are similar to phases of materials. Below 0.494 volume fraction, the system behavior is gas-like, at 0.545 volume fraction there is a solid transition, and the glass transition occurs at 0.58 to 0.60 volume fraction[249]. In the regime between the gas and solid states, there is a region of two phase coexistence. Rapid increase in volume fraction of particles leads to the glassy phase. In systems with short-range attraction, the glass transition is always near the fluid-two phase boundary and slightly above it[250]. For short range attraction, the crystal region can produce a "repulsive" crystal (where separation distance is larger than the attraction), and an "attractive" crystal (in the attractive well), as well as glass phase. In order to form crystals, the system must operate within the 2-phase low-density fluid-crystal coexistence regime, but below the glass curve (i.e. lower particle concentration). By nucleating to the left of the glass curve, it is possible to enter the crystalline region non-adiabatically and avoid glass formation. It is necessary to exclude the 2-phase region, as the formed crystals will not be of high quality. This leaves only the region to the right of the glass curve, to the bottom by phase separation, and to the top by the gas-side of the gas-crystal phase-coexistence as the likely region for forming good crystals. This suggests that for a fixed short range of interaction, there is a "practical crystallization region" in the temperature-density plane, and there is a limited regime of interaction ranges where the slot is accessible experimentally. This is given as regime I in Figure 6 of reference 161. The exact range of the attraction is relative to the particle diameter, and the parameter given (b=30) does not seem to be directly explained, but it is short-ranged. The screening parameter relates to an exponential function (-b), and is in units of reciprocal of the hard-core diameter.

For the behavior of the crystallizing system, the ratio of the attractive to the repulsive range is described as the important parameter[251]. For a large ratio, typical behavior of a van der Waals fluid is obtained. When the range of the attraction narrows, the glass transition at 0.48 becomes temperature dependent and moves to lower density. A separate and distinct glass driven by short range attraction is formed and can exist in metastable equilibrium with the repulsive glass. Particles in the short-range attractive fluid benefit only while they are in each other's attractive well.

The process of nucleating a (single) crystal region and growing an ordered colloidal film is a difficult process based on kinetic constraints of controlling the phase space of increasing particle concentration. Operationally, there are additional concerns with surface defects, solvent-substrate wetting,

evaporation rates, and the kinetics of nucleation and growth. Observation of the nucleation and growth of colloidal crystals on substrates have been performed using confocal microscopy[252]. Laser scanning confocal microscopy used to observe direct imaging of nucleation and growth of crystalline regions. Nuclei were rough surfaced and the same structure as the solid phase. The surface tension of the critical nuclei was determined to be $\gamma \sim 0.027 k_B T/a^2$ and agrees with density functional theory and hard sphere systems. The nucleus was modeled as an ellipsoid rather than as a sphere. Nucleation is favored near a wall due to attractive interactions between the spheres and the wall and image charges in the surface[253]. This helps explain the formation of higher particle concentrations near the wall and 2D hexagonal layers before 3D crystals are formed.

Routes for forming colloidal crystal arrays and examples

There are several approaches for creating a slowly increasing concentration of particles so that crystallization will nucleate and grow to form a near single crystal photonic lattice. The longest known process utilizes sedimentation of a dilute particle suspension to concentrate the particles. The process can take extremely long times (months) depending on the particle size and density mismatch with the solvent. Weak centrifugation can be employed in some cases, but the films are generally not well controlled, and can be polycrystalline. There is another example using electrophoresis with conductive substrates, and it requires particles with significant electrostatic charge[254]. Nanoparticles are claimed to be infiltrated using the same procedure. A patterned conductive electrode under UV light creates a current and field gradient and sweeps particles into exposed areas[255]. Domain sizes are 10-20 microns in this method, which prevents long range application.

A more common technique in evaluation uses convective evaporation to initiate and grow colloidal photonic lattices[256,257,258,259]. A particle suspension is allowed to evaporate with a highly wetting slide vertically immersed in the suspension. As the evaporation rate is more rapid in the thin meniscus, convection currents provide a flux of particles into the rapid evaporation zone. These particles can crystallize due to the capillary forces in partially immersed spheres and create films based on the evaporation rate and the particle concentration. The time for evaporation must be slow, causing the process to take several days. Particle stability is again a critical factor, as adhered particles behind the drying front lead to poor meniscus properties and optical flaws257. A method using horizontal samples and applied ultrasonic power to increase uniformity has also been demonstrated, but has not found widespread use due to problems with wetting behavior[260].

Another popular technique utilizes forced filtration[261], in which the substrate and cover plates are separated by a spacer membrane, and microchannels are etched in the spacer to allow for solvent to be filtered but trapping the particles. Application of ultrasonic vibration is also used to promote crystallization. It is relatively fast, has good control over the number of layers, and works for numerous aqueous suspensions. Similar approaches utilize microchannels and either electrocapillarity or evaporative convection of the solvent to order particles in the microchannels[262,263]. These methods have the advantage that the width of the channel can assist in forming a more perfect array of particles, and thereby improve optical characteristics.

A route that is less investigated applies the phase transition of polymers to the control over volume fraction of the particle phase[264]. This approach is similar to that of electrostatically stabilized colloids, in that the particles are not in direct contact. In this case, poly(N-isopropyl acrylamide) microgels are used to act as surface responsive polymers based on thermal transitions in conformation and effective size. The polymeric phase acts to slow crystallization growth kinetics for the electrostatically stabilized silica spheres.

As discussed, crystalline perfection is critical to evaluate for optical properties. Image analysis can be applied to calculate scattering functions and perfection for these lattices, but may be time consuming[265]. A significant requirement for forming devices using colloidal photonic lattices is incorporation of high index of refraction materials such as nanoparticle titania or active materials like organic dyes. There are examples of forming photonic lattices using mixtures of templating particles and

nanoparticles[266,267]. Crystallization is very slow, and defects such as grain boundaries are more prevalent. Active materials containing polymeric dye modified polymers have been evaluated in photonic lattice systems. The photonic structure has proven capable of creating a strong emission directionality preference in transmission, and may prove applicable to LED applications. Overlap of the dye emission band and the stop band of the PL affects the emission as (1) PL intensity is suppressed at the stop band (2) the PL spectrum acquires an angular anisotropy in agreement with angular dispersion of the stop band of the PL (3) the emission excited through the back surface has a frequency-dependant directionality resulting from interference conditions for radiation at different frequencies (4) the ASE band appears at the stop band edge, likely from electronic and photonic interplay of stop-band structures.

All these routes contain a common purpose of increasing particle concentration is a controlled manner to nucleate a crystalline region followed by growth processes. As the initial materials are constrained by requirements of sphericity, monodispersity in size, and colloidal stability, they are typically used as templates for the infiltration of high index of refraction materials in the form of nanoparticles, sol-gel precursors, or electrodeposited materials. If the materials have active photonic properties such as fluoroescence, the photonic lattice does affect optical properties through optical interferrence behavior. Of all the routes applied to control of these properties, none are externally directed and allow for real-time control or patterning. The development of such a system will provide a significant advance to the technology for forming colloidal photonic lattices.

Experimental

Synthesis of polymerically derivatized photo-sensitive particles has been detailed previously. In these studies, silica particles of 284 nm and 927 nm diameters have been derivatized with poly(methyl methacrylate) polymer containing 20 mol % spirobenzopyran units. The polymer layers were grown using ATRP synthesis, and the details have been given previously. The layer thicknesses of the polymer coating are 5% of the radius for the 1 micron particles, and 21.4% of the radius for the 284 nm particles. These particles have demonstrated reversible aggregation in toluene after successive UV/visible light treatment.

Sedimentation of the particles was studied using confocal microscopy at UIUC. It should be noted here that due to the very weak fluorescence signal of the SP/MMA particles, the confocal microscopy imaging was performed in reflectance mode. Therefore, the number of particle layers that could be imaged reliably was limited to approximately 10-15 for the 927 nm colloids. Moreover, extracting quantitative information such as particle center of mass from the obtained images was not possible due to strong scattering signal from the neighboring particle layers. Finally, 284 nm particles could not be resolved adequately and most of the experiments were carried out with larger, 927 nm spheres. Tests were performed using these particles without UV exposure and following UV exposure.

Routes for forming colloidal crystal arrays were attempted in non-aqueous solvents, including tetrahydrofuran (THF), toluene, and anisole. The sedimentation, forced filtration, and dip coating routes were attempted. Prior to forced filtration cell assembly, the Mylar spacers (12 micron thick) were dipped in 0.01 vol.% THF dispersion of 927 nm or 284 nm SP/MMA modified colloids. The cells were assembled with the Mylar spacer still wet from the coating suspension. Similar results were obtained, however, when the spacers were coated with other silica particles (as long as these were smaller than the particles being crystallized) or not coated at all. After assembly, solvent was pushed though each cell edge sequentially until all of the trapped air bubbles were washed away. Dispersions introduced into the cells after this procedure were typically 0.25 vol.% (in this case, the tube holding colloids needs to be at least 6 cm in height and 0.5 cm diameter in order to supply enough particles to fill the cell completely), although 1 vol.% dispersions gave similar results. While 1 micron colloids filled the cell completely in approx. 1 day, the 284 nm particles clogged the cell after approx. the same time preventing its complete filling.

Patterning was examined using the confocal microscope and a UV beam on polymer coated surfaces and particle sediments. Particle adsorption during sedimentation was studied on these patterned surfaces.

Results

Xia Cell Experiments, Particle Monolayers and Sediment Structure

Attempts to create crystals out of SP/MMA coated silica particles suspended in tetrahydrofuran (THF), toluene or anisole were mostly unsuccessful. Both sedimentation and Xia cell methods yielded random-closed packed structures with either 284 nm or 927 nm diameter particles. Representative confocal microscopy pictures of the formed structures are shown in Figures 16 and 17.

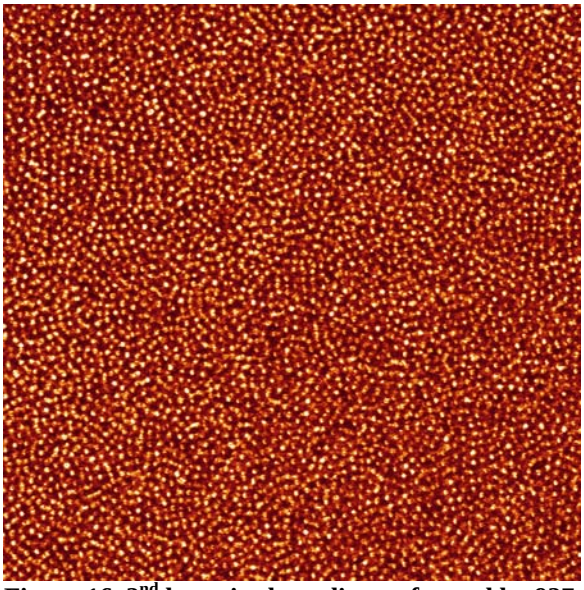

Figure 16 2nd layer in the sediment formed by 927 nm SP/MMA particles.

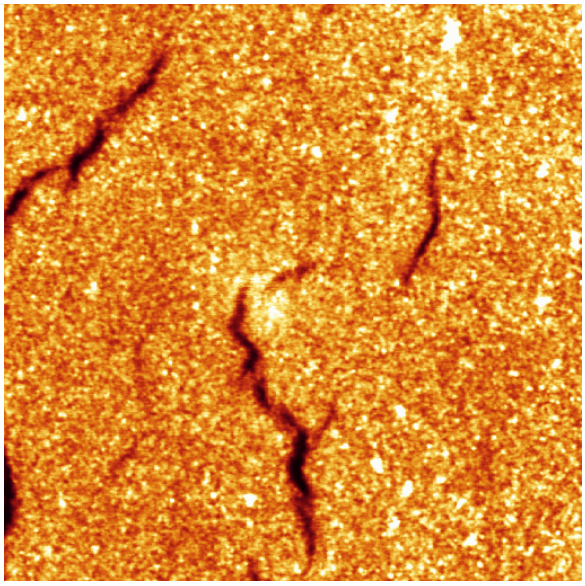

Figure 17 cross-section through Xia cell made with 284 SP/MMA particles.

Only in one case (out of 20 attempts), did forced filtration yield opalescent regions within a cell formed from 1 micron colloids. Because a thick microscope glass slide was used for a substrate, however, analysis using confocal microscopy was not possible.

Dip coating of clean glass slides and octadecyltrichlorosilane (OTS) treated slides from SP/MMA particulate suspensions yielded sub-monolayer crystalline domains as shown in Figure 18. Obtaining an ordered area with at least 2-3 layers colloids was very difficult when using THF, toluene, or anisole as solvents.

Structure of sediment from 927 nm SP/MMA particle suspension in toluene was examined before and after UV irradiation. It was found that without UV treatment, sediments were dense and random close-packed. Upon UV irradiation, however, the sediments were comprised of loosely packed aggregates. Series of images in Figure 18 show cross-sections at various sediment heights (z) after 1 hour sedimentation time for 0.3 vol.% suspension with (right column) and without (left column) UV treatment. Figure 20 illustrates the reconstructed 3-D sediment structure (top images) as well as cross-section in the x-z plane (bottom images) for the data shown in Figure 18.

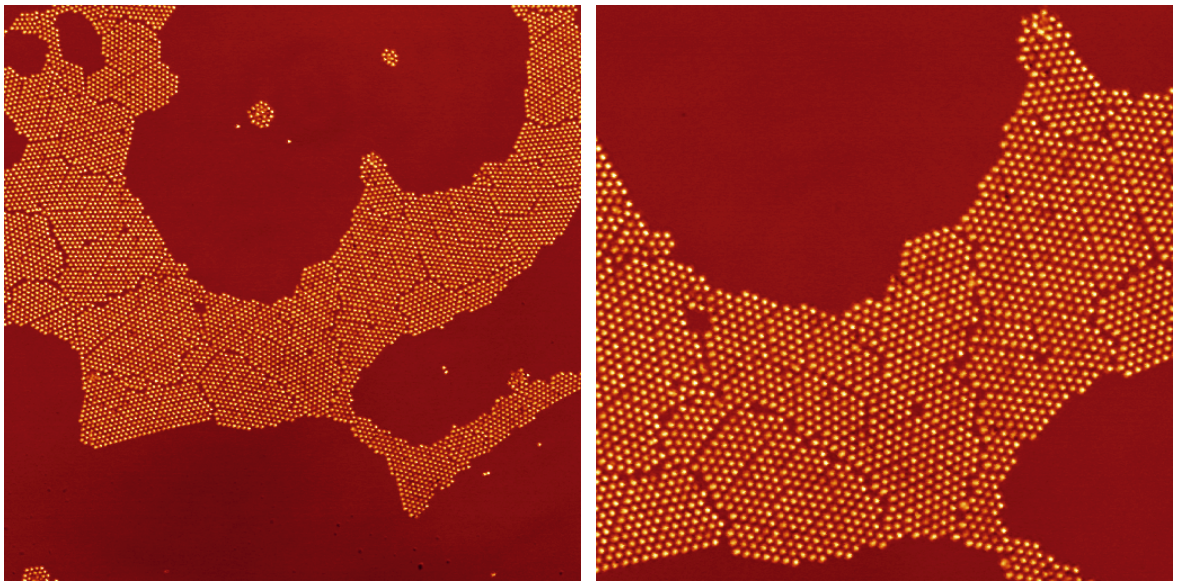

Figure 18 OTS treated glass slide after dip coating from suspension of 927 nm SP/MMA particles in THF at a concentration of 1 vol. %. The picture on the right is a higher magnification of the picture on the left.

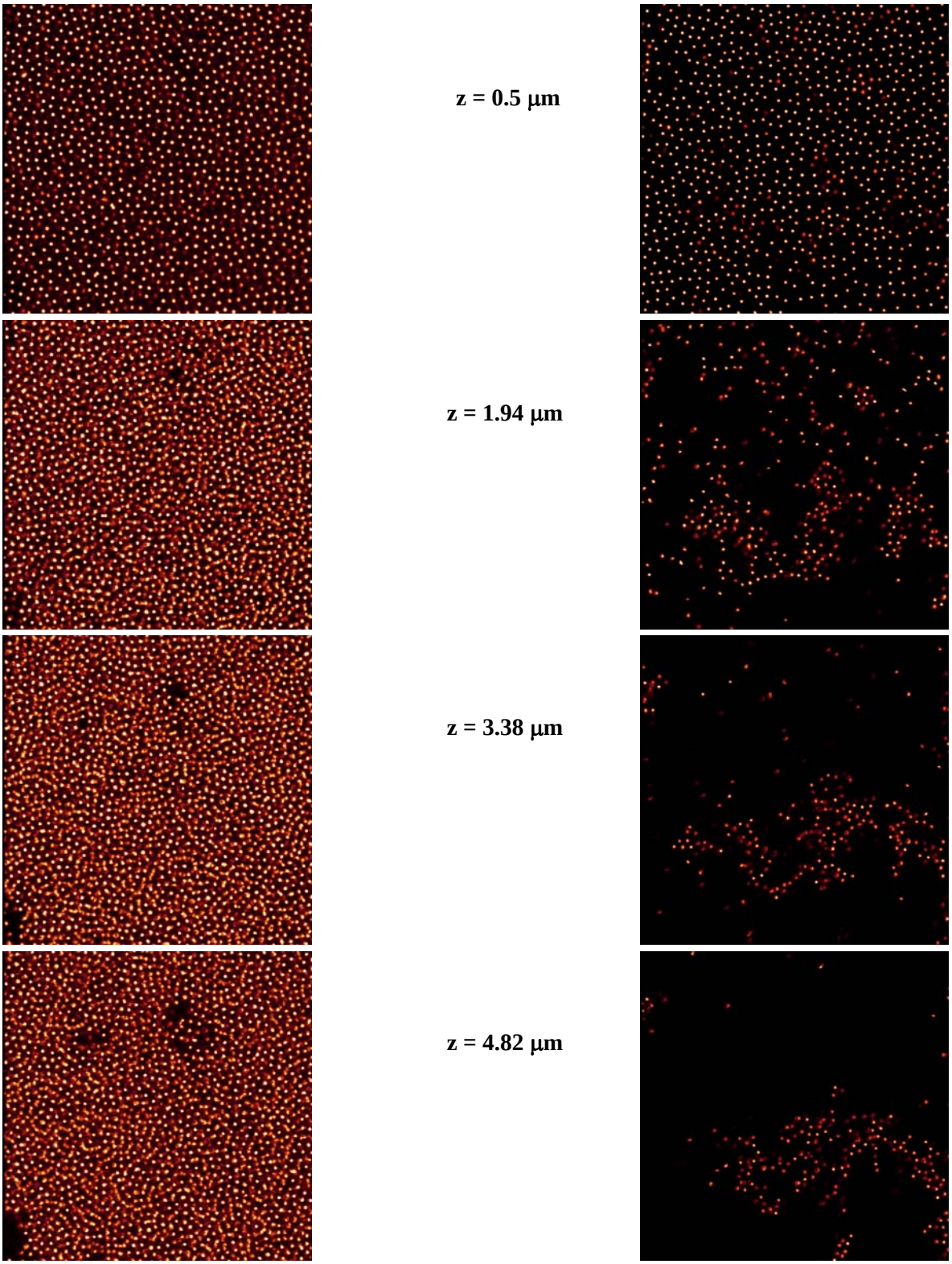

Figure 19 Cross-sections of sediment at various heights (z) for 0.3 vol.% suspension of 927 nm SP/MMA colloids in toluene after 1 hour sedimentation time. Left column - sample not exposed to UV irradiation. Right column – sample after 5 min UV irradiation.

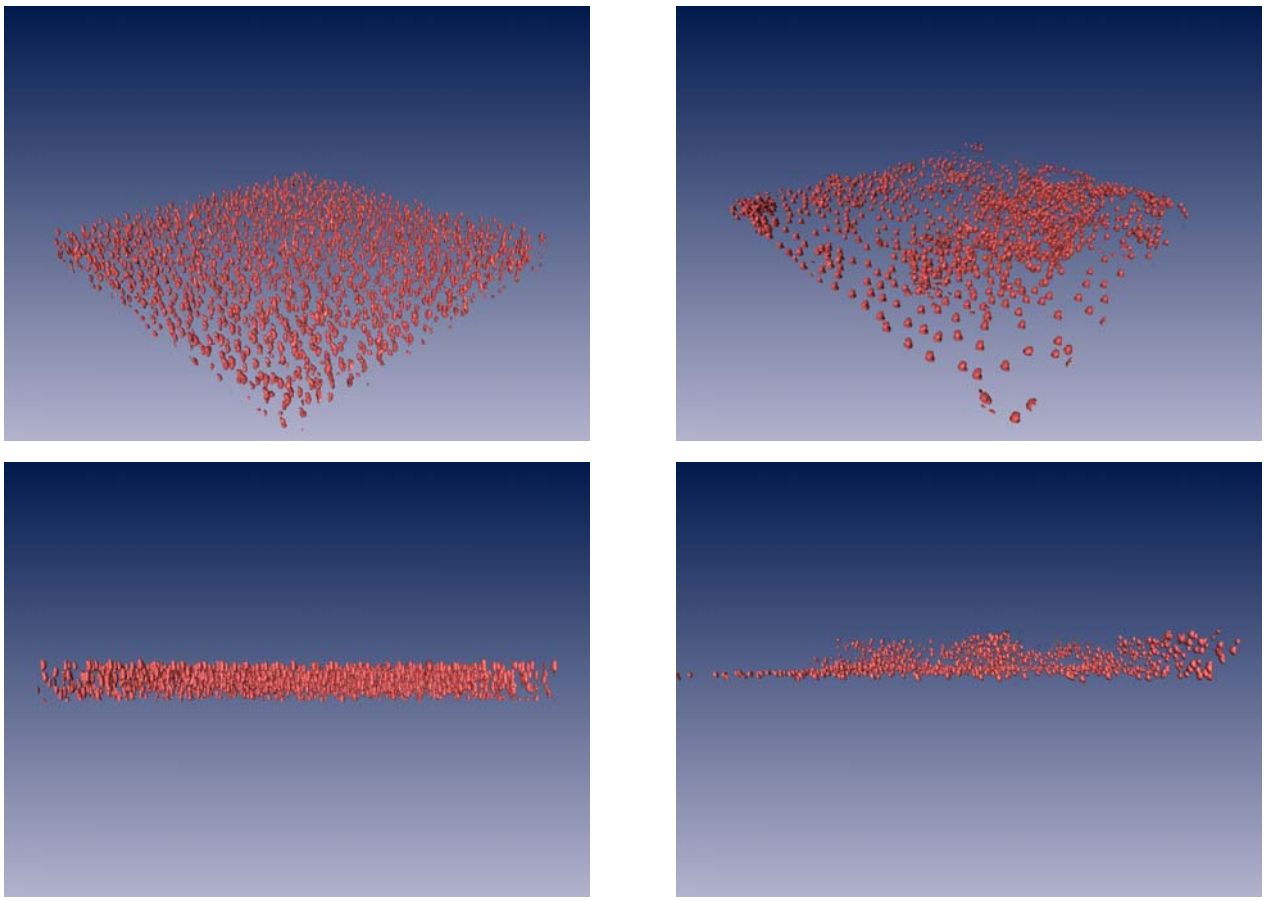

Figure 20 Reconstruction of 3-D sediment structure (top images) and x-z cross sections (bottom images) for 0.3 vol.% suspension of 927 nm SP/MMA colloids in toluene after 1 hour sedimentation time. Left column - sample not exposed to UV irradiation. Right column – sample after 5 min UV irradiation.

Pattern creation with UV beam in the SP/MMA particle structures

Due to the high two-photon cross-section of the spyrobenzopyran (SP) molecule, it was possible to direct switching of these molecules to and from the merocyanine (ME) form by using UV (λ = 353 nm) and visible (λ = 540 nm) irradiation. In this way, 3-D patterns of SP or ME species could be written into the SP/MMA structures. Series of images below shows a cross-section through a Xia cell made with 284 nm SP/MMA particles before UV irradiation (Figure 21a), after writing a box with UV beam (Figure 21b) and finally, after writing another, smaller box with visible light (Figure 21c). The observed contrast in the image between UV irradiated and untreated/visible irradiated regions comes from the difference in refractive index between the SP and ME forms.

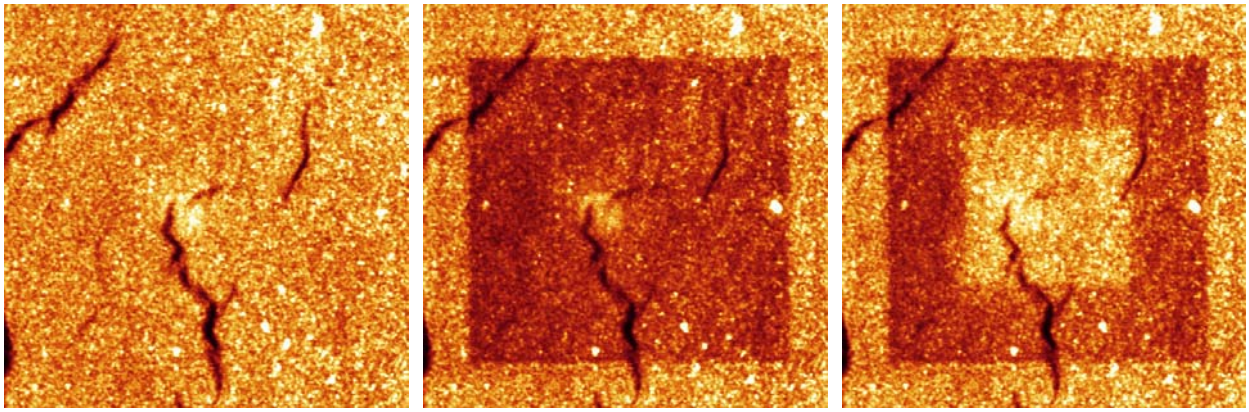

a **b** **c**

Figure 211 Cross-section through a Xia cell made with 284 nm SP/MMA particles (a) **before UV irradiation,** (b) **after writing a box with UV beam and** (c) **after writing another, smaller box with visible light. The sample was immersed in toluene.**

Similarly, Figure 22 below illustrates the same effect for 927 nm SP/MMA particles dip coated onto an OTS treated glass substrate.

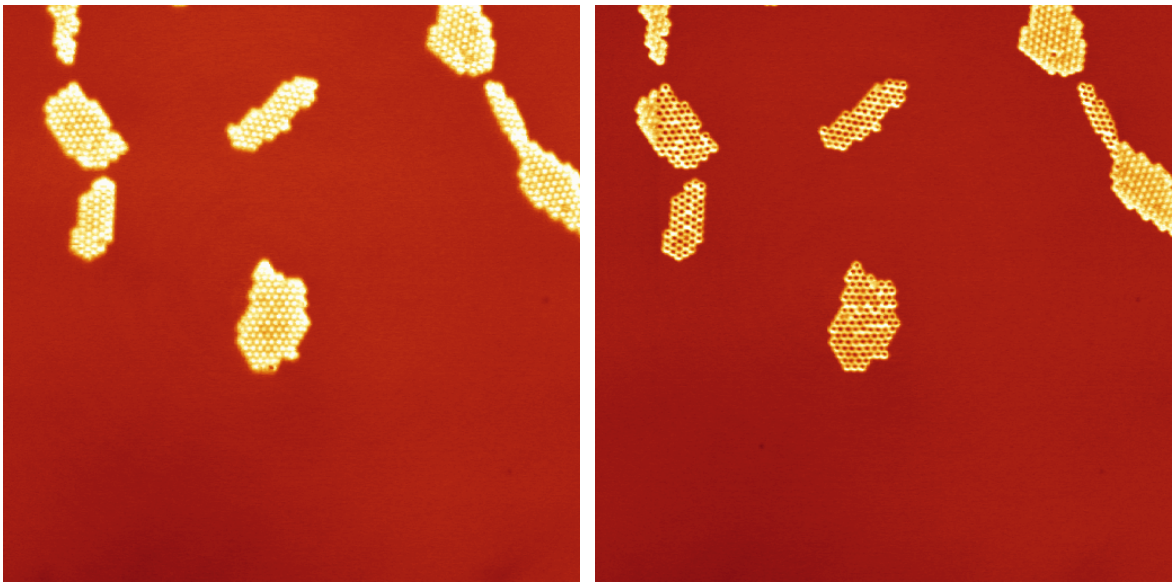

a **b**

Figure 222 OTS treated glass slide after dip coating from suspension of 927 nm SP/MMA particles in THF at a concentration of 1 vol. %. (a) **before UV irradiation, and** (b) **after writing a smaller box with UV beam. The sample was immersed in toluene.**

In summary, it was possible to locally carry out the switching from SP to ME forms and vice versa by using a laser beam at λ = 353 nm and λ = 540 nm. However, the expected changes in structure upon switching were not observed. In other words, while SP/MMA polymer layers are expected to shrink when exposed to UV irradiation and expand upon treatment with visible light, no evidence of this effect was found here. This could be due to the rather small polymer coating on the 927 nm colloids (i.e., coating thickness = 5% of particle radius). In the case of smaller, 284 nm colloids, although the coating thickness relative to the particle size was greater (i.e., coating thickness = 21.4% of particle radius), the resolution limit of the microscope prevented quantitative analysis.

Colloid Adsorption Experiments

Sedimentation of SP/MMA colloids from toluene onto SP/MMA coated surface was performed to determine whether particles adhere preferentially to non-exposed or UV exposed regions. As shown in the Figure 23 below, colloids appear to stick to the surface not exposed to the UV irradiation quite readily. Instead of diffusing over the surface for long periods of time, the particles appear to stick irreversibly only after short diffusion. In this particular case, a 927 nm SP/MMA colloid stuck to the surface after approximately 12 seconds.

In the case of UV irradiated surfaces the time frame for particle diffusion and adsorption was found to be slightly shorter. Figure 24 shows a diffusion and capture event for the same sample as in Figure 23, but after 5 minute UV irradiation.

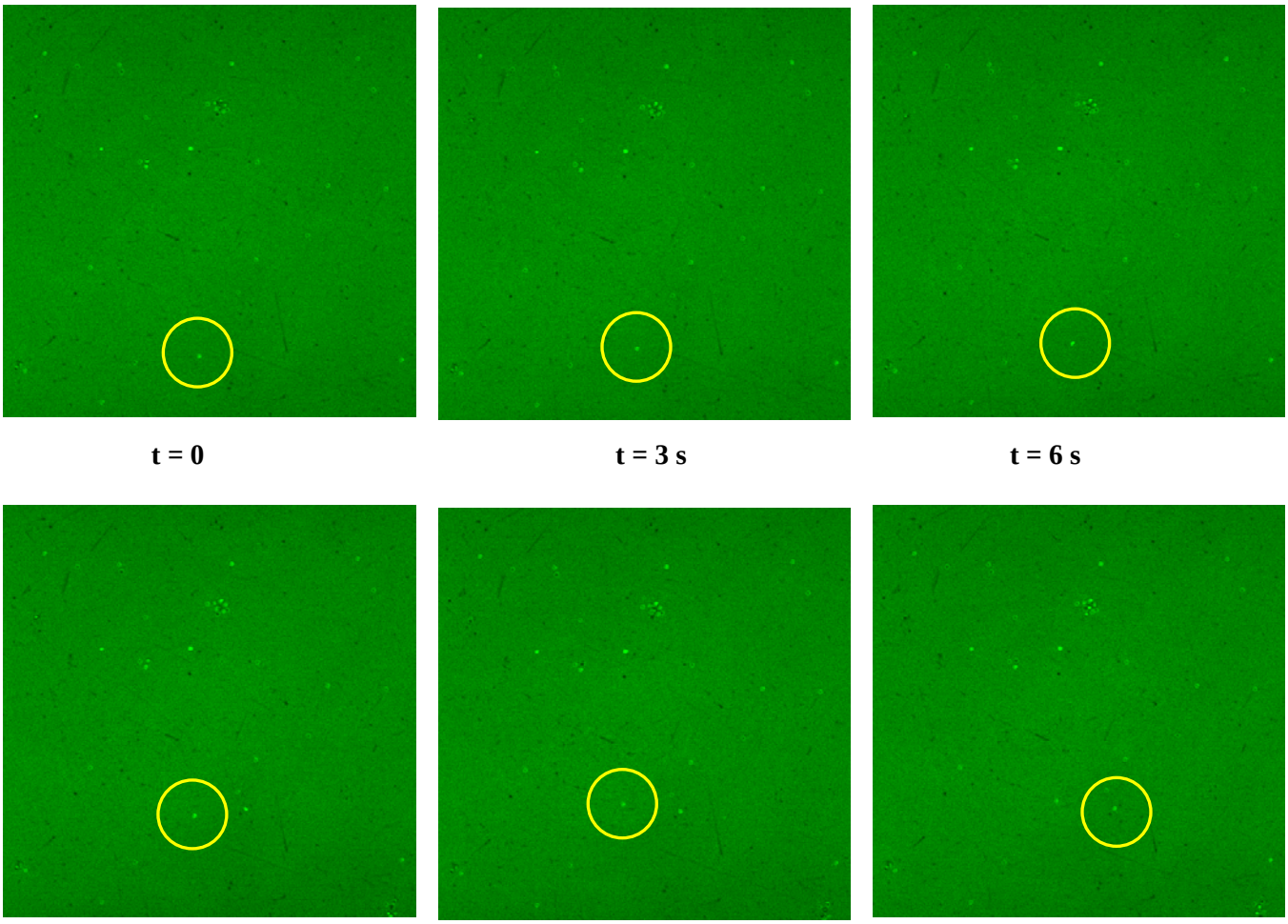

Figure 23 Sedimentation of 927 nm SP/MMA colloids from toluene onto SP/MMA treated surface. This time series data shows a colloid undergoing Brownian diffusion along a surface for approximately 12 seconds before irreversibly adsorbing.

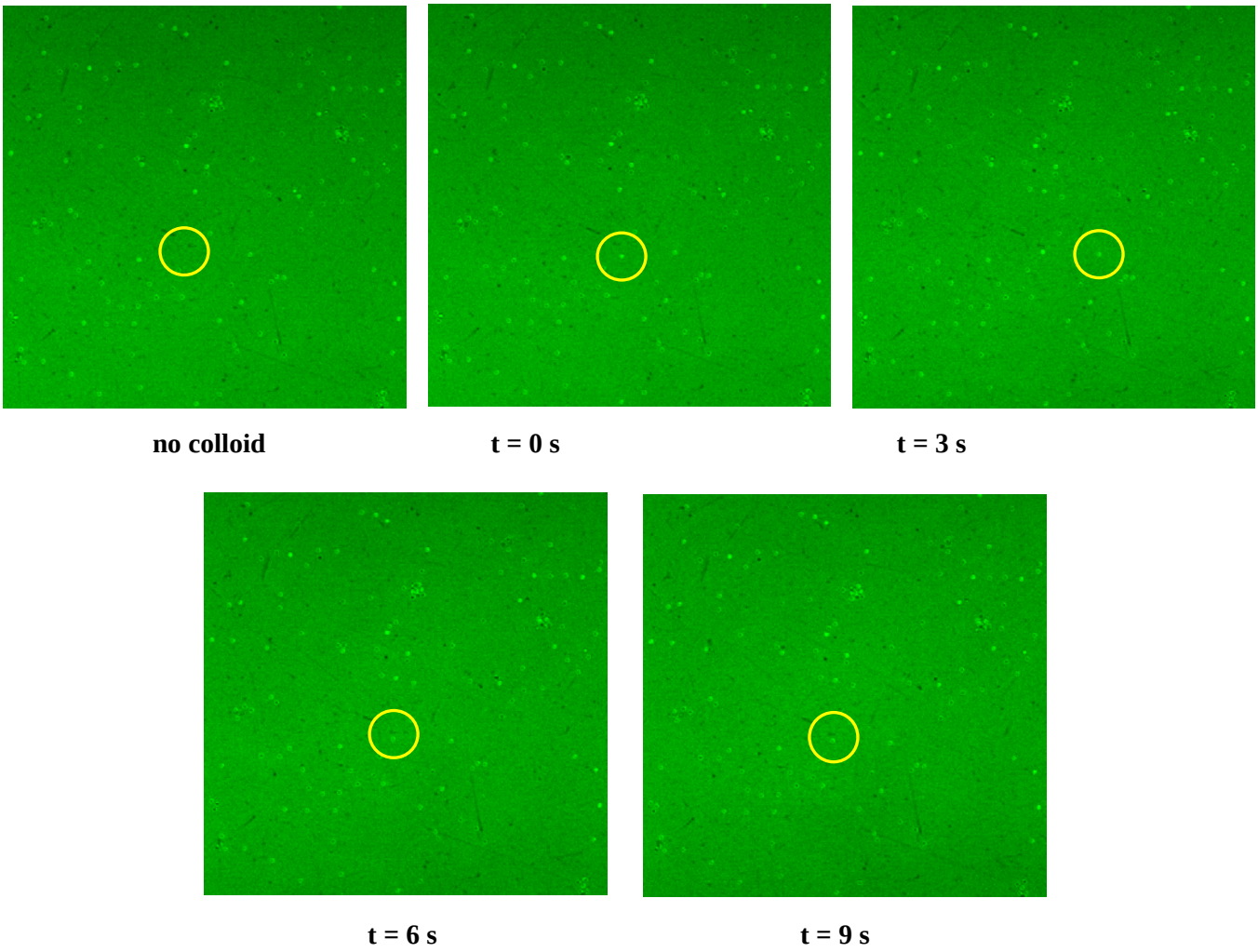

Figure 24 Sedimentation of 927 nm SP/MMA colloids from toluene onto SP/MMA treated surface after UV irradiation. This time series data shows a colloid undergoing Brownian diffusion along a surface for approximately 6 seconds before irreversibly adsorbing.

In order to further characterize the attraction between switched photo-chromic substrates and photo-chromic particles, adhesion tests were performed using an enclosed cell within the confocal microscope. The 927 nm particle suspensions were sonicated in toluene prior to deposition into the cell. Particle concentrations were varied during the test in order to monitor adhesion events in a timely manner. The substrate was cleaned and loaded into the cell, then rinsed with pure toluene. Patterns were written using the UV laser source. The initial particle concentration injected into the cell was 0.01 vol% (time, t = 0). As few adhesion events were observed, a suspension at 0.03% was added at t = 300 s. This solution was found to have some aggregates, attributed to poor dispersion. A suspension of 0.1% was then added at approx. t = 720 s, and a significantly larger number of sedimenting colloidal particles was observed. At the end of experiment (t = 1100 s) the surface was washed with pure toluene to remove the unadhered particles. Three more washes were performed to remove all of the free colloids still in the cell.

Figure 25 shows the particle adsorption onto UV exposed and unexposed regions determined from the acquired confocal images. The data is plotted as a ratio of the area covered by adsorbed colloids to the total available area of the exposed and unexposed regions vs. time. As can be seen from the figure,

flocculated particle clusters adsorb almost exclusively onto the UV exposed area (*i.e.*, t = 300 – 720 s period). However, even individual colloids are significantly more likely to absorb onto the UV exposed area (*i.e.*, t = 720 – 1100 s). The increase in number of particles registered with the confocal microscope is obviously dependant on the experiment duration (*i.e.*, particle fraction). However, the strongly adhering particles are still retained after extensive rinsing performed at the conclusion of the experiment. In order to better visualize the kinetics of particle association into the exposed and unexposed regions, the ratio of adsorbed particles in the exposed to unexposed regions is shown in Figure 26. Specifically, the selectivity factor defined as the ratio: (area of colloidal particles adsorbed onto the UV exposed region normalized by the total available area in the exposed region)/(area of colloidal particles adsorbed onto the unexposed region normalized by the total available area of the unexposed region) is plotted against time. As can be seen, the addition of the 0.1 vol% suspension began causing particle adhesion over much of the substrate, including the unexposed region. Following the rinsing procedure that left only the most strongly adsorbed particles on the surface, the selectivity ratio was calculated to be 3.1. This data suggests that SP/MMA modified colloids are 3.1 times as likely to adsorb onto the UV exposed surfaces during a typical sedimentation experiment.

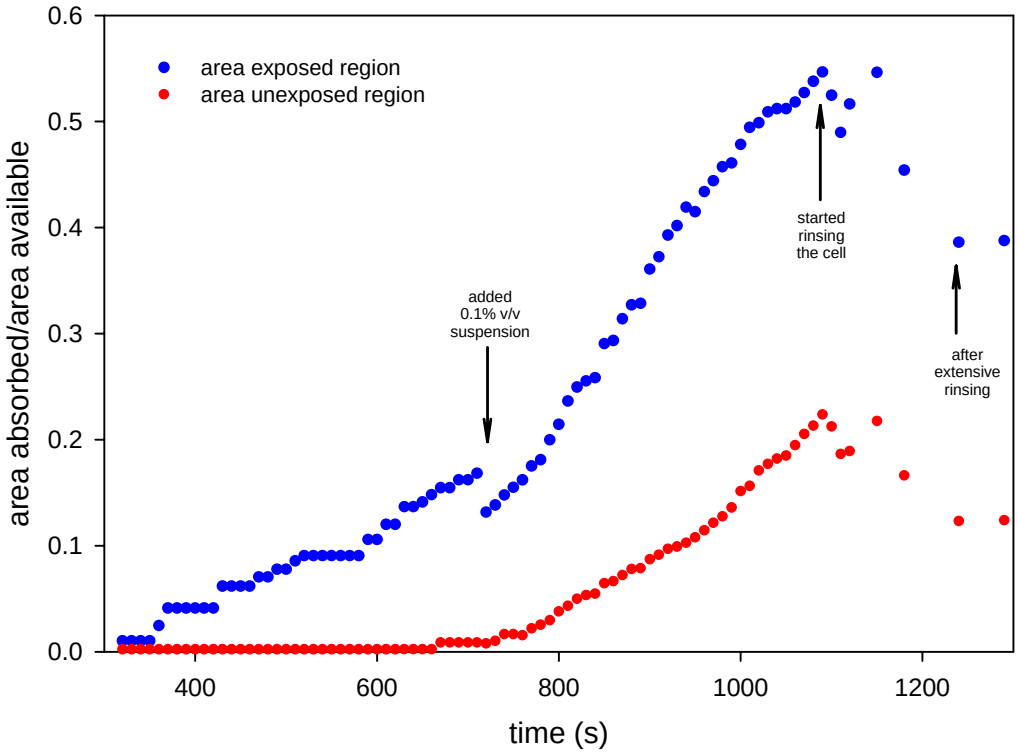

Figure 235 Comparison of particle adsorption on exposed vs. unexposed photo-controlled films in the sedimentation cell configuration. *y-axis*: area of stuck particles in exposed region/total area of exposed region or area of stuck particles in unexposed region/total area of unexposed region.

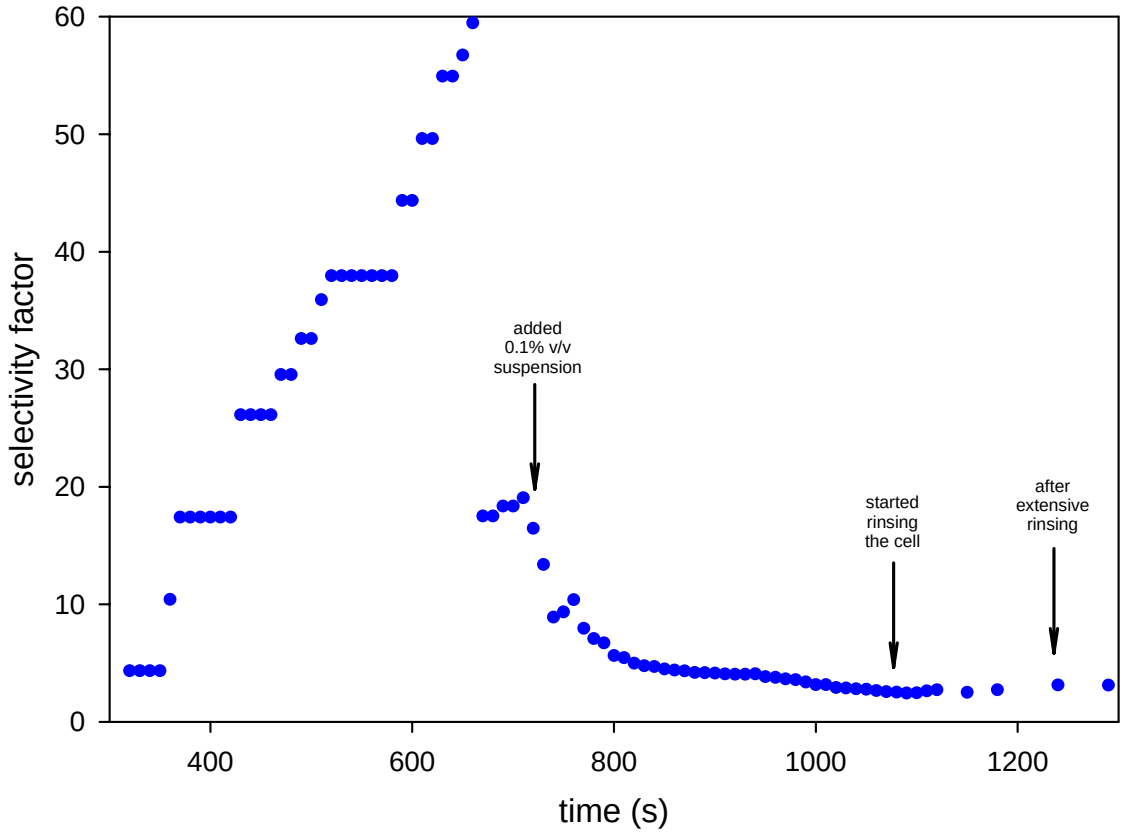

Figure 246 Preferential adsorption of particles onto the UV exposed areas in the sedimentation cell configuration. The data represent the ratio: (area of colloidal particles adsorbed onto the UV exposed region normalized by the total available area in the exposed region)/(area of colloidal particles adsorbed onto the unexposed region normalized by the total available area of the unexposed region). This ratio defines the selectivity factor.

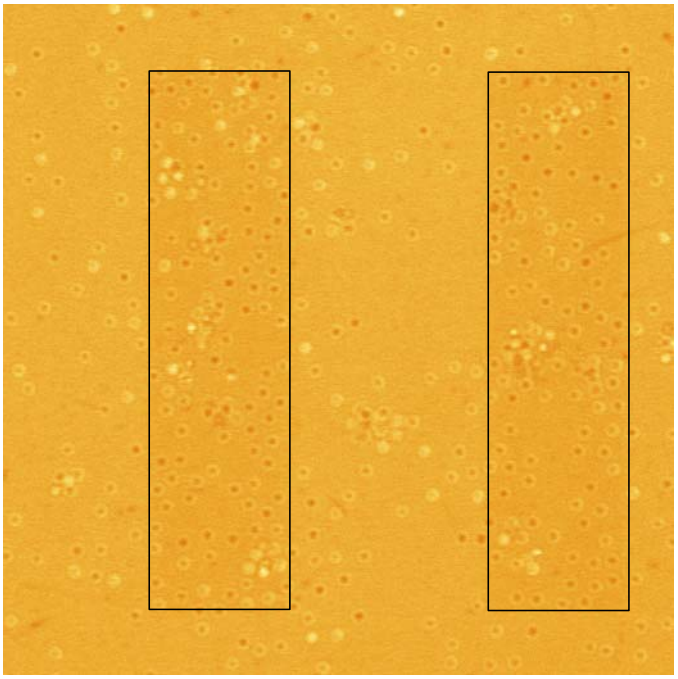

Figure 27 Confocal image of SP/MMA modified surface after colloid deposition and extensive toluene rinsing in a sedimentation cell. Marked rectangles in the figure denote areas exposed to UV radiation.

It should be mentioned that when a flow cell geometry was employed for similar adsorption experiment, the selectivity ratio was found to be 10.8. This enhancement was most likely caused by a better removal of unattached, diffusing colloids from the unexposed regions during the pulsed flow through the flow cell. Figure 28 shows the adhered particles after the extensive rinsing, along with adjacent areas of unexposed substrate. Statistics of adhesion for this flow cell experiment are compared in Table 12.

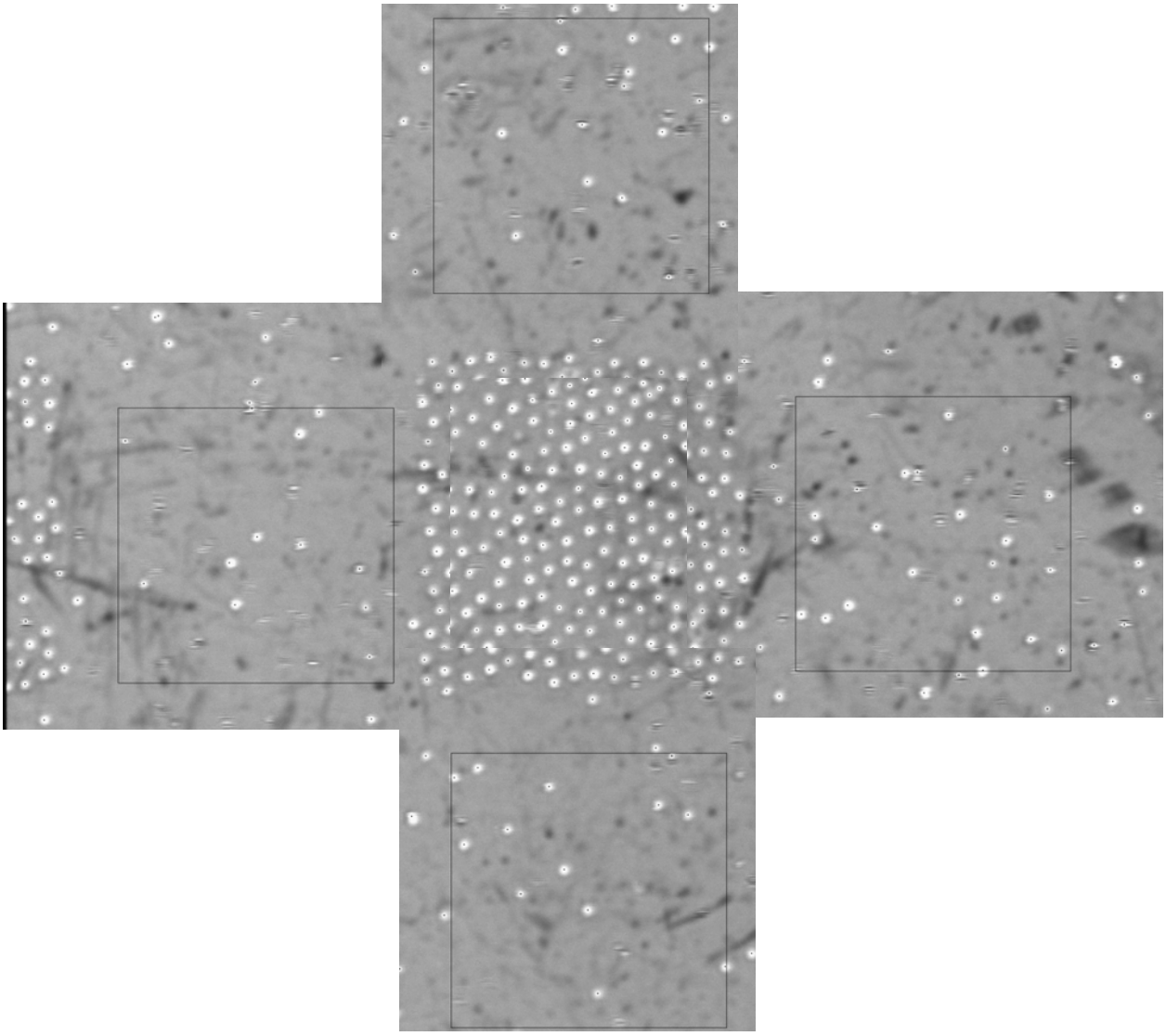

Figure 28 Confocal image of preferential adsorption in exposed areas. Boxes are given to indicate the comparison with unexposed areas and statistics of particle adsorption.

Table 12 Statistics of particle adsorption on exposed vs. unexposed surfaces for the flow cell experiment. The selectivity factor for the patterned area is 10.8, defined as the area of particles adsorbed on the pattern region per unit area / area adsorbed on the unpatterned region per unit area. The % fill is the ratio of the number of adsorbed particles compared to the area of a hexagonally close packed array of monodisperse spheres.

	Description	# Adsorbed	Area Density ($\#/\mu m^2$)	% Fill
	ROI	148	0.512	59.2
Unexposed	Top	12	0.042	4.8
	Bottom	13	0.045	5.2
	Left	9	0.031	3.6
	Right	21	0.073	8.4
	Unpatterned Mean	13.75	0.048	5.5

Discussion

The routes tested for creating ordered structures in this particle system exhibited behavior that inhibited the crystallization process. The dip coating procedure is not well adapted to the formation of multilayer ordered structures, as the pulling speed can exceed the flux of particles to the drying front. Additionally, there are concerns with the non-aqueous solvents tested for these particles, as the surface tension, viscosity, and evaporation rates are not equal and may not promote the kinetics required for crystallization. However, ordering was seen in isolated monolayer particle assemblies. This process is likely due to the meniscus attraction between particles immersed in a fluid layer that is thinner than the particle diameter[268].

The forced filtration route was also not very successful for creating ordered structures although success was achieved in one sample. It is possible that the grafted polymer layers affect the restructuring of particles through increased local viscosity or dampening of the applied acoustic power. There is additionally a maximum frequency for acoustic adsorption based on particle size. The frequency of these experiments was not controlled, and there is potential for improved performance if the ultrasonic vibration is optimized. Finally, it is possible that the surface layers of the grafted polymers are interdigitated, which would create local adhesion and prevent rearrangement. These series of observations show that crystallization is possible in these particles, but that the process is unlike that of hard spheres. The most likely candidates for the deviations are the non-aqueous solvents used and the grafted photo-switchable polymer layer on the particles.

The sedimentation studies performed with the confocal microscope provide more insight into the behavior of the particles. Sedimentation of dispersed particles without UV photo-switching creates dense layers without long-range order. Particles show some diffusion at the surface, but do not appear to exhibit sufficient stability against aggregation to achieve the lowest energy packing state (crystallinity) before achieving adhesion. The sediments exhibit glassy structure. The presence of the polymer layers on the particles may be impacting crystal nucleation and growth kinetics. Polymer coated particles in organic solvents have demonstrated colloidal crystallization in certain cases, but the formation was partially related to electrostatic repulsion present between the particles[269]. Figure 15 shows approximately uniform particle separation distances (i.e. short range order) but no long range order. The growth of ordered structures was greatly lowered by the presence of microgel particles (thought to be weakly adsorbed to the

silica particle surfaces). The polymeric layer may exhibit interdigitation of surface groups or effectively an increased local viscosity between neighboring particles.

Upon UV exposure to initiate photo-switching, the aggregate structure becomes significantly different. The substrate layer shows a distribution of single particles, and on focusing within the sample, agglomerated particles are visible as open, loosely packed structures. This shows that the UV initiated aggregation process causes rapid agglomeration with sufficient strength to prevent rearrangement, but that some particles are not incorporated into the growing particle assemblies. These observations suggest that a short-range attraction is generated by the photo-switching interaction, and the kinetics of attraction may also be limited by the photo-isomerization and complex formation within the methylmethacrylate chain. Particles in near proximity aggregate, yet some particles are too distant to be attracted into aggregates.

The mechanism of aggregation is proposed to relate to the increase in dipole moment in SP units when they convert to the merocyanine (open) form which is zwitterionic. The ionic form associates with methacrylate units in the polymer to form a weak complex. For a grafted polymer chain in proximity to a neighboring SPMMA coated particle, interchain complexes are possible. For isolated particles, intrachain complexes are the only route possible for lowering free energy. This creates a system in which UV exposure causes a rapid period of aggregation but exhibits a saturation or termination of attraction. This hypothesis could support the observations seen here where both aggregates and discrete particles sediment after photo-switching the surface layers.

Dervatized SP/MMA polymeric surfaces were also examined for patterning by UV exposure. Adhesion was found to be enhanced in he UV treated regions, although particles also adhered onto the unexposed areas. The selectivity with which colloids adsorbed onto the UV irradiated areas could be enhanced by using a flow through geometry instead of the standard quiescent sedimentation cell.

A desired property for “zone refining” of particle arrays is the reversible association and repulsion of derivatized particles. This would create volume and structural changes in the sedimented particle layers. This was tested by “writing” with a UV beam and/or visible beam on a sediment layer, as shown in Figure 20 and on particle monolayers in Figure 21. In each case, the particles show no propensity for spontaneous restructuring through photo-switching. It does not create a sustained long range attraction or repulsion based on wetting or hydrophobic forces. It also does not cause swelling or deswelling in the polymer layer. This prevents local melting of colloidal structure, and requires ultrasonic power input to redisperse particles in contact.

Thus, in order to direct colloidal deposition with UV light, another solvent and/or polymer system needs to be investigated. Specifically, with the chromophores in one state (e.g., SP form) the colloidal interactions need to be repulsive (or attractive), but with the chromophores in the other optical state (e.g., ME form) these same interactions need to change to attraction (or repulsion, respectively).

Conclusions

The sedimentation behavior and particle structure in a photo-aggregating system was examined using confocal microscopy. Crystallization of these monodisperse particles can be forced, but is more difficult than in hard sphere systems. The aggregates formed by destabilization of the polymer layers grown from each surface are open rather than dense, and there remain individual particles after the photo-switching exposure. There was also no long-range attraction between surfaces bearing patterns of exposed and unexposed area. The proposed mechanism for the aggregation interaction is a short range attraction based on the formation of complexes between the zwitterionic switched units and the methacrylate units in the polymer backbone. Aggregation is short range and complete within a finite period. This prevents the possibility of reversibly melting and crystallizing a particle sediment to form more perfect colloidal crystals in this system.

Appendix A: Photo-controlled Colloidal Crystal Arrays

A milestone in the initial proposal was to create photo-controlled photonic crystals, which would have the property of reversible tuning of the photonic band gap based on the response of the photochromic molecules. After the first year of the program, we determined that the response of a fluid-filled gel photonic crystal array would be diffusion limited in signal response as well as susceptible to solvent loss in the gel. In addition, the application of photo-control of a photonic lattice in the dry state requires the existence of a photo-responsive polymer. Searches in the literature for such a material did not produce many candidates. Most studies were performed on flat surfaces and indicated 2-dimensional stress leading to island formation, but even these responses required humid atmospheric conditions[270,271]. These responses are similar to that of Langmuir monolayers on aqueous surfaces, which also suggests that photochromic content and packing of polymer must be concentrated141. One solid state example found in our search of an organic photomechanical response was for diarylethene molecular crystal[272]. This required crystallization of the molecule, and we did not pursue the fabrication of this material for impregnation in a colloidal photonic lattice. Recently, a polymeric example of a polymer with photomechanical response has been published190. However, the specific strain created by photoswitching was not reported. It is possible to synthesize the photochromic polymer and melt infiltrate the material in a colloidal photonic lattice produced by convective evaporation or other means, to attempt the formation of a polymeric film producing optical shift of the photochromic response. The efficiency of this response will still relate to the optical properties of the network, and might be improved by incorporating high index nanoparticles in the polymer film.

The decision was made to focus efforts instead on photo-control of particle interactions to create more perfect crystals through a zone refining process, or to control the position and orientation of line defects to create optical pathways. In this section, we detail recent publications that did achieve the formation of photo-responsive polymerized colloidal crystal arrays (PCCAs) utilizing azobenzene and spiropyran derivative hydrogels to shift the wavelength of the bandgap[273]. These systems approach the problem through the formation of a PCCA using highly charged polystyrene colloids in exhaustively deionized water. The electrostatic repulsion of the spheres causes them to crystalize in a non-contacting FCC lattice (with defects). The aqueous phase contains monomers for the polymerization of a hydrogel, generally crosslinked acrylamide or N-isopropyl acrylamide. In this synthesis, the hydrogel matrix contains epoxide chemistries that are not reacted during the formation of the PCCA. The photochromic units are added in a second step to bond with the gel phase. Once reacted, the hydrogel can display photocontrolled solubility responses, and undergo a reversible swelling/deswelling reaction. The development required the isolation of a unique azobenzene compound which has a high activation barrier between the trans and cis isomers, and it is also water soluble. Other azobenzene compounds have not demonstrated good stability in polar solvents, and tend to assume the cis isomer. The spiropyran compound was derivatized with maleimide, and required the second stage reaction in DMSO.

The response of such a network is limited by the diffusion of solvent in the material, so that a rapid switching reaction is inhibited. For macroscopic gels the times for switching are in the seconds to minutes range, but over smaller areas of ~200 μm, hydrogels can swell in the μsecond range. Additionally, the peak shift in the photonic bandgap is only 15 nm for the azobenzene system and 10-11 nm for the spiropyran system, and can not be modulated between the two states[274]. The polymeric materials used also do not have high refractive index contrast, and the photonic bandgap is weak and narrow as a result. The photo-recovery time for the spiropyran system was 35 hours in the dark, and they did not show stability at tests above 25 ºC. These publications suggest use of these materials as novel recordable and readable memory devices.

Finally, there is a report of a photonic crystal impregnated with photochromic organic moeities displaying unique optical response[275,276]. A polymeric photonic crystal was formed by impressing an opal with coumarin 6 dye containing polymer. A spectral redistribution of the luminescence was observed

from the opal structure. Under increasing optical pumping power, a band of amplified spontaneous emission was observed at the stop-band edge. The dye was not chemically bound to the polymer, and a photoinitiator was also impregnated. The fluorescence was not quenched by using the dye in a diluted state. These films show a strong emission directionality dependance from the back side (transmittance) of the stimulating radiation, but very little emission dependance from the front side (reflection). This suggests that laying a PL over an LED stimulator leads to some directional emission from the back side. Thicker crystals lead to higher factors of directionality dependance. Raising refractive index contrast is still important to obtain a full band gap.

Overlap of the dye emission band and the stop band of the PL affects the emission as (1) PL intensity is suppressed at the stop band, (2) the PL spectrum acquires an angular anisotropy in agreement with angular dispersion of the stop band of the PL, (3) the emission excited through the back surface has a frequency-dependant directionality resulting from interference conditions for radiation at different frequencies, and (4) the ASE band appears at the stop band edge, likely from electronic and photonic interplay of stop-band structures. A second study also details features of luminescence in PL structures similar to the prior reference[277].

Appendix B: Photo-switchable Application to Microfluidic Devices

Micrometer scale fluid pumps and valves are formed in customized channels using colloidal particulates as flow directing components71. Optical trapping is used to manipulate either individual colloids, “dumbbells”, or photo-polymerized colloidal assemblies to form rotating, oscillating, or switchable geometries to elegantly control flow. The colloids form the micro-components and eliminate the need for difficult fabrication methods to create cantilevers and actuators. However, an optical trapping system and laser are required, but the authors suggest that other routes for control of particle motion such as electrophoresis or magnetic fields could also be used. The following figure illustrates the motions utilized in the colloidal microfluidic control devices.

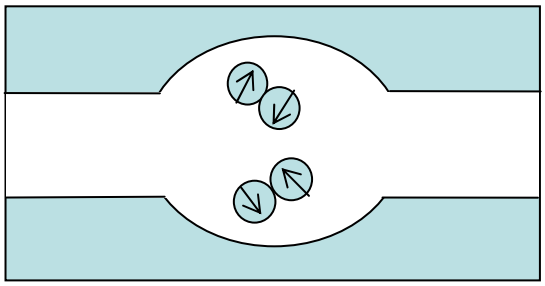

Two-Lobe Gear Pump

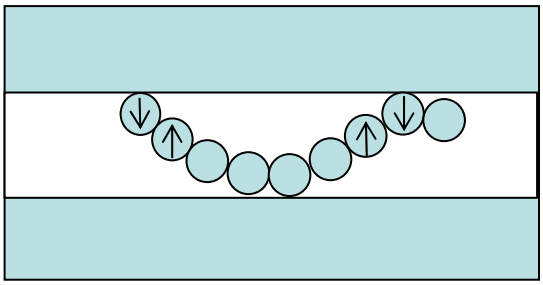

“Serpentine” Pump

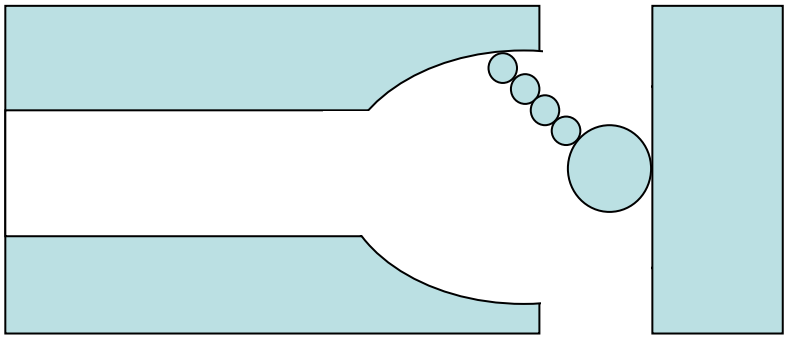

Passive Colloidal Valve

A. Terray, J. Oakey, and D.W.M. Marr, *Science* **296** (2002) 1841-1844.

Electrowetting has also demonstrated control of fluid flow through the conformation adjustment of molecules by an applied electric field[278]. Microfluidic components can also be derivatized with photo-switchable groups to control fluid flow. An azobenzene derivative based on calix[4]resorcinarenes has shown the capability to control the motion of some non-aqueous liquids through contact angle differences based on photo-switching53,91[279]. Also, photo-modulated control of contact angle has demonstrated the ability to separate water and air or immiscible fluids in microchannels. Fluid approaching a Y junction can be separated by UV controlled hydrophilicity of one channel and visible light hydrophobicity of the other channel. Water flows down the hydrophilic channel and air or hydrocarbon down the hydrophobic channel with no moving parts. However, switching the hydrophobicity takes several hundred seconds, and must be improved for future application.

REFERENCES

[1] J.C., Huie, "Guided Molecular Self-Assembly: A Review of Recent Efforts," *Smart Mater. Struct.* **12**(2003) 264-271.

[2] A., Kumar, A.B., Mandale, M., Sastry, "Sequential electrostatic assembly of amine-derivatized gold and carboxylic acid-derivatized silver colloidal particles on glass substrates" *Langmuir* **16** (2000) 6921-6926

[3] A., Groisman, M., Enzelberger, S.R., Quake, "Microfluidic Memory and Control Devices," *Science* **300** (2003) 955-958.

[4] M., Irie, "Diarylethene for Memories and Switches," *Chem. Rev.* **100** (2000) 1685-1716.

[5] G., Berkovic, V., Krongauz, V., Weiss, "Spiropyrans and Spirooxazines for Memories and Switches," *Chem.. Rev.* **100** (2000) 1741-1753.

[6] J. A., Delaire, K., Nakatani, "Linear and Nonlinear Optical Properties of Photochromic Molecules and Materials," C*hem.. Rev.* **100** (2000) 1817-1845.

[7] Y., Yokoyama, "Fulgides for Memories and Switches," *Chem. Rev.* **100** (2000) 1717-1739.

[8] G., Cik, M., Bardosova, "Reversible Optical Memory," *Chemicke Listy* **87** (1993) 690-696.

[9] G., Qian, M. Wang, "Recent developments of organic-inorganic hybrid optical functional materials and related devices," *Journal of the Chinese Ceramic Society* **29** (2001) 596-601.

[10] V. A., Mallia, N., Tamaoki, "Design of chiral dimesogens containing cholesteryl groups; formation of new molecular organizations and their application to molecular photonics," *Chemical Society Reviews* **33** (2004) 76-84.

[11] O., Tsutsumi, T. Ikeda, "Photochemical modulation of alignment of liquid crystals and photonic applications," *Current Opinion in Solid State & Materials Science* **6** (2002) 563-568.

[12] Y., Zhao, "Design and study of new azobenzene liquid crystal/polymer materials," *Chinese Journal of Polymer Science* **21** (2003) 621-629.

[13] V., Shibaev, A., Bobrovsky, N., Boiko, "Light-responsive chiral photochromic liquid crystalline polymer systems," *Journal of Photochemistry and Photobiology A* **155** (2003) 3-19.

[14] T., Seki, "Dynamic photoresponsive functions in organized layer systems comprised of azobenzene-containing polymers," *Polymer Journal* **36** (2004) 435-454.

[15] O., Pieroni, F., Ciardelli, "Photoresponsive Polymeric Materials," *Trends in Polymer Science* **3** (1995) 282-287.

[16] M., Irie, "Photoresponsive Polymers," *Advances in Polymer Science* **94** (1990) 27-67.

[17] O., Pieroni, A., Fissi, F., Ciardelli, "Light-induced effects in photoresponsive polymers," *Photochemistry and Photobiology* **44** (1986) 785-791.

[18] J. L. R., Williams, R. C., Daly, "Photochemical probes in polymers," *Prog. Polym. Sci.* **5** (1977) 61-93.

[19] D. A., Topchiyev, "Photochromism of spiropyrans in polymeric media, some aspects and possibilities of regulating the spectral-kinetic characteristics. Review," *Polymer Science* **32** (1990) 2361-2383.

[20] S., Xie, A., Natansohn, P., Rochon, "Recent developments in aromatic azo polymers research," *Chemistry of Materials* **5** (1993) 403-411.

[21] A., Momotake, T. Arai, "Synthesis, exited state properties, and dynamic structural change of photoresponsive dendrimers," *Polymer* **45** (2004) 5369-5390.

[22] T., Kinoshita, "Photoresponsive membrane systems," *Journal of Photochemistry and Photobiology B* **42** (1998) 12-19.

[23] B.L., Feringa, R.A., van Delden, N., Loumura, E.M., Geertsema, "Chrioptical Molecular Switches," *Chem. Rev.* **100** (2000) 1789-1816.

[24] W.-W., Zhang, Z.-M., Ren, H.-F., Li, C.-S., Lu, C.-J., Hu, H.-Z., Zhu, Q.-J., Meng, "Study on Self-Assembled Monolayers of Functionalized Azobenzene Thiols on Gold: XPS, Electrochemical Properties, and Surface-Enhanced Raman Spectroscopy," *J. Coll. Interf. Sci.* **255**(2002) 150-157.
[25] S.K., Prasa, G.G., Nair, "Effects of Photo-Controlled Nanophase Segregation in a Re-entrant Nematic Liquid Crystal," *Adv. Mater.* **13** (2001) 40-43.
[26] K., Ishihara, A., Okazaki, N., Negishi, I., Shinohara, T., Okano, K., Kataoka, Y., Sakurai, "Photo-Induced Change in Wettability and Binding Ability of Azoaromatic Polymers," *J. Appl Polym. Sci.* **27** (1982) 239-245.
[27] T., Sheng, K. A., Smith, T. A., Hatton, "Photoreversible Surfactants Exhibiting Unusually Large, Reversible Surface Tension Changes under Varying Illumination Conditions," *Langmuir* **19** (2003) 10764-10773.
[28] C., Ruslim, K., Ichimura, "Conformation-Assisted Amplification of Chirality Transfer of Chiral Z-Azobenzenes," *Adv. Mater.* **13** (2001) 37-40.
[29] B., Zou, D., Qiu, X., Hou, L., Wu, X., Zhang, L., Chi, H., Fuchs, "Surface Micelles of Single Chain Amphiphiles Bearing Azobenzene," *Langmuir* **18** (2002) 8006-8009.
[30] T., Seki, H., Sekizawa, K., Ichimura, "Morphological Changes in Monolayer of a Photosensitive Polymer Observed by Brewster Angle Microscopy," *Polymer* **38** (1997) 725-728.
[31] K., Murata, M., Aoki, T., Suzuki, T., Harada, H., Kawabata, T., Komori, F., Obseto, K., Ueda, S., Shinkai, "Thermal and Light Control of the Sol-Gel Phase Transition in Cholesterol-Based Organic Gels. Novel Helical Aggregation Modes As Detected by Circular Dichroism and Electron Microscopic Observation," *J. Am. Chem. Soc.* **116** (1994) 6664-6676.
[32] J., Mamiya, K., Kanie, T., Hiyama, T., Ikeda, T., Kato, "A rodlike organogelator: fibrous aggregation of azobenzene derivatives with a syn-chiral carbonate moiety," *Chem. Commun.* (2002) 18870-1871.
[33] S., van der Laan, B. L., Feringa, R. M., Kellogg, J., van Esch, "Remarkable Polymorphism in Gels of New Azobenzene Bis-urea Gelators," *Langmuir* **18** (2002) 7136-7140.
[34] T., Seki, T., Fukuchi, K., Ichimura, "Role of Hydrogen Bonding in Azobenzene-Urea Assemblies. The Packing State and Photoresponse Behavior in Langmuir Monolayers," *Langmuir* **18** (2002) 5462-5467.
[35] M., Irie, W., Schnabel, "On the Dynamics of Photostimulated Conformational Changes of Polystyrene with Pendant Azobenzene Groups in Solution," *Macromolecules* **18** (1985) 394-398.
[36] M., Irie, Y., Hirano, S., Hashimoto, K., Hayashi, "Photoresponsive Polymers. 2. Reversible Solution Viscosity Change of Polyamides Having Azobenzene Residues in the Main Chain," *Macromolecules* **14** (1981) 262-267.
[37] M., Irie, T., Suzuki, "Photoresponsive Polymers. Reversible Solution Viscosity Change of Poly(dimethylsiloxane) with azobenzene residues in the main chain," *Amakromol. Chem., Rapid Commun.* **8** (1987) 607-610.
[38] M., Irie, H., Tanaka, "Photoresponsive Polymers. 5. Reversible Solubility Change of Polystryrene Having Azobenzene Pendant Groups," *Macromolecules* **16** (1983) 210-214.
[39] M., Irie, R., Iga, "Photostimulated Reversible Sol-Gel Transition of Polystyrene with Pendant Azobenzene Groups in Carbon Disulfide," *Makromol. Chem. Rapid Commun.* **6** (1985) 403-405.
[40] M., Irie, "Stimuli-Responsive Poly(N-isopropylacrylamide). Photo- and Chemical-Induced Phase Transitions," *Adv. Polymer Science* **110** (1993) 49-65.
[41] M., Irie, D. Kungwatchakun, "Stimuli Responsive Polymers. Photostimulated Reversible Phase Separation of Aquesous Solutions of Poly(N-isopropylacrylamide) with Pendant Azobenzene Groups," *Proc. Japan Acad.* **68** (1992) 127-132.
[42] K., Balashev, I., Panaiotov, J. E., Proust, "Propagation of Photoinduced Surface Pressure Perturbation along a Mixed Benzospiropyran-Octadecanol Monolayer," *Langmuir* **13** (1997) 5373-5377.
[43] M., Matsumoto, T., Nakazawa, V. A., Mallia, N., Tamaoki, R., Azumi, H., Sakai, M., Abe, "Thermal Hysteresis in the Photoresponsivity of a Langmuir Film of Amphiphilic Spiropyran," *J. Am. Chem. Soc.* **126** (2004) 1006-1007.

[44] R., Rosario, D., Gust, M., Hayes, F., Jahnke, J., Springer, A. A., Garcia, "Photon-Modulated Wettability Changes on Spiropyran-Coated Surfaces," *Langmuir* **18** (2002) 8062-8069.
[45] J. M., Galvin, G. B., Schuster, "Preparation and Characterization of Mixed Thin Films Containing Spiropyrans and Long Chain Alkyl Silanes: Towards a Command Surface for Liquid Crystal Realignment," *Supramolecular Sci.* **5**(1999) 89-100.
[46] H., Asanuma, K., Shirasuka, T., Yoshida, T., Takarada, X., Liang, M., Komiyama, "Spiropyran as a Regulator of DNA Hybridization with Reversed Switching Mode to That of Azobenzene," *Chem. Lett.* (2001) 108-109.
[47] K., Arai, Y., Shitara, T., Ohyama, "Preparation of Photochromic Spiropyrans Linked to Methyl Cellulose and Photoregulation of their Properties," *J. Mater. Chem.* **6** (1996) 11-14.
[48] T. M., Cooper, V., Tondiglia, L. V., Natarajan, M., Shapiro, K., Obermeier, R. L., Crane, "Holographic Grating Formation in Poly(spiropyran l-glutamate)," *Appl. Optics* **32** (1993) 674-677.
[49] S., Rath, O., Mager, T., Klingler, H., Port, "Nano-optical Reversible Switching of Organic Photochromes," *J. of Microscopy* **203** (2001) 182-187.
[50] D. -J., Che, G., Li, B. -S., Du, Z., Zhang, Y. H., Li, "Photolysis of diacylferrocenes and their photo-ligand exchange reactions with 1,10-phenanthroline," *Inorg. Chimica Acta* **261** (1997) 121-127.
[51] C. G. F., Cooper, J. C., MacDonald, R., Soto, W. G., McGimpsey, "Non-Covalent Assembly of a Photoswitchable Surface," *J. Am. Chem. Soc.* **126** (2004) 1032-1033.
[52] N. Tanio, M., Irie, "Photooptical Switching of Polymer Film Waveguide Containing Photochromic Diarylethenes," *Jpn. J. Appl. Phys.* **33** (1994) 1550-1553.
[53] S.-K. Oh, M. Nakagawa, and K. Ichimura, "Photocontrol of liquid motion on an Azobenzene monolayer," *J. Mater. Chem.* **12** (2002) 2262-2269.
[54] G. G. A., Janssens-Maenhout, T., Schulenberg, "An alternative description of the interfacial energy of a liquid in contact with a solid," *J. Colloid Interf. Sci*. **257** (2003) 141–153
[55] C., Rulison, "So You Want to Measure Surface Energy," Kruss USA, 9305 Monroe Road, Suite B, Charlotte, NC, 28270-1488.
[56] J., Tsibouklis, P., Graham, P. J., Eaton, J. R., Smith, T. G., Nevell, J. D., Smart, R. J., Ewen, "Poly (perfluoroalkyl methacrylate) Film Structures: Surface Organization Phenomena, Surface Energy Determinations, and Force of Adhesion Measurements," *Macromolecules* **33** (2000) 8460-8465.
[57] M., Irie, R., Iga, "Reversible Wettability Change of Poly[butyl methacrylate-co-a-(2-hydroxyphenyl)-a-(4-vinylphenyl) benzyl alcohol]," *Makromol. Chem., Rapid Commun.* **8** (1987) 569-572.
[58] S., Mendez, L. K., Ista, G. P., Lopez, "Use of Stimuli Responsive Polymers Grafted on Mixed Self-Assembled Monolayers to Tune Transitions in Surface Energy," *Langmuir* **19**(2003) 8115-8116.
[59] L. N., Lucas, J., van Esch, R. M., Kellogg, B. L., Feringa, "Photocontrolled Assembly of Molecular Switches," *Chem. Commun.* (2001) 759-760.
[60] S., Mandal, A., Gole, N., Lala, R., Gonnade, V., Ganvir, M., Sastry, "Studies on the Reversible Aggregation of Cysteine-Capped Colloidal Silver Particles Interconnected via Hydrogen Bonds," *Langmuir* **17** (2001) 6262-6268.
[61] S. R. J., Oliver, N., Bowden, G. M., Whitesides, "Self-Assembly of Hexagonal Rod Arrays Based on Capillary Forces," *J. Coll. Interf. Sci.* **224** (2000) 425-428.
[62] D., Gan, L. A., Lyon, "Tunable Swelling Kinetics in Core-Shell Hydrogel Nanoparticles," *J. Am. Chem. Soc.* **123** (2001) 7511-7517.
[63] M., Taguchi, G., Li, Z., Gu, O., Sato, Y., Einaga, "Magnetic Vesicles of Amphiphilic Spiropyran Containing Iron Oxide Particles on a Solid Substrate," *Chem. Mater.* **15** (2003) 4756-4760.
[64] K., Sugiyama, H., Nakano, K., Ohga, "Preparation and characterization of photoresponsive poly(methyl methacrylate) microspheres bearing phosphorylcholine-analogous and spirooxazine moieties," *Macromol. Chem. Phys.* **195** (1994) 3915-3928.
[65] M., Ueda, K., Kudo, K., Ichimura, "Photochromic Behavior of a Spirobenzopyran Chemisorbed on a Colloidal Silica Surface," *J. Mater. Chem.* **5** (1995) 1007-1011.

[66] M., Ueda, H. -B., Kim, K., Ichimura, “Photocontrolled Aggregation of Colloidal Silica,” *J. Mater. Chem.* **4** (1994) 883-889.
[67] M., Ueda, H. -B., Kim, K., Ichimura, “Photocontrol of dispersibility of colloidal silica," *Materials Letters* **20** (1994) 245-249.
[68] M., Ueda, N., Fukushima, K., Kudo, K., Ichimura, “Photocontrolled Dispersibility of Colloidal Silica by Surface Adsorption of a Calix[4]resorcinarene having Azobenzene Groups,” *J. Mater. Chem.* **7** (1997) 641-645.
[69] S. D., Evans, S. R., Johnson, H., Ringsdorf, L., M. Williams, H., Wolf, "Photoswitching of azobenzene derivatives formed on planar and colloidal gold surfaces," *Langmuir* **14** (1998) 6436-6440.
[70] P., Jia-Ling, J., Hanna, H., Kokado, "Photobinding of colloidal particles by means of surface modification. II. Surface Azido density and dispersibility," *Journal of Imaging Science* **32** (1989) 232-237.
[71] A., Terray, J., Oakey, and D. W. M., Marr, “Microfluidic Control Using Colloidal Devices,” *Science* **296** (2002) 1841-1844.
[72] S., Kidoaki, S., Ohya, Y., Nakayama, T., Matsuda, “Thermoresponsive Structural Change of a Poly (N-isopropylacrylamide) Graft Layer Measured with an Atomic Force Microscope,” *Langmuir* **17** (2001) 2402-2407.
[73] M., Irie, W., Schnabel, “Photoresponsive Polymers. On the Dynamics of Conformational Changes of Polyamides with Backbone Azobenzene Groups,” *Macromolecules* **14** (1981) 1246-1249.
[74] Y. S., Park, Y., Ito, Y., Imanishi, "Photocontrol Gating by Polymer Brushes Grafted on Porous Glass Fiter," *Macromolecules* **31** (1998) 2606-2610.
[75] T., Hugel, N. B., Holland, A., Cattani, L., Moroder, M., Seitz, H. E., Gaub, "Single-Molecule Optomechanical Cycle," *Science* **296** (2002) 1103-1106.
[76] Y., Ito, "Pattern change of stimuli-responsive polymers," *Kobunshi Ronbunshu* **56** (1999) 617-625.
[77] Y., Ito, "Signal-responsive permeation through porous membrane grafted with polymer brushes," *Kobunshi Ronbunshu* **55** (1998) 171-181.
[78] D. J., Chung, Y., Ito, Y., Imanishi, "Preparation of Porous Membranes Grafted with Poly(spiropyran-containing methacrylate) and Photocontrol of Permeability," *J. Appl. Polym. Sci.* **51** (1994) 2027-2033.
[79] C., Graf, W., Schartl, K., Fisher, N., Hugenberg, M., Schmidt, "Dye-labeled poly(organosiloxane) microgels with core-shell architecture," *Langmuir* **15** (1999) 6170-6180.
[80] K. N., Jayachandran, A., Takacs-Cox, D. E., Brooks, "Synthesis and Characterization of Polymer Brushes of Poly(*N*,*N*-dimethylacrylamide) from Polystyrene Latex by Aqueous Atom Transfer Radical Polymerization," *Macromolecules* **35** (2002) 4247-4257.
[81] B., Fong, P. S., Russo, “Organophilic Colloidal Particles with a Synthetic Polypeptide Coating,” *Langmuir* **15** (1999) 4421-4426.
[82] K., Suzuki, T., Yumura, Y., Tanaka, M., Akashi, "Stimuli-responsive release from porous silica/stimuli-responsive gel hybrid particle," *Am. Chem. Soc., Polymer Preprints* **41** (2000) 1191-1192.
[83] D., Kuckling, C. D., Vo, S. E., Wohlrab, "Preparation of nanogels with temperature-responsive core and pH-responsive arms by photo-cross linking," *Langmuir* **18** (2002) 4263-4269.
[84] C. D., Jones, L. A., Lyon, "Shell-restricted swelling and core compression in poly(*N*-isopropylacrylamide) core-shell microgels," *Macromolecules* **36** (2003) 1988-1993.
[85] J. N., Kizhakkedathu, R., Norris-Jones, D. E., Brooks, "Synthesis of well-defined environmentally-responsive polymer brushes by aqueous ATRP," *Macromolecules* **37** (2004) 734-743.
[86] J. H., Kim, T. R., Lee, "Thermo- and pH-responsive hydrogel-coated gold nanoparticles," *Chemistry of Materials* **16** (2004) 3647-3651.
[87] X. C., Xiao, L. Y., Chu, W. M., Chen, S., Wang, R., Xie, "Preparation of submicrometer-sized monodispersed thermoresponsive core-shell hydrogel microspheres," *Langmuir* **20** (2004) 5247-5253.
[88] A. Elaissari, T., Delair, C., Pichot, "Thermally sensitive, hydrophilic, and reactive latex particles as versatile supports for biomolecules immobilization," *Progress in Colloid and Polmer Science* **124** (2004) 82-87.

[89] L. M., Siewierski, W. J., Brittain, S., Petrash, M. D., Foster, "Photoresponsive Monolayers Containing In-Chain Azobenzene", Langmuir **12**, 5838 (1996).
[90] S.-K., Oh, M., Nakagawa, K., Ichimura, "Self-Assembled Monolayers Derived from Calix[4]resorcinarens Exhibiting Excellent Desorption-Resistance and Their Applicability to Surface Energy Photocontrol", *Chem. Lett.* **4**, 349 (1999).
[91] K., Ichimura, S. -K., Oh, M., Nakagawa, "Light-Driven Motion of Liquids on a Photoresponsive Surface", *Science* **288**, 1624 (2000).
[92] T., Seki, H. Sekizawa, S. -Ya, Morino, K., Ichimura, "Inherent and Cooperative Photomechanical Motions in Monolayers of an Azobenzene Containing Polymer at the Air-Water Interface", *J. Phys. Chem. B* **102**, 5313 (1998).
[93] G., Moller, H., Harke, H., Motschmann, D., Prescher, "Controlling Microdroplet Formation by Light", *Langmuir* **14**, 4955 (1998).
[94] K. C., Vrancken, K., Possemiers, P., Van Der Voot, E. F., Vansant, "Surface modification of silica gels with aminoorganosilanes", *Colloids Surfaces A* **98**, 235 (1995).
[95] J. H., Moon, J. W., Shin, S. Y., Kim, J. W., Park, "Formation of Uniform Amonosilane Thin Layers: An Imine Formation To Measure Relative Surface Density of the Amine Group", *Langmuir* **12**, 4621 (1996).
[96] D. F., Siqueira Petri, G., Wenz, P., Schunk, T., Schimmel, "An Improved Method for the Assembly of Amino-Terminated Monolayers on SiO_2 and the Vapor Deposition on Gold Layers", *Langmuir* **15**, 4520 (1999).
[97] E. A., Vogler, J. C., Graper, G. R., Harper, H. W., Sugg, L. M., Lender, W. J., Brittain, "Contact activation of the plasma coagulation cascade. I. Precoagulant surface chemistry and energy", *J. Biomed. Mater. Res.* **29**, 1005 (1995).
[98] A., Liebmann-Vinson, L. M., Lender, M. D., Foster, E. A., Vogler, C. F., Majkrzak, S., Satija, "A Neutron Reflectrometry Study of Human Serum Albumin Adsorption *in Situ*", *Langmuir* **12**, 2256 (1996).
[99] A., Heise, H., Menzel, H., Yim, M. D., Foster, R. H., Wieringa, A. J., Shouten, V., Erb, M., Stamm, "Grafting of Polypeptides on Solid Substrates by Initiation of *N*-Carboxyanhydride Polymerization by Amino-Terminated Self-Assembled Monolayers", *Langmuir* **13**, 723 (1997).
[100] A., Heise, M., Stamm, M., Rauscher, H., Duschner, H., Menzel, "Mixed silane self assembled monolayers and their in situ modification", *Thin Solid Films* **327-329**, 199 (1998).
[101] G. E., Fryxell, P. C., Rieke, L. L., Wood, M. H., Engelhard, R. E., Williford, G. L., Graff, A. A., Campbell, R. J., Wiacek, L., Lee, A., Halverson, "Nucleophilic Displacements in Mixed Self-Assembled Monolayers", *Langmuir* **12**, 5064 (1996).
[102] T., Koide, G., Takei, T., Kitamori, H. -B., Kim, "Photocontrolled Fluid Flows by Photoresponsive Spirobenzopyran-coated Surface in Microchannels," *7th International Conference on Miniaturized Chemical and Biochemical Analysis Systems*, Oct. 5-9, 2003, Squaw Valley, CA, USA.
[103] R., Rosario, D., Gust, A. A., Garcia, M., Hayes, J. L., Taraci, T., Clement, J. W., Dailey, S. T., Picraux, "Lotus Effect Amplifies Light-Induced Contact Angle Switching," *J. Phys. Chem. B* **108** (2004) 12640-12642.
[104] E. E., Polymeropoulos, and D., Mobius, "'Photochromism in Monolayers" *Ber. Bunsenges. Phys. Chem.* **83** (1979) 1215-1222.
[105] S., Hayashida, H., Sato, S., Sugawara, "Large Photo-induced Thickness Change in Evaporated Spiropyran Films," *J. Chem. Soc. Chem. Commun.* (1985) 134-135.
[106] S., Hayashida, H., Sato, S., Sugawara, "Photochromic Evaporated Films of Spiropyrans with Long Alkyl Chains," *Jpn. J. Appl. Phys. 1, Regul. Pap. Short Notes (Japan)* **24** (1985) 1436-1439.
[107] S., Terrettaz, H., Tachibana, M., Matsumoto, "Investigation of Photosensitive Langmuir-Blodgett Monolayers by in Situ Atomic Force Microscopy and Absorption Spectroscopy," *Langmuir* **14** (1998) 7511-7518.

[108] H., Tachibana, Y., Yamanaka, M., Matsumoto, "Temperature Effect on Photochromic Reaction in Langmuir-Blodgett Films of Amphiphilic Spiropyran and Their Morphological Changes," *J. Phys. Chem. B* **105** (2001) 10282-10286.

[109] M., Matsumoto, T., Nakazawa, R., Azumi, H., Tachibana, Y., Yamanaka, H., Sakai, M., Abe, "Light-Induced J-Aggregation of Merocyanin in Langmuir and Langmuir-Blodgett Films," *J. Phys. Chem. B* **106** (2002) 11487-11491.

[110] H., Tachibana, Y., Yamanaka, M., Matsumoto, "Surface and photochemical properties of Langmuir monolayer and Langmuir-Blodgett films of a spiropyran derivative," *J. Matter. Chem.* **12** (2002) 938-942.

[111] E., Ando, J., Miyazaki, K., Morimoto, "J-Aggregation of Photochromic Spiropyran in Langmuir-Blodgett Films," *Thin Solid Films* **133** (1985) 21-28.

[112] R., Steiger, R., Kitzing, P., Junod, *J. Photogr. Sci.* **21** (1973) 107.

[113] D., Mobius, *Adv. Mater.* **7** (1995) 437.

[114] S., Tazuke, S., Kurihara, H., Yamaguchi, T., Ikeda, "Photochemically Triggered Physical Amplification of Photoresponsiveness," *J. Phys. Chem.* **91** (1987) 249-251.

[115] C. J., Drummond, S., Albers, D. N., Furlong, D., Wells, "Photocontrol of Surface Activity and Self-Assembly with a Spirobenzopyran Surfactant," *Langmuir* **7** (1991) 2409-2411.

[116] E., Katz, M., Liondagan, I., Willner, "Control of Electrochemical Processes by Photoisomerizable Spiropyran Monolayers Immobilized onto Au Electrodes – Amperometric Transduction of Optical Signals," *J. Electroanalytical Chem.* **382** (1995) 25-31.

[117] E. E., Polymeropoulos, D., Mobius, H., Kuhn, "Photoconduction in monolayer assemblies with functional units of sensitizing and conducting molecular components," *J. Chem. Phys.* **68** (1978) 3918-3931.

[118] B. C., Bunker, B. I., Kim, J. E., Houston, R., Rosario, A. A., Garcia, M., Hayes, D., Gust, S. T., Picraux, "Direct Observation of Photo Switching in Tethered Spiropyrans Using the Interfacial Force Microscope," *Nano Lett.* **3** (2003) 1723-1727.

[119] M. Irie, A. Menju, K. Hayashi, "Photoresponsive Polymers. Reversible Solution Viscosity Change of Poly(methyl methacrylate) Having Spirobenzopyran Side Groups," *Macromolecules* **12** (1979) 1176-1180.

[120] H. R. Allcock, C. Kim, "Photochromic polyphosphazenes with spiropyran units," *Macromolecules* **24** (1991) 2846-2851.

[121] J. Labsky, I., Koropecky, S., Nespurek, J., Kalal, "The photochromism of spiropyrans bound on side-chains of soluble polymers," *European Polymer Journal* **17** (1981) 309-313.

[122] Y., Kalisky, D. J., Williams, "Laser photolysis of photoinduced aggregation in polymer containing spiropyran units," *Macromolecules* **17** (1984) 292-296.

[123] M., Irie, T., Iwayanagi, Y., Taniguchi, "Photoresponsive Polymers. 7. Reversible Solubility Change of Polystyrene Having Pendant Spirobenzopyran Groups and Its Application to Photoresists," *Macromolecules* **18** (1985) 2418-2422.

[124] E., Goldburt, F., Shvartsman, V., Krongauz, "Intramolecular interactions in photochromic spiropyran merocyanine polymer," *Macromolecules* **17** (1984) 1225-1230.

[125] K. Kimura, M. Sumida, M. Yokoyama, "Drastic metal-ion enhancement in photoinduced aggregation of copolymer carrying crown ether and spirobenzopyran moieties," *Chem. Commun.* (1997) 1417-1418.

[126] C. Konak, R. C. Rathi, P. Kopeckova, J. Kopecek, "Photoregulated Association of Water-Soluble Copolymers with Spirobenzopyran-Containing Side Chains," *Macromolecules* **30** (1997) 5553-5556.

[127] Konak, R. C. Rathi, P. Kopeckova, J. Kopecek, "Photoassociation of Water-soluble Copolymers Containing Photochromic Spirobenzopyran Moieties," *Polym. Adv. Technol.* **9** (1998) 641-648.

[128] K., Kimura, N., Nakamura, H., Sakamoto, R. M., Uda, M., Sumida, M., Yokoyama, "Cation Complexation, Photochromism, and Aggregation of Copolymers Carrying Crown Ether and Spirobenzopyran Moieties at the Side Chains," *Bull. Chem. Soc. Jpn.* **76** (2003) 209-215.

[129] M. Moniruzzaman, G. F. Fernando,C. Sabey, D. Winter, R. A. Badcock, J. Akhavan, E. Krofli, "Synthesis and characterization of a novel class of photo-actuating and photo-rheological polymers," *Proceedings of the SPIE - The International Society for Optical Engineering* **5464** (2004) 209-220.

[130] M. Irie, A. Menju, K. Hayashi, G. Smets, "Reversible viscosity change of photochromic spirobenzopyran copolymer solutions," *J. Polym. Sci. C: Polym. Lett.* **17** (1979) 29-31.

[131] M. Irie, A., K. Hayashi, G. Smets, "Reversible viscosity change of photochromic spirobenzopyran copolymer solutions," *Photographic Science and Engineering* **23** (1979) 191-193.

[132] A. Menju, K. Hayashi, M. Irie, "Photoresponsive Polymers. 3. Reversible Solution Viscosity Change of Poly(methacrylic acid) Having Spirobenzopyran Pendant Groups in Methanol," *Macromolecules* **14** (1981) 755-758.

[133] O. Pieroni, A. Fissi, F. Ciardelli, "Photochromic poly(α-amino acid)s: Photomodulation of molecular and supramolecular structure," *Reactive and Functional Polymers* **26** (1995) 185-199.

[134] M. Kameda, K. Sumaru, T. Kanamori, T. Shinbo, "Probing the dielectric environment surrounding poly(N-isopropylacrylamide) in aqueous solution with covalently attached spirobenzopyran," *Langmuir* **20** (2004) 9315-9319.

[135] P. Uznanski, J. Pecherz, M. Kryszewski, "Spiropyrans as counterions in photochrome-containing polyelectrolyte," *Molecular Crystals and Liquid Crystals Science and Technology, Section A: Molecular Crystals and Liquid Crystals* **246** (1994) 351-354.

[136] T. M. Cooper, K. A. Obermeier, L. V. Natarajan, R. L. Crane, "Kinetic study of the helix to coil dark reaction of poly(spiropyran-L-glutamate)," *Photochemistry and Photobiology* **55** (1992) 1-7.

[137] A. E., Ivanov, N. L., Eremeev, P. O., Wahlund, I. Y., Galaev, B., Mattiasson, "Photosensitive copolymer of N-isopropylacrylamide and methacryloyl derivative of spyrobenzopyran," *Polymer* **43** (2002) 3819-3823.

[138] K., Sumaru, M., Kameda, T., Kanamori, T., Shinbo, "Characteristic phase transition of aqueous solution of poly(N- isopropylacrylamide) functionalized with spirobenzopyran," *Macromolecules* **37** (2004) 4949-4955

[139] Y. –K., Choi, E., Kim, "Synthesis and Polymerization of 6-(Alkyloxyphenyl)carbonyl Substituted Spirobenzopyran," *Tetrahedron Letters* **39** (1998) 8861-8864.

[140] B. Mecheri, P. Baglioni, O. Pieroni, G. Caminati, "Molecular switching in nano-structured photochromic films of biopolymers," *Materials Science and Engineering C* **23** (2003) 893-896.

[141] H. Gruler, R. Vilanove, F. Rondelez, "Reversible photochemical strain in Langmuir monolayers," *Physical Review Letters* **44** (1980) 590-592.

[142] N. Higashi, K. Shimizu, M. Niwa, "Surface monolayers of poly(L-glutamic acid)-functionalized amphiphiles: Effect of attachment of spiropyran to the polymer segment," *J. Colloid Interface Sci.* **185** (1997) 44-48.

[143] R., Vilanove, H., Hervet, H., Gruler, F., Rondelez, "Photochromism of Monolayers of Poly(methyl methacrylate) Having Spirobenzopyran Side Groups," *Macromolecules* **16** (1983) 825-831.

[144] V. Weiss, A. A. Friesem, V. A. Krongauz, "Organic materials for real-time holographic recording," *Journal of Imaging Science and Technology* **41** (1997) 371-382.

[145] A. V. Lyubimov, N. L. Zaichenko, V. S. Marevtsev, "Photochromic network polymers," *Journal of Photochemistry and Photobioloty A – Chemistry* **120** (1999) 55-62.

[146] V., Weiss, A. A., Friesem, V. A., Krongauz, "Optical recording in the mid-IR in photochromic polymers," *Proceedings of SPIE - The International Society for Optical Engineering* **1972** (1993) 151-156.

[147] E. J. C., Kellar, G., Williams, V., Krongauz, S., Yitzchaik, "Dielectric-ralaxation spectroscopy and molecular-dynamics of a liquid-crystalline polyacrylate containing spiropyran goups," *Journal of Materials Chemistry* **1** (1991) 331-337.

[148] J., Verborgt, G., Smets, "Photochromic Behavior of Copolymers of Indolinospirobenzopyrane Methacrylic Derivatives," *J. Polym. Sci.* **12** (1974) 2511-2523.

[149] Y., Tezuka, T., Majima, H., Yajima, S., Goto, T., Ishii, "Kinetic Matrix Effect of Photochromic Reactions of Spirobenzopyran Dispersed in or Covalently Bound to Poly(alkyl methacrylate) Matrices," *J. Photopolym. Sci. Technol.* **8** (1995) 55-64.

[150] J. G. Zhi, B. Y. Zhang, B. L. Zang, G. H. Shi, "Synthesis and properties of photochromic cholesteric liquid crystalline polysiloxane containing chiral mesogens and azobenzene photochromic groups," *Journal of Applied Polymer Science* **85** (2002) 2155-2162.

[151] C. H. Kim, D. K. Kim, J. H. Lee, K. S. Lee, "Photochromism of liquid crystalline polymers with spiropyran derivatives," *Molecular Crystals and Liquid Crystals* **370** (2001) 131-134.

[152] L. V. Natarajan, T. J. Bunning, S. Y. Kim, "Photochromic liquid crystalline cyclic siloxanes containing spiropyran groups," *Macromolecules* **27** (1994) 7248-7253.

[153] S. Yitzchaik, I. Cabrera, F. Buchholtz, V. Krongauz, "Photochromism of liquid-crystal polyacrylates containing spiropyran groups," *Macromolecules* **23** (1990) 707-713.

[154] L. V. Natarajan, T. J. Bunning, H. E. Klei, R. L. Crane, W. W. Adams, "Novel photochromic cholesteric liquid crystal siloxane," *Macromolecules* **24** (1991) 6554-6556.

[155] L. V. Natarajan, V. Tondiglia, T. J. Bunning, R. L. Crane, W. W. Adams, "Liquid crystalline siloxanes containing spiropyran chromophores as reversible optical data storage materials," *Advanced Materials for Optics and Electronics* **1** (1992) 293-297.

[156] J., Ratner, N., Kahana, A., Warshawsky, V., Krongauz, "Photochromic polysulfones. 2. Photochromic properties of polymeric polysulfone carrying pendant spiropyran and spirooxazine groups," *Industrial & Engineering Chemistry Research* **35** (1996) 1307-1315.

[157] G., Smets, "New Developments in Photochromic Polymers," *J. Polym. Sci.* **13** (1975) 2223-2231.

[158] G., Smets, J., Braeken, M., Irie, "Photomechanical effects in photochromic systems," *Pure Appl. Chem.* **50** (1978) 845-856.

[159] N., Negishi, T., Iida, K., Ishihara, I., Shinohara, "Photoregulated Binding Ability of a Polymeric Adsorbent Contining a Spiro[2*H*-chromen-2,2'-indoline] Moiety," *Makromol. Chem., Rapid Commun.* **2** (1981) 617-620.

[160] A., Higuchi, A., Hamamura, Y., Shindo, H., Kitamura, B. O., Yoon, T., Mori, T., Uyama, A., Umezawa, "Photon-Modulated Changes of Cell Attachments on Poly(spiropyran-*co*-methyl methacrylate) Membranes," *Biomacromolecules* **5** (2004) 1770-1774.

[161] V. A., Krongauz, E., Golburt, "Crystallization of Poly(spiro methacrylate) with Cooperative Spiropyran-Merocyanine Conversion," *Macromolecules* **14** (1981) 1382-1386.

[162] J. H. Kim, S. Y. Ban, S. Kaihua, D. H. Choi, "Photochromic behavior of new bifunctional copolymer containing spiropyran and chalcone moiety in the side chain," *Dyes and Pigments* **58** (2003) 105-112.

[163] A. K. Bobrovsky, N. I. Boiko, V. P. Shibaev, "Photosensitive cholesteric copolymers with spiropyran-containing side groups. I. Phase behaviour and photo-optical properties," *Liquid Crystals* **27** (2000) 57-62.

[164] B. H. Lee, J. H. Kim, M. J. Cho, S. H. Lee, D. H. Choi, "Photochromic behavior of spiropyran in the photoreactive polymer containing chalcone moieties," *Dyes and Pigments* **61** (2004) 235-242.

[165] N., Kobayashi, S., Sato, K., Takazawa, K., Ikeda, R., Hirohashi, "A new polymer electrolyte for reversible photoresponsive ionic conduction," *Electrochimica Acta* **40** (1995) 2309-2311.

[166] M. –H., Lee, X., Li, E., Kim, "Preparation of photochromic cellulose derivatives containing spirobenzopyran," *Molecular Crystals and Liquid Crystals* **349** (2000) 51-54.

[167] Y., Imai, K., Adachi, K., Naka, Y., Chujo, "Photochromic organic-inorganic polymer hybrids from spiropyran-modified poly(N,N-dimethylacrylamide)," *Polymer Bulletin* **44** (2000) 9-15.

[168] D., Levy, D., Avnir, "Effects of the Changes in the Properties of Silica Cage along the Gel/Xerogel Transition on the Photochromic Behavior of Trapped Spiropyrans," *J. Phys. Chem.* **92** (1988) 4734-4738.

[169] R., Nakao, F., Noda, T., Horii, Y., Abe, "Thermal Stability of the Spironaphthoxazine Colored Form in Polymeric Siloxanes," *Polym. Adv. Technol.* **13** (2002) 81-86.

[170] R., Nakao, N., Ueda, Y., Abe, T., Horii, H., Inoue, "Polymeric Siloxanes with a Substituent and the Spirobenzopyran Moiety: Effect of Polar Substituent on the Photochromic Properties," *Polym. Adv. Technol.* **7** (1996) 863-866.

[171] S., Hayashida, H., Sato, S., Sugawara, "Photo-Induced Wettability Change in Films Containing Spiropyran Microcrystals," *Polymer Journal* **18** (1986) 227-235.

[172] I. V. Chapurin, S. V. Robu, E. V. Rotari, O. Y. Korshak, R. A. Lessard, "Development and characterization of negative photochromic compounds." *Proceedings of the SPIE - The International Society for Optical Engineering* **4642** (2002) 50-54.

[173] I. Chapurin, B. Robu, L. Vlad, R. A. Lessard, A. Tork, C. Lafond, M. Bolte, "Spectral and holographic characterization of new photochromic compounds based on substituted spiropyrans," *Proceedings of the SPIE* **4296** (2001) 337-340.

[174] H. Eckhardt, A. Bose, V. A. Krongauz, "Formation of molecular H- and J-stacks by the spiropyran-merocyanine transformation in a polymer matrix," *Polymer* **28** (1987) 1959-1964.

[175] H. S. Blair, C. B. McArdle, "Photoresponsive polymeric systems. I. Mixed monomolecular films of some synthetic polymers and indolinospiropyrans," *Polymer* **25** (1984) 999-1005.

[176] S. S. Xue, G. Manivannan, R. A. Lessard, "Holographic and spectroscopic characterization of spiropyran doped poly(methyl methacrylate) films," *Thin Solid Films* **253** (1994) 228-232.

[177] J. S. Lin, "Interaction between dispersed photochromic compound and polymer matrix," *European Polymer Journal* **39** (2003) 1693-1700.

[178] S., Abe, Y., Nishimura, I., Yamazaki, N., Ohta, "Remarkable electric field effect on the absorption intensity of a molecular aggregate of photomerocyanine in a PMMA polymer film," *Chemistry Letters* (1999) 165-166.

[179] A., Tork, F., Boudreault, M., Roberge, A. M., Ritcey, R. A., Lessard, T. V., Galstian, "Photochromic behavior of spiropyran in polymer matrices," *Applied Optics* **40** (2001) 1180-1186.

[180] R., Piyaket, I., Cokgor, F. B., McCormick, S., Esener, A. S., Dvornikov, P. M., Rentzepis, "Two-photon-induced photochromic reactions in spirobenzopyran-doped poly(methyl methacrylate) thin-film waveguides," *Optics Letters* **21** (1996) 1032-1034.

[181] K., Horie, K., Hirao, N., Kenmochi, I., Mita, "Photochromic reaction of spirobenzopyran, azobenzene, and fuldgide at 4 K in polymer films," *Makromol. Chem., Rapid Commun.* **9** (1988) 267-273.

[182] A. Athanassiou, K. Lakiotaki, M. Kalyva, S. Georgiou, C. Fotakis, "Laser-controlled molecular actuators," *Laser Physics* **13** (2003) 664-668.

[183] S. Kurihara, M. Higuchi, T. Ogata, T. Nonaka, "Photoinduced membrane potential change of methacrylate polymers containing various spiropyrans," *Journal of Membrane Science* **93** (1994) 69-78.

[184] T., Ishiwatari, T., Kondo, M., Mitsuishi, "Photochromism of spirobenzopyran in the membrane of surfactant vesicle and in the cavity of cyclodextrins," *Colloid and Polymer Science* **274** (1996) 1000-1005.

[185] Y., Hasebe, I., Anzai, A., Ueno, T., Osa, "Photo-excitable membranes ion-selective photoresponse of polyvinyl chloride-spirobenzopyran membranes doped with nonactin and valinomycin," *Chemical and Pharmaceutical Bulletin (Tokyo)* **37** (1989) 1307-1310.

[186] I., Anzai, H., Sasaki, A., Ueno, T., Osa, "Photoinduced membrane-potential changes – poly(vinyl-chloride) spirobenzopyran membrane as an organic photo-sensor," *Makromol. Chem., Rapid Comm.* **7** (1986) 133-137.

[187] H., Sasaki, A., Ueno, J., Anzai, T., Osa, "Benzo-15-crown-5 linked spirobenzopyran. 1. Photocontrol of cation-binding ability and photoinduced membrane-potential changes," *Bull. Chem. Soc. Jpn.* **59** (1986) 1953-1956.

[188] S., Kato, M., Aizawa, S., Suzuki, "Effect of lipid on photo-induced potential change across spiropyran membrane," *Kobunshi Ronbunshu* **34** (1977) 793-799.

[189] R. L. White, Y. Y. Hsu, T. M. Cooper, J. D. Gresser, D. L. Wise, D. J. Trantolo, "Photochromic liquid hydrogels as hosts for holographic materials," *Materials Research Society Symposium Proceedings* **488** (1997) 453-458.

[190] A. Athanassiou, K. Lakiotaki, V. Tornari, S. Georgiou, C. Fotakis, "Photocontrolled mechanical phenomena in photochromic doped polymeric systems," *Applied Physics A* **76** (2003) 97-100.

[191] M. Levitus, M. Talhavini, R. M. Negri, T. D. Z. Atvars, P. F. Aramendia, , "Novel kinetic model in amorphous polymers. Spiropyran-merocyanine system revisited," *Journal of Physical Chemistry B* **101** (1997) 7680-7686.

[192] A. Athanassiou, M. Kalyva, K. Lakiotaki, S. Georgiou, C. Fotakis, "Laser controlled mechanical actuation of photochromic-polymer microsystems," *Reviews on Advanced Materials Science* **5** (2003) 245-251.

[193] S. O. Konorov, A. B. Fedotov, A. M. Zheltikov, "Three-dimensional reversible laser micromachining with subnanojoule femtosecond pulses based on two-photon photochromism," *Applied Physics B: Lasers and Optics* **76** (2003) 707-710.

[194] P. Uznanski, A. Wojda, M. Kryszewski, "Phototransformation of merocyanine forms of spiropyrans in amorphous polymeric media," *European Polymer Journal* **26** (1990) 141-143.

[195] S. O., Konorov, D. A., Sidorov-Biryukov, I., Bugar, D., Chorvat, D. Chorvat, A. M. Zheltikov, "Femtosecond time-resolved two-photon absorption resonant four-wave mixing in three-dimensional spiropyran-PMMA samples," *Journal of Raman Spectroscopy* **34** (2003) 1013-1017.

[196] U., Albrecht, H., Schafer, R., Richert, "Dispersive 1st-order reaction. 2. Photochromic model system," *Chemical Physics* **182** (1994) 61-68.

[197] R., Richert, A., Elschner, H., Bassler, "Experimental study of non-exponential relaxation process in random organic solids," *Zeitschrift fur Physikalische Chemie, Neue Folge* **149** (1986) 63-75.

[198] H., Ishitobi, Z., Sekkat, S., Kawata, "Dynamical studies of optically induced orientation processes in photochromic isomers: Experiment and theory," *Molecular Crystals and Liquid Crystals* **344** (2000) 107-112.

[199] S. O., Konorov, D. A., Sidorov-Biryukov, I., Bugar, D.,Chorvat, D., Chorvat, A. M., Zheltikov, "Quantum-controlled color: chirp- and polarization-sensitive two-photon photochromism of spiropyrans in the solid phase" *Chemical Physics Letters* **381** (2003) 572-578.

[200] X. F., Guo, D., Zhang, Y., Gui, M. X., Wax, J. C., Li, Y. Q., Liu, D. B., Zhu, "Reversible photoregulation of the electrical conductivity of spiropyran-doped polyaniline for information recording and nondestructive processing," *Advanced Materials* **16** (2004) 636-640 + 577.

[201] M. P. Srinivasan, K. K. S. Lau, "Molecular orientation in mixed LB films containing photochromic molecules," *Thin Solid Films* **307** (1997) 266-273.

[202] D. A., Holden, H., Ringsdorf, V., Deblauwe, G., Smets, "Photosensitive monolayers. Studies of surface-active spiropyrans at the air-water interface," *J. Phys. Chem.* **88** (1984) 716-720.

[203] H. S., Blair, H. I., Pogue, "Investigation of photoresponsive effects in polymer monolayers," *Polymer* **20** (1979) 99-103.

[204] I., Cokgor, A. S., Dvornikov, R., Piyaket, S. C., Esener, P. M., Rentzepis, D. W., Garvey, M. G., Kuzyk, "Spyrobenzopyran-doped core PMMA fibers," *Proceedings of SPIE* **3623** (1999) 215-223.

[205] J., Aubard, C., MBossa, J. P., Bertigny,R., Dubest, G., Levi, E., Boshet, R., Guglielmetti, "Surface enhanced Raman spectroscopy of photochromic spiroxazines and related spiropyrans," *Molecular Crystals and Liquid Crystals Science and Technology A* **246** (1994) 275-278.

[206] C. Guermeur, C. Sanchez, B. Schaudel, K. Nakatani, J. A. Delaire, F. DelMonte, D. Levy, " Investigation of dye-matrix interactions in sol-gel-derived hybrid organic-inorganic nanocomposites," *Proceedings of the SPIE - The International Society for Optical Engineering* **3136** (1997) 10-19.

[207] Jae Young Bae, Ji-In Jung, Byeong-Soo Bae, "Photochromism in spiropyran impregnated fluorinated mesoporous organosilicate films," *Journal of Materials Research* **19** (2004) 2503-2509.

[208] A. S., Cherkasov, N. S., Shelekhov, Yu. V., Solomatin, O. V., Bandyuk, "Photochemistry of spiropyrans in a porous glass impregnated with polymethyl methacrylate," *Optika i Spektroskopiya* **81** (1996) 802-806.

[209] I., Casades, M., Alvaro, H., Garcia, M. N., Pillai, "Modified mesoporous MCM-41 as hosts for photochromic spirobenzopyrans," *Photochemical & Photobiological Sciences* **1** (2002) 219-223.

[210] R. A. Lessard, G. Manivannan, “Photochromism used in holographic recording: a review,” *Proceedings of the SPIE - The International Society for Optical Engineering* **3347** (1998) 11-19.
[211] K., Maeda, "Photochromism in organized media," *Journal of Synthetic Organic Chemistry Japan* **49** (1991) 554-565.
[212] F. M., Raymo, S., Giordani, “Singnal Processing at the Molecular Lever,” *J. Am. Chem. Soc.* **123** (2001) 4651-4652.
[213] O. Y. M., Mitsunobu, “Preparation of Esters of Carboxylic and Phosphoric Acid via Quaternary Phosphonium Salts,” *Bull. Chem. Soc. Jpn.* **40** (1967) 2380-2382.
[214] O. Y. M., Mitsunobu, “Stereospecific and Stereoselective Reactions. I. Preparation of Amines from Alcohols,” *J. Am. Chem. Soc.* **94** (1972) 679-680.
[215] O. Y. M., Mitsunobu, “The Use of Diethyl Azodicarboxylate and Triphenylphosphine in Synthesis and Transformation of Natural Products,” *Synthesis* (1981) 1-28.
[216] E. L., Zaitseva, A. L., Prohoda, L. H., Kurkovskaya, R., Shifrina, N. S., Kardash, D. A., Krapkina, V., A., Krongauz, *Chem. Heterocycl. Compd.* **12** (1973) 1476.
[217] K., Matyjaszewski, P. J., Miller, N., Shukla, B., Immaraporn, A., Gelman, B. B., Luokala, T. M., Siclovan, G., Kickelbick, T., Vallant, H., Hoffmann, T., Pakula, "Polymers at Interfaces: Using Atom Transfer Radical Polymerization in the Controlled Growth of Homopolymers and Block Copolymers from Silicon Surfaces in the Absence of Untethered Sacrificial Initiator," *Macromolecules* **32** (1999) 8716-8724.
[218] M., Kamigaito, T., Ando, M., Sawamoto, “Metal-Catlyzed Living Radical Polymerization,” *Chem. Rev.* **101** (2001) 3689-3745.
[219] K. Matyjaszewski, "Macromolecular Engineering by Controlled/Living Ionic and Radical Polymerizations," *Macromol. Symp.* **174** (2001) 51-67.
[220] J. Qiu, B. Charleux, K. Matyjaszewski, "Controlled/living radical polymerization in aqueous media: homogenous and heterogenous systems," *Prog. Polym. Sci.* **26** (2001) 2083-2134.
[221] J. Pyun, T. Kowalewski, K. Matyjaszewski, "Synthesis of Polymer Brushes Using Atom Transfer Radical Polymerization," *Macromol. Rapid Commun.* **24** (2003) 1043-1059.
[222] X. Huang and M.J. Wirth, “Surface-Initiated Radical Polymerization on Porous Silica,” *Anal. Chem.* **69** (1997) 4577-4580.
[223] X. Huang, L.J. Doneski and M.J. Wirth, “Surface-Confined Living Radical Polymerization for Coatings in Capillary Electrophoresis,” *Anal. Chem.* **70** (1998) 4023-4029.
[224] H. Fisher, *Macromolecules* **30** (1997) 5666.
[225] H. Fisher, *J. Am. Chem. Soc.* **108** (1986) 3925.
[226] A. Kajiwara, K. Matyjaszewski, "EPR study of the atom transfer radical polymerization (ATRP) of (meth)acrylates," *Macromol. Rapid Commun.* **19** (1998) 319-321.
[227] M. Ejaz, S. Yamamoto, K. Ohno, Y. Tsujii, T. Fukuda, *Macromolecules* **31** (1998) 5934.
[228] M. Husseman, E. E. Malmstrom, M. McNamara, M. Mate, D. Mecerreyes, D. G. Benoit, J. L. Hedrick, P. Mansky, E. Huang, T. P. Russell, C. J. Hawker, *Macromolecules* **32** (1999) 1424.
[229] N. Negishi, T. Tsunemitsu, K. Ishihara, I. Shinohara, T. Okano, K. Kataoka, T. Akaike, Y. Sakurai, *Kobunshi Ronbushu* **37** (1980) 287.
[230] M. M. Guerrini, B. Charleux, J. –P. Vairon, "Functionalized latexes as substrates for atom transfer radical polymerization," *Macromol. Rapid Commun.* **21** (2000) 669-674.
[231] T. von Werne, T. E. Patten, "Preparation of Structurally Well-Defined Polymer–Nanoparticle Hybrids with Controlled/Living Radical Polymerization," *J. Am. Chem. Soc.* **121** (1999) 7409-7410.
[232] H. Bottcher, M. L. Hallensleben, S. Nuβ, H. Wurm, *Polym. Bull.* **44** (2000) 223-229.
[233] T. K. Mandal, M. S. Fleming, D. R. Walt, "Production of Hollow Polymeric Microspheres by Surface-Confined Living Radical Polymerization on Silica Templates," *Chem. Mater.* **12** (2000) 3481-3487.
[234] G. Carrot, S. Diamanti, M. Manuszak, B. Charleux, J. –P. Vairon, "Atom Transfer Radical Polymerization of *n*-Butyl Acrylate from Silica Nanoparticles," *J. Polym. Science A: Polym. Chem.* **39** (2001) 4294-4301.

[235] D. Bontempo, N. Tirelli, K. Feldman, G. Masci, V. Crescenzi, J. A. Hubbell, "Atom Transfer Radical Polymerization as a Tool for Surface Functionalization," *Adv. Matter.* **14** (2002) 1239-1241.
[236] K. Min, J. Hu, C. Wang, A. Elaissari, "Surface Modification of Polystyrene Latex Particles via Atom Transfer Radical Polymerization," *J. Polym. Science A: Polym. Chem.* **40** (2002) 892-900.
[237] B. Gu, A. Sen, "Synthesis of Aluminum Oxide/Gradient Copolymer Composites by Atom Transfer Radical Polymerization," *Macromolecules* **35** (2002) 8913-8916.
[238] D. Bontempo, N. Tirelli, G. Masci, V. Crescenzi, J. A. Hubbell, "Thick Coating and Functionalization of Organic Surfaces via ATRP in Water," *Macromol. Rapid Commun.* **23** (2002) 417-422.
[239] G. Zheng, H. D. H. Stover, "Grafting of Polystyrene from Narrow Disperse Polymer Particles by Surface-Initiated Atom Transfer Radical Polymerization," *Macromolecules* **35** (2002) 6828-6834.
[240] D. A. Savin, J. Pyun, G. D. Patterson, T. Kowalewski, K. Matyjaszewski, "Synthesis and Characterization of Silica-*graft*-Polystyrene Hybrid Nanoparticles: Effect of Constraint on the Glass-Transition Temperature of Spherical Polymer Brushes," *J. Polym. Science B: Polymer Physics* **40** (2002) 2667-2676.
[241] H. Mori, D. C. Seng, M. Zhang, A. H. E. Muller, "Hybrid Nanoparticles with Hyperbranched Polymer Shells via Self-Condensing Atom Transfer Radical Polymerization from Silica Surfaces," *Langmuir* **18** (2002) 3682-3693.
[242] J. Pyun, S. Jia, T. Kowalewski, G. D. Patterson, K. Matyjaszewski, "Synthesis and Characterization of Organic/Inorganic Hybrid Nanoparticles: Kinetics of Surface-Initiated Atom Transfer Radical Polymerization and Morphology of Hybrid Nanoparticle Ultrathin Films," *Macromolecules* **36** (2003) 5094-5104.
[243] T. Liu, S. Jia, T. Kowalewski, K. Matyjaszewski, "Grafting of Poly(*n*-butyl acrylate) from Functionalized Carbon Black Surface by Atom Transfer Radical Polymerization," *Langmuir* **19** (2003) 6342-6345.
[244] J. –B. Kim, W. Huang, M. L. Bruening, G. L. Baker, "Synthesis of Triblock Copolymer Brushes by Surface-Initiated Atom Transfer Radical Polymerization," *Macromolecules* **35** (2002) 5410-5416.
[245] G. H. Brown, "Techniques of Chemistry," Vol. **3**, Wiley, New York (1971) 49-289.
[246] M. Irie, K. Hayashi, A. Menju, "Photoresponsive polymers IV. Photocontrol of viscosity and pH value in aqueous systems using poly(methacrylic acid) having spirobenzopyran side groups" *Polymer Photochemistry* **1** (1981) 233-242.
[247] S.A. Asher, J. Holtz, J. Weissman, and G. Pan, "Mesoscopically Periodic Photonic-Crystal Materials for Linear and Nonlinear Optics and Chemical Sensing," *MRS Bulletin* 10 (1998) 44-50.
[248] Y. Iwayama, J. Yamanaka, Y. Tagiguchi,, M. Takasaka, K. Ito, T. Shinohara, T. Sawada, and M. Yonese, "Optically Tunable Celled Photonic Crystal Covering Almost the Entire Visible Light Wavelength Region," *Langmuir* 19 (2003) 977-980.
[249] P.N. Pusey, W. Van Megen, S.M. Underwood, P. Bartlett and R.H. Ottewill, "Colloidal Fluids, Crystals and Glasses," *Physics A* 176 (1991) 16-27.
[250] G. Foffi, G.D. McCullagh, A. Lawlor, E. Zaccarelli, K.A. Dawson, F. Sciortino, P. Tartaglia, D. Pini, and G. Stell, "Phase Equilibria and Glass Transition in Colloidal Systems with Short-ranged Attractive Interactions: Application to Protein Crystallization," *Phys. Rev. E* 65 (2002) 031407.
[251] K.A. Dawson, "The glass paradigm for colloidal glasses, gels, and other arrested States driven by Attractive Interactions," *Current Opinion Coll. Interf. Sci.* 7 (2002) 218-227.
[252] U. Gasser, E.R. Weeks, A. Schofield, P.N. Pusey, and D.A. Weitz, "Real-Space Imaging of Nucleation and Growth in Colloidal Crystallization," *Science* 292 (2001) 258-262.
[253] S. Tandon, R. Kesavamoorthy, and S.A. Asher, "Image Charge Effects on Colloidal Crystal Ordering," *J. Chem. Phys.* 109 (1998) 6490-6496.
[254] A.L. Rogach, N.A. Kotov, D.S. Koktysh, J.W. Ostrander, and G. A. Ragoisha, "Electrophoretic Deposition of Latex-Based 3D Colloidal Photonic Crystals: A Technique for Rapid Production of High-Quality Opals." *Chem. Mater.* 12 (2000) 2721-2726.

[255] R.C. Hayward, D.A. Saville, and I.A. Aksay, "Electrophoretic Assembly of Colloidal Crystals with Optically Tunable Micropatterns," *Nature* 404 (2000) 56-59.
[256] A.S. Dimitrov and K. Nagayama, "Continuous Convective Assembling of Fine Particles into Two-Dimensional Arrays on Solid Surfaces," *Langmuir* 12 (1996) 1303-1311.
[257] L. Shmuylovich, A.Q. Shen, and H.A. Stone, "Surface Morphology of Drying Latex Films: Multiple Ring Formation," *Langmuir* 18 (2002) 3441-3445.
[258] P. Jiang, K.S. Hwang, D.M. Mittleman, J.F. Bertone, and V.L. Colvin, "Template-Directed Preparation of Macroporous Polymers with Oriented and Crystalline Arrays of Voids," *J. Am. Chem. Soc.* 121 (1999) 11630-11637.
[259] D.M. Mittleman, J.F. Bertone, P. Jiang, K.S. Hwang, and V.L. Colvin, "Optical Properties of Planar Colloidal Crystals: Dynamical Diffraction and the Scalar Wave Approximation," *J. Chem. Phys.* 111 (1999) 345-354.
[260] M. Sasaki and K Hane, "Ultrasonically Facilitated Two-dimensional Crystallization of Colloid Particles," *J. Appl. Phys.* 80 (1996) 5427-5431.
[261] S.H. Park and Y. Xia, "Assembly of Mesoscale Particles over Large Areas and Its Application in Fabricating Tunable Optical Filters," *Langmuir* 15 (1999) 266-273.
[262] J.-Y. Shiu, C.-W. Kuo, and P. Chen, "Actively Controlled Self-Assembly of Colloidal Crystals in Microfluidic Networks by Electrocapillary Forces," *J. Am. Chem. Soc. Comm.*
[263] S.M. Yang, H. Miguez, and G.A. Ozin, "Opal Circuits of Light –Planarized Microphotonic Crystal Chips," *Adv. Funct. Mater.* 12 (2002) 425-431.
[264] T. Okubo, H. Hase, H. Kimura, and E. Kokufuta, "Thermosensitive Colloidal Crystals of Silica Spheres in the Presence of Gel Spheres of Poly(N-Isopropyl Acrylamide)," *Langmuir* 18 (2002) 6783-6788.
[265] J. Ballato, J. DiMaio, T.D.Taylor, E. Gulliver, D.-G. Han, R.E. Riman, and D.L. Carroll, "Structure Determination in Colloidal Crystal Photonic Bandgap Structures," *J. Am. Ceram. Soc.* 85 (2002) 1366-1368.
[266] G. Subramania, K. Constant, R. Biswas, M.M. Sigalas, and K.-M. Ho, "Inverse Face-Centered Cubic Thin Film Photonic Crystals," *Adv. Mater.* 13 (2001) 443-446.
[267] G. Subramania, K. Constant, R. Biswas, M.M. Sigalas, and K.-M. Ho, "Optical Photonic Crystals Fabricated from Colloidal Systems," *Appl. Phys. Lett.* 74 (1999) 3933-3935.
[268] P.A. Kralchevsky and K. Nagayama, "Capillary Forces between Colloidal Particles," *Langmuir* 10, (1994) 23-36.
[269] K. Yoshinaga, M. Chiyoda, H. Ishiki, and T. Okubo, "Colloidal Cystallization of Monodisperse and Polymer-modified Colloidal Silica in Organic Solvents," *Coll. And Surf. A* 204 (2002) 285-293.
[270] T. Seki, K. Tanaka, and K. Ichimura, "Photomechanical Response in Monolayered Polymer Films on Mica at High Humidity," *Macromolecules* **30** (1997) 6401-6403.
[271] T. Seki, H. Sekizawa, K. Tanaka, Y. Matsuzawa, and K. Ichimura, "Photoresponsive Monolayers on Water and Solid Surfaces," *Supramolecular Sci.* **5** (1998) 373-377.
[272] "Light Changes Color and Size of Crystal," *Laser Focus World* June 2001, p. 63.
[273] M.K. Maurer, PHOTORESPONSIVE POLYMERIZED CRYSTALLINE COLLOIDAL ARRAYS AND CHEMICAL SENSORS, Ph.D. Dissertation, University of Pittsburgh, 2004.
[274] M. Kamenjicki, I.K. Ladnev, and S.A. Asher, "Photoresponsive Azobenzene Photonic Crystals," *J. Phys. Chem. B* **108** (2004) 12637-12639.
[275] S.G. Romanov, T. Maka, C.M. Sotomayor Torres, M. Muller, and R. Zentel, "Photonic Band-Gap Effects upon the Light Emission from a Dye-Polymer-Opal Composite," *Appl. Phys. Lett.* 75 (1999) 1057-1059.
[276] S. G. Romanov, T. Maka, C. M. Sotomayor Torres, M. Muller, and R. Zentel, "Emission Properties of Dye-Polymer-Opal Photonic Crystals" *J. Lightwave Tech.*, **17**, (1999) 2121-2127.
[277] T. Yamasaki and T. Tsutsui, "Spontaneous Emission from Fluorescent Molecules Embedded in Photonic Crystals Consisting of Polystyrene Microspheres," *Appl. Phys. Lett.* **72** (1998) 1957-1959.

[278] M.G. Pollack, R.B. Fair, and A.D. Shenderov, "Electrowetting-based Actuation of Liquid Droplets for Microfluidic Applications," *Appl. Phys. Lett.* **77** (2000) 1725-1726.

[279] S.-K. Oh, M. Nakagawa, K. Ichimura, "Light-Guided Movement of a Liquid Droplet," *Mol. Cryst. And Liq. Cryst.* **345** (2000) 311-316.

Distribution:

1	MS0311	Joe Thomes
1	MS0750	Justin Marbury
1	MS0887	Michael. Cieslak, 1800
1	MS0888	Greg Jamison
1	MS0888	Chad Staiger
2	MS0899	Technical Library, 9616
1	MS9018	Central Technical Files, 8945-1
1	MS1411	Jun. Liu, 1846
8	MS1411	N. S. Bell, 1846
1	MS1411	Marcin Piech